

DETERMINATION OF LOADS ON A FLEXIBLE WING OF A FIGHTER JET  
VIA SURROGATE MODELS

A THESIS SUBMITTED TO  
THE GRADUATE SCHOOL OF NATURAL AND APPLIED SCIENCES  
OF  
MIDDLE EAST TECHNICAL UNIVERSITY

BY

ÖZGÜR ZAFER

IN PARTIAL FULFILLMENT OF THE REQUIREMENTS  
FOR  
THE DEGREE OF MASTER OF SCIENCE  
IN  
AEROSPACE ENGINEERING

JANUARY 2023



Approval of the thesis:

**DETERMINATION OF LOADS ON A FLEXIBLE WING OF A FIGHTER  
JET VIA SURROGATE MODELS**

submitted by **ÖZGÜR ZAFER** in partial fulfillment of the requirements for the degree of **Master of Science in Aerospace Engineering, Middle East Technical University** by,

Prof. Dr. Halil Kalıpcılar  
Dean, Graduate School of **Natural and Applied Sciences**

\_\_\_\_\_

Prof. Dr. Serkan Özgen  
Head of the Department, **Aerospace Engineering**

\_\_\_\_\_

Assoc. Prof. Dr. Melin Şahin  
Supervisor, **Aerospace Engineering, METU**

\_\_\_\_\_

**Examining Committee Members:**

Asst. Prof. Dr. Ali Türker Kutay  
Aerospace Engineering, METU

\_\_\_\_\_

Assoc. Prof. Dr. Melin Şahin  
Aerospace Engineering, METU

\_\_\_\_\_

Assoc. Prof. Dr. Nilay Sezer Uzol  
Aerospace Engineering, METU

\_\_\_\_\_

Asst. Prof. Dr. Görkem Eğemen Güloğlu  
Aerospace Engineering, METU

\_\_\_\_\_

Assoc. Prof. Dr. Mustafa Kaya  
Aerospace Engineering, AYBU

\_\_\_\_\_

Date: 26.01.2023

**I hereby declare that all information in this document has been obtained and presented in accordance with academic rules and ethical conduct. I also declare that, as required by these rules and conduct, I have fully cited and referenced all material and results that are not original to this work.**

Name Last name : Özgür Zafer

Signature :

## **ABSTRACT**

### **DETERMINATION OF LOADS ON A FLEXIBLE WING OF A FIGHTER JET VIA SURROGATE MODELS**

Zafer, Özgür  
M.Sc., Aerospace Engineering  
Supervisor: Assoc. Prof. Dr. Melin Şahin

January 2023, 106 pages

This study presents the load analysis of a flexible wing for a fighter jet. The main purpose is to demonstrate the application of a rapid methodology for aero-structural coupling and the determination of flexible wing loads suitable for the initial design stages of a fighter jet. The present methodology allows designers to include flexibility effects early on and to explore the design space quickly for flexible wing loads. The methodology uses an aerodynamic database obtained with high-fidelity computational fluid dynamics (CFD) and loads at unknown flight parameters are calculated with surrogate models. Surrogate models reduce the computational time by replacing computationally expensive CFD simulations with approximate functions which are much faster to evaluate. In order to acquire the loads on a flexible wing of the fighter jet, required models for aero-structural coupling, namely; aerodynamic, structural and surrogate models are developed. The aerodynamic model of the generic fighter aircraft is a three-dimensional wing-body configuration and aerodynamic analysis is conducted using Euler simulations in ANSYS Fluent. The results obtained from the aerodynamic analysis are validated with the available experimental results. On the other hand, the structural model is a two-dimensional

beam stick model (BSM) to decrease the computational time. The BSM generated from a wing's finite element model (FEM) and the modal properties of BSM are tuned to achieve similar modal characteristics as that of the FEM. To generate an aerodynamic database efficiently, surrogate models are also utilized and are then compared in terms of the generation of the aerodynamic database with minimal CFD simulations. According to this criterion, the surrogate model is selected for this particular research problem.

The aeroelastic model is generated using the aerodynamic loads obtained from the optimized surrogate model and mode shapes from the BSM. Flexible wing loads are calculated from the present model and verified with Nastran FlighLoads (FLDS) module which uses low-fidelity, linear aerodynamic theory to calculate aerodynamic loads. Once the validation process is completed, the developed aeroelastic model takes the high-fidelity CFD solutions as input to determine the flexible wing loads and compares the final computed results with the FLDS. In conclusion, the proposed methodology produces satisfactory results compared to the CFD simulations, hence, it can be used in the early design phase to significantly reduce computational time and cost.

Keywords: Load Analysis, Aero-Structural Coupling, Beam Stick Model, Computational Fluid Dynamics, Surrogate Modeling

## ÖZ

### **BİR SAVAŞ UÇAĞININ ESNEK KANADI ÜZERİNDEKİ YÜKLERİN VEKİL MODELLER KULLANILARAK BELİRLENMESİ**

Zafer, Özgür  
Yüksek Lisans, Havacılık ve Uzay Mühendisliği Bölümü  
Tez Yöneticisi: Doç. Dr. Melin Şahin

Ocak 2023, 106 sayfa

Bu çalışmada bir savaş uçağı esnek bir kanadının yük analizleri yapılmaktadır. Ana amaç, aero-yapısal etkileşimi için hızlı bir metodolojinin uygulanmasını ve bir savaş uçağının ilk tasarım aşamalarına uygun esnek kanat yüklerinin belirlenmesini göstermektir. Bu metodoloji, tasarımcıların esneklik etkilerini erkenden dahil etmelerine ve esnek kanat yükleri için tasarım bölgelerini hızlı bir şekilde keşfetmelerine olanak tanıyacaktır. Metodoloji, yüksek doğrulukta hesaplamalı akışkanlar dinamiği (HAD) ile elde edilen bir aerodinamik veri tabanı kullanmakta ve bilinmeyen uçuş parametrelerindeki yükler vekil modellerle hesaplanmaktadır. Vekil modeller, pahalıya mal olan HAD simülasyonlarını, çok daha hızlı olan yaklaşık fonksiyonlarla değiştirerek hesaplama süresini de azaltmaktadır.

Savaş uçağı esnek kanadının yüklerini elde etmek için aero-yapısal etkileşim için gerekli modeller, yani aerodinamik, yapısal ve vekil modeller geliştirilmiştir. Jenerik savaş uçağının aerodinamik modeli, üç boyutlu bir kanat-gövde konfigürasyonudur ve aerodinamik analizi, ANSYS Fluent ile Euler simülasyonları kullanılarak gerçekleştirilmektedir. Aerodinamik analizden elde edilen sonuçlar, mevcut deneysel sonuçlarla da doğrulanmıştır. Diğer taraftan yapısal model, hesaplama süresini azaltmak için iki boyutlu bir giriş çubuk olarak da modellenmiştir. Bir

kanadın sonlu eleman modelinden (SEM) üretilen kiriş çubuğu modeli ve bu modelin modal özellikleri, SEM'inkine benzer modal özelliklere ulaşmak için ayarlanmış ve verimli bir aerodinamik veri tabanı oluşturmak için vekil modeller kullanılmıştır. Bu vekil modeller, minimum HAD simülasyonları ile aerodinamik veri tabanının oluşturulması açısından da karşılaştırılmıştır. Bu kritere göre, bahsi geçen araştırma problemi için en uygun vekil model seçilmiştir.

Aeroelastik model, optimize edilmiş vekil modelden elde edilen aerodinamik yükler ve kiriş çubuğu modelinden gelen mod şekilleri kullanılarak oluşturulmuştur. Esnek kanat yükleri, mevcut modelle hesaplanmış ve aerodinamik yükleri hesaplamak için düşük doğrulukta, lineer aerodinamik teori kullanan Nastran FlighLoads (FLDS) modülü ile doğrulanmıştır. Doğrulama işlemi tamamlandıktan sonra, geliştirilen aeroelastik model, yüksek doğruluklu HAD çözümlerini esnek kanat yüklerini belirlemek için bir girdi olarak almış ve hesaplanan nihai sonuçlar FLDS ile karşılaştırılmıştır. Sonuç olarak, önerilen bu metodoloji, HAD simülasyonlarına kıyasla tatmin edici sonuçlar elde edilmiş ve bu nedenle hesaplama süresini ve maliyeti önemli ölçüde azalttığı için erken tasarım aşamasında kullanılabilceğini de göstermiştir.

Keywords: Yük analizi, Aero-yapısal Etkileşimi, Kiriş Çubuğu Modeli, Hesaplamalı Akışkanlar Dinamiği, Vekil Modelleme



To My Family

## ACKNOWLEDGMENTS

I would like to express my deepest gratitude to my supervisor Assoc. Prof. Dr. Melin Şahin for his valuable advice, assistance, giving me opportunity to work with him and patience through this study.

I am grateful to Abdul Rampurawala for supporting me patiently about technical subjects throughout the study and for all contributions to my entire engineering skills.

I would like to thank to my colleagues Hasnain Tahir, Mehmet Yılmaztürk, Sercan Öztürk, Murat Aydın, Burak Keskin, Abdullah Enes Coşkun and Tolga Kayabaşı for their all precious supports throughout this thesis study.

I also would like to thank to Enes Akkül and Süleyman Özkan for their strong friendships.

Finally, I would like to present my deepest thanks to my parents Durdiya Zafer, and İbrahim Zafer for their endless supports in my whole life.

## TABLE OF CONTENTS

ABSTRACT .....	v
ÖZ .....	vii
ACKNOWLEDGMENTS .....	x
TABLE OF CONTENTS .....	xi
LIST OF TABLES .....	xv
LIST OF FIGURES .....	xvi
CHAPTERS	
1 INTRODUCTION .....	1
1.1 Background and Motivation of the Study .....	1
1.2 Objectives of the study .....	2
1.3 Limitations of the study .....	3
1.4 Outline of the study .....	3
2 LITERATURE REVIEW .....	5
2.1 Introduction .....	5
2.2 Initial Design for a Fighter Aircraft .....	5
2.3 Loads Analysis for Fixed-Wing Aircraft .....	6
2.4 Established Computational Approaches for Aero-Structural Analyses .....	7
2.4.1 Low-Fidelity Methods in Aero-Structural Analyses .....	9
2.4.2 High-Fidelity Methods in Aero-Structural Analyses .....	10

2.5	High-Fidelity-Based Computational Rapid Approaches for Aero-Structural Analyses .....	10
2.5.1	Data Fit Models .....	11
2.5.2	Projection-Based Reduced Order Models.....	11
2.5.3	Hierarchical Models .....	12
2.6	Conclusions.....	12
3	PROPOSED METHODOLOGY .....	15
3.1	Introduction.....	15
3.2	Aero-Structural Coupling of a Generic Fighter Wing .....	15
3.3	Conclusions.....	19
4	AERODYNAMIC MODELING AND ANALYSES OF THE GENERIC FIGHTER AIRCRAFT .....	21
4.1	Introduction.....	21
4.2	Aerodynamic Model of the Generic Fighter Aircraft.....	21
4.2.1	Configuration of the Generic Fighter Aircraft .....	21
4.2.2	Aerodynamic Mesh of the Generic Fighter Aircraft .....	22
4.3	Aerodynamic Model of the Generic Fighter Aircraft.....	25
4.3.1	Solver Settings of Fluent.....	25
4.3.2	Analysis Results of Fluent .....	26
4.4	Conclusions.....	40
5	STRUCTURAL MODELING OF THE GENERIC FIGHTER AIRCRAFT WING.....	41
5.1	Introduction.....	41
5.2	Finite Element Model of the Generic Fighter .....	41
5.3	Beam Stick Model for Generic Fighter Wing.....	42

5.4	Validation of the Generated Beam Stick Model .....	48
5.5	Conclusions.....	50
6	AERODYNAMIC DATABASE GENERATION FOR GENERIC FIGHTER VIA SURROGATE MODELS .....	51
6.1	Introduction.....	51
6.2	Aerodynamic Database Generation Methodology for Generic Fighter....	52
6.2.1	Aerodynamic Database Generation with Surrogate Modeling Toolbox 57	
6.2.2	Aerodynamic Database Generation with Artificial Neural Networks 62	
6.3	Comparisons of Surrogate Modeling Methods .....	66
6.4	Conclusions.....	69
7	AERO-STRUCTURAL ANALYSES OF THE GENERIC FIGHTER WING 71	
7.1	Introduction.....	71
7.2	Aero-Structural Coupling of the Generic Fighter Wing.....	71
7.3	Validation of the Proposed Methodology.....	75
7.4	Aero-Structural Analysis Results of the Generic Fighter Wing.....	83
7.5	Conclusions.....	86
	CONCLUSIONS .....	89
8.1	General Conclusions.....	89
8.2	Recommendations for future works .....	90
	REFERENCES.....	91
	APPENDICES	
A.	Initial Training and Test Points for Aerodynamic Database Generation .	99

B.	Aerodynamic Database Generation with Three Different Databases.....	101
C.	Response Surfaces for Surrogate Models .....	103

## LIST OF TABLES

### TABLES

Table 2.1 Load analysis types for fixed-wing aircraft.....	7
Table 3.1 Aerodynamic database structure .....	18
Table 5.1 Natural frequencies of the FEM and BSM .....	49
Table 6.1 Number of points used to create an aerodynamic database.....	61
Table 6.2 Hyperparameters investigated in PyTorch .....	63
Table 6.3 Hyperparameters investigated in MATLAB ANN Toolbox .....	65
Table 6.4 Comparison of average elapsed time and number of training points used for KRG and ANN.....	67
Table 7.1 Total wing $F_z$ forces [kN] for different Mach and AoA values.....	85
Table 7.2 Elapsed time comparison for FLDS and Rapid Method .....	86

## LIST OF FIGURES

### FIGURES

Figure 2.1 Collar aeroelastic triangle [5] .....	8
Figure 2.2 Varying levels of complexity in modeling for fluids and structures [7]..	9
Figure 3.1 Generic fighter wing planform and BSM Nodes.....	17
Figure 4.1 Generic fighter configuration and dimensions [58].....	22
Figure 4.2 Generic fighter surface mesh [58] .....	23
Figure 4.3 Generic fighter volume mesh .....	23
Figure 4.4 Mesh for Fluid Domain.....	24
Figure 4.5 Surface pressure comparison for generic fighter $M=0.85$ , $AoA=2.12^\circ$ at 59% span (left), at 85% span (right) [58].....	24
Figure 4.6 Hierarchy of governing equations [59] .....	25
Figure 4.7 Residuals vs iteration number.....	27
Figure 4.8 Surface pressure comparison for generic fighter $M=0.85$ , $AoA=2.12^\circ$ at 59% span.....	28
Figure 4.9 Surface pressure comparison for generic fighter $M=0.85$ , $AoA=2.12^\circ$ at 85% span.....	28
Figure 4.10 $C_L$ vs. $AoA$ curve for different Mach numbers.....	30
Figure 4.11 $C_L$ vs. $AoA$ curve for Mach numbers $< 1$ .....	31
Figure 4.12 $C_L$ vs. $AoA$ curve for Mach numbers $> 1$ .....	31
Figure 4.13 Root (black), mid (red) and tip (blue) sections on the generic fighter.	32
Figure 4.14 $C_L$ vs. $AoA$ curve for different Mach numbers and three selected wing sections.....	33
Figure 4.15 Surface $C_p$ distributions at Mach 0.6 for $0^\circ$ , $2^\circ$ and $4^\circ$ $AoA$ .....	34
Figure 4.16 Surface $C_p$ distributions at Mach 0.6 for $6^\circ$ , $8^\circ$ and $10^\circ$ $AoA$ .....	35
Figure 4.17 Surface $C_p$ distributions at Mach 0.6 for $12^\circ$ , $14^\circ$ and $16^\circ$ $AoA$ .....	35
Figure 4.18 Surface $C_p$ distributions at Mach 0.6 for $18^\circ$ , $20^\circ$ and $22^\circ$ $AoA$ .....	36
Figure 4.19 Surface $C_p$ distributions at Mach 0.9 for $0^\circ$ , $2^\circ$ and $4^\circ$ $AoA$ .....	37
Figure 4.20 Surface $C_p$ distributions at Mach 0.9 for $6^\circ$ , $8^\circ$ and $10^\circ$ $AoA$ .....	37



Figure 4.21 Surface $C_p$ distributions at Mach 0.9 for 12°, 14° and 16° AoA .....	38
Figure 4.22 Surface $C_p$ distributions at Mach 1.4 for 0°, 2° and 4° AoA .....	39
Figure 4.23 Surface $C_p$ distributions at Mach 1.4 for 6°, 8° and 10° AoA .....	39
Figure 5.1 Structural finite element model for the generic fighter [58] .....	42
Figure 5.2 Equivalent beam reduction procedures [63].....	43
Figure 5.3 Top view for undeflected wing (red) and deflected wing (black) with BSM nodes .....	44
Figure 5.4 Isometric view for undeflected wing (red) and deflected wing (black) with BSM nodes .....	44
Figure 5.5 Lift distribution along the span for different numbers of beam stick nodes .....	45
Figure 5.6 Flexural and torsional rigidity of BSM.....	46
Figure 5.7 Beam stick nodes on the FEM.....	47
Figure 5.8 BSM nodes and RBE2 elements and leading and trailing edge of the wing .....	48
Figure 5.9 (a) The First Bending mode (b) The first torsion mode (c) The Second bending mode for FEM (left) and BSM (right).....	49
Figure 6.1 Computational time – number of simulations for CFD simulations in this study.....	53
Figure 6.2 Aerodynamic database generated for generic fighter .....	54
Figure 6.3 Initial training and test points for aerodynamic database.....	55
Figure 6.4 Cut planes on the generic fighter wing .....	55
Figure 6.5 Flowchart for optimized database generation.....	56
Figure 6.6 SMT Architecture [57].....	58
Figure 6.7 Advantages and disadvantages of surrogate modeling methods in SMT [57].....	59
Figure 6.8 Comparisons of surrogate modeling methods in SMT .....	61
Figure 6.9 Maximum relative error (left) and elapsed time (right) - training points for ANN with Pytorch.....	64

Figure 6.10 Maximum relative error (left) and elapsed time (right) - training points for ANN with MATLAB .....	66
Figure 6.11 Model performance-data volume for different methods [67].....	68
Figure 7.1 Flowchart for the proposed methodology .....	72
Figure 7.2 Generic fighter configuration (red) and FLDS configuration (black) ...	75
Figure 7.3 (a) 240 panels (b) 480 panels (c) 960 panels (d) 1920 for the FLDS model.....	77
Figure 7.4 $F_z$ vs number of panels .....	78
Figure 7.5 Wing $F_z$ and $M_y$ values for changing AoA.....	79
Figure 7.6 Center of pressure locations and the BSM on the wing for different Mach numbers at AoA = 4° .....	80
Figure 7.7 Center of pressure locations and the BSM on the wing for different Mach numbers at AoA = 16° .....	80
Figure 7.8 $F_z$ and $M_y$ distributions for the wing for different Mach numbers and AoA = 4° .....	82
Figure 7.9 $F_z$ and $M_y$ distributions for the wing for different Mach numbers at AoA = 4° .....	83
Figure 7.10 $F_z$ and $M_y$ distributions for the wing for different Mach numbers and AoA = 16° .....	84

## **CHAPTER 1**

### **INTRODUCTION**

#### **1.1 Background and Motivation of the Study**

Load assessment of aircraft and its components is essential to the aircraft development process. At the preliminary design stage of aircraft development, aerodynamic loads must be computed on the most current iteration of the external shape to size the aircraft structure. The newly sized structure is then assessed for its impact on the loads, aeroelastic and aerodynamic performance of the aircraft. Therefore, load computations are central in the overall flight physics process and it is vital for achieving a good level of accuracy to ensure the optimum weight, performance, dimensions and safety of the aircraft. The operation envelope for a fighter aircraft ranges from low subsonic with very high angles of attack to supersonic high g maneuvers. Aerodynamic forces acting on the aircraft during these extreme maneuvers cause large deformations of the elastic structure. Changed external shape requires the recalculation of the aerodynamic forces. The wing is the main component, which is exposed to the aeroelastic effects, and therefore there is a need for integrating loads on a flexible wing into the fighter aircraft design process in the early stages.

The accuracy of the load's computations depends on the fidelity of the aerodynamics methods used; ideally, wind tunnel models would provide the most accurate results in the absence of flight test data. However, it is not feasible as the external shape and

structure are not mature enough for a wind tunnel or a flight test. The less accurate but feasible option is to use low-fidelity panel methods. Still, these methods are not capable of modeling aerodynamic nonlinearities such as shocks, separation and vertical flows, which are all important characteristics of fighter aircraft flow regimes. Another option is to use high-fidelity computational fluid dynamics (CFD) computations which require long lead times and high computational resources for the number of calculations needed for the load's process. Since one of the options lacks the necessary accuracy to model aerodynamics and the other option requires high computational times and resources, and for this reason, there is a need for rapid methodology with reasonable accuracy, and therefore in this study, it is proposed to use a CFD-based surrogate model to overcome the constraint of high computational cost and provide a similar accuracy level with high-fidelity solutions.

## **1.2 Objectives of the study**

The main objective of this thesis is the development of a rapid methodology to compute flexible wing loads of fighter aircraft using CFD-based surrogate models. The models and tools required for achieving this main objective are summarized below as:

- Constructing a high-fidelity aerodynamic model of a fighter aircraft to obtain a better estimate of the aerodynamic loads in the flight conditions that the fighter aircraft operates.
- Constructing a beam stick model for a fighter aircraft wing.
- Conducting high-fidelity 3D Computational Fluid Dynamics (CFD) analysis and creating a database that includes the envelope of a fighter aircraft.
- Selecting the surrogate model and predicting the loads for the desired flight conditions.
- Constructing an aeroelastic model for a fighter aircraft wing.
- Validating the aeroelastic model via a commercial finite element software (MSC NASTRAN) used in the industry.

### **1.3 Limitations of the study**

The main limitations of this study can be listed as follows:

- Aircraft is assumed rigid and viscous effects are neglected in aerodynamic solutions (i.e. Euler solutions).
- Wing sections are assumed to be rigid in chord-wise direction; hence change in camber due to chord-wise bending of the sectional profile is not modeled.
- For the aero–structural coupling, a time-independent formulation is used.
- The induced incidence distribution is predicted via a numerical approach applicable to non-planar wings.

### **1.4 Outline of the study**

The organization of this thesis can be given as follows:

In Chapter 2, the literature survey about computational approaches for aero-structural analyses for fixed-wing aircraft is given briefly. This section also provides the types and properties of established computational methods in the industry. High-fidelity-based rapid computational methods are also presented in this chapter.

In Chapter 3, the proposed CFD-based rapid methodology for aero-structural coupling and determination of flexible wing loads, is described in detail. The methodology allows designers to include flexibility effects at the early stages of fighter jet design.

In Chapter 4, the aerodynamic model of the generic fighter aircraft is constructed and the aerodynamic analyses are performed to calculate aerodynamic loads for different Mach and angle of attack (AoA) combinations.

In Chapter 5, the structural model of the generic fighter aircraft wing is presented. A beam stick model is generated at the elastic axis of a finite element model (FEM). and then compared with FEM in terms of natural frequencies and mode shapes.

In Chapter 6, aerodynamic loads for each node of the stick model for all Mach and AoA combinations are generated. The tools and surrogate models utilized in this study are also explained. Afterward, the database structure and each surrogate model's performance of generation of the aerodynamic database are given. Finally, the surrogate model for the research problem is selected in this chapter.

In Chapter 7, aerodynamic loads from the surrogate model and the eigenvalues and corresponding eigenvectors of the beam stick model are coupled through a code written in Python programming language. The loads on the flexible wing for different flow regimes are presented and then the results are then compared with an established approach used in the industry.

In Chapter 8, the general conclusions are presented and recommendations for future work are provided.

## **CHAPTER 2**

### **LITERATURE REVIEW**

#### **2.1 Introduction**

This chapter summarizes the studies that have been carried out in connection with the topic of this thesis. First, general information about the initial design phase of the fighter aircraft is given. Second, established approaches to aero-structural analysis in the design phases are explained. This part presents low-fidelity panel and high-fidelity coupling methods of Computational Fluid Dynamics (CFD) and Computational Structural Mechanics (CSM). The third part presents high fidelity-based rapid approaches for aero-structural analyses. In the literature, this is also known as surrogate models. Surrogate models include data fit, projection-based reduced order, and hierarchical models.

#### **2.2 Initial Design for a Fighter Aircraft**

Aircraft design stages are divided into three parts in the literature: conceptual design, preliminary design, and detail design [1]. In the conceptual design phase, requirements guide the process. All of the designs first try to meet requirements. In this stage, initial estimates of the aircraft's weight, size, and performance are conducted. Trade-off studies are performed among the design alternatives satisfying the requirements. The resulting conceptual design aircraft is further analyzed in the preliminary design phase to make necessary changes and perform optimization studies. In this stage, high-fidelity analyses and wind tunnel tests are carried out to obtain more reliable data and freeze the aircraft configuration. Detail design is the phase where the designed parts are started to be manufactured. Experimental tests

and high-fidelity computational simulations are continued in this phase but also ground, and flight tests are performed during this phase.

In the initial design stage, aircraft weight is one of the most critical parameters that should be determined because it affects its performance in many aspects. It is vital to design an aircraft as light as possible but strong enough to endure the forces it experiences during its lifetime. The load analysis determines the forces acting on the aircraft during maneuvers, turbulence, landings, and ground operations [2]. Therefore, it is essential to conduct load analysis in the initial design stages. For conventional aircraft, a loads envelope may require the order of 100000 simulations to find all critical load cases. For unconventional aircraft with little or no engineering experience available, up to 10 million computations may be required [3]. Load analysis can be performed by assuming the structure is rigid or flexible. Although assuming a rigid structure decreases the complexity of the problem, this may cause expensive modifications in the later stages. Deflection of the structure tends to redistribute the aerodynamic load significantly. Structural members must be designed for the aerodynamic load distribution related to the deformed structure, not the initial shape [4]. In order to determine these aero-structural coupling effects, the most reliable data sources are flight tests or wind tunnels. However, it is not feasible to use those in the preliminary stages since the external shape and structure are not mature enough. Therefore, in these stages, it is feasible to use computational approaches.

### **2.3 Loads Analysis for Fixed-Wing Aircraft**

In the previous section, the initial design phase of the fighter type of aircraft is described. This section, on the other hand, discusses the research on load analysis for fixed-wing aircraft in the literature. In the literature, for fixed-wing aircraft usually, load analysis is applied to either the transport or fighter type of aircraft. Another classification type is the assumption of rigidity where the load analysis is conducted on rigid aircraft which does not consider the structure's deformation.



The second type assumes the aircraft structure as flexible and the loads analysis performed on this type can be named as aero-structural analysis because it considers both the aerodynamics and the structures of the aircraft. These classifications show the studies conducted based on the fixed-wing aircraft type and the structure rigidity assumption.

Table 2.1 Load analysis types for fixed-wing aircraft

	Rigid	Flexible
Transport	[3],[22],[24],[39],[40],[41],[42] [43],[44],[45],[46]	[3],[4],[47],[48],[49],[50],[52],[53]
Fighter	[38],[51],[54]	[36],[37]

In the literature, loads analysis is mainly conducted on the transport type of aircraft and analysis of the fighter type of aircraft is limited. This thesis focuses on the load analysis of flexible fighter aircraft loads.

#### 2.4 Established Computational Approaches for Aero-Structural Analyses

Aeroelasticity studies the interaction between aerodynamic, elastic, and inertial forces acting on a structure. It is classified as static and dynamic aeroelasticity in the literature. Figure 2.1 shows the Collar's aeroelastic triangle, which demonstrates the interaction between aerodynamic, elastic, and inertial forces. Static aeroelasticity is due to the interaction between elastic forces and aerodynamic forces. This influences the lift distribution on the aircraft and can cause statically unstable conditions such as divergence and control surface reversal. The interaction between elastic, aerodynamic, and inertial forces is considered in dynamic aeroelasticity. Dynamic aeroelasticity includes the phenomena of flutter. Flutter is a dynamically unstable self-excited vibration in which the structure extracts energy from the air stream and can cause catastrophic structural failure [5].

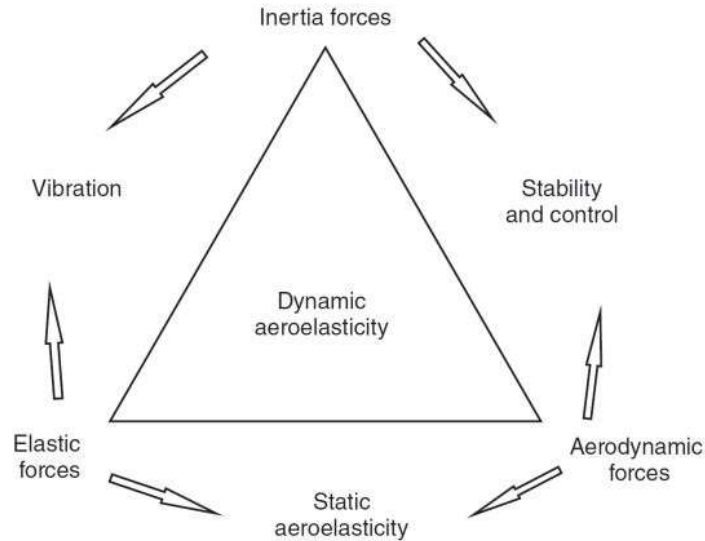


Figure 2.1 Collar aeroelastic triangle [5]

Aero-structural analyses can be performed on different fidelity levels computationally. Figure 2.2 shows different complexity levels used to model the interaction between fluids and structures. Aerodynamic data may be used in multiple levels of fidelity in aircraft design stages. They are starting with low-fidelity Lookup tables for the high-fidelity Navier-Stokes solutions. In the arrow direction, the complexity of physics is increasing for fluids. Similarly, the data for structures can be obtained starting from the shape functions assumed with low-fidelity detailed three-dimensional finite elements. In the arrow direction geometry complexity decreases.

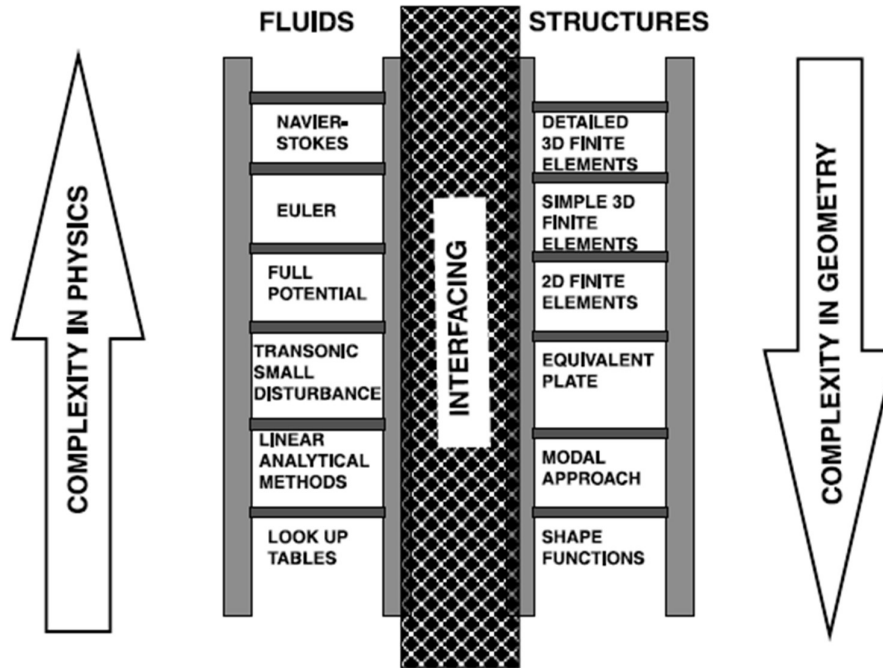


Figure 2.2 Varying levels of complexity in modeling for fluids and structures [7]

By changing the complexity used in the fluids and structures, the accuracy and the computational time generally increase. In the design cycle of an aircraft, there are established methods that use different levels of fidelity.

#### 2.4.1 Low-Fidelity Methods in Aero-Structural Analyses

Linear analytical and transonic small disturbance methods generally have low fidelity in aeroelastic problems. One of the most used commercial tools using low-fidelity methods to solve aeroelastic problems is MSC Nastran and MSC FlightLoads [6]. For aerodynamic calculations MSC Nastran uses the Doublet-Lattice method (DLM) for subsonic flows and uses ZONA51 for supersonic flows [6]. The theory for DLM is presented in [9],[10],[11],[12],[13] and it uses linearized aerodynamic potential theory. The undisturbed flow is uniform and it can be either steady or

varying harmonically. All lifting surfaces are assumed to lie nearly parallel to the flow. On the other hand, ZONA51 is a supersonic lifting surface theory that accounts for the interference among multiple lifting surfaces. It is a linearized aerodynamic small disturbance theory that assumes all interfering lifting surfaces lie nearly parallel to the flow. Like the DLM, the linearized supersonic theory does not account for any thickness effects of the lifting surfaces. ZONA51 is presented in [14].

#### **2.4.2 High-Fidelity Methods in Aero-Structural Analyses**

Low-fidelity methods in the aero-structural analyses use linear potential flow theory or transonic small disturbance theory in their aerodynamic solutions. These methods assume linearity; however, this assumption has the disadvantage of neglecting significant effects such as transonic flow, stall, and friction drag in the case of aerodynamics [3]. Because these methods cannot predict the non-linear effects encountered by the aircraft in the non-linear flow regimes, high-fidelity methods need to be used [15]. The accuracy of the aeroelastic model can be increased by using high-fidelity aerodynamic models based on the Navier-Stokes equations or Euler equations [16]. Navier-Stokes equations solve for viscous flows, and Euler equations assume inviscid flow and are reduced forms of the Navier-Stokes equations.

#### **2.5 High-Fidelity-Based Computational Rapid Approaches for Aero-Structural Analyses**

In the previous sections, low and high-fidelity approaches in the aero-structural analyses are described. However, these approaches have their limitations. Low-fidelity methods are linear and cannot capture non-linear effects, which are essential for the design of a fighter aircraft. On the other hand, high-fidelity methods can capture the non-linear effects, but they need high computational resources. One high-fidelity aero-structural analysis could take days to perform aerodynamic-structure iterations [4].

High-fidelity-based rapid approaches are not trying to solve the differential equations but instead use the high-fidelity methods' solutions to create a model. Hence, this approach is data-based and rapid because it can find the desired parameter much faster than high-fidelity methods. In the literature, this type of model is known as the “surrogate model” [8]. The main advantages of using surrogate models are their simplicity and ability to handle complex problems regardless of the nature of the problem and the source from which the modes of the system originate [17]. Surrogate models are categorized into three main classes: data-fit models, projection-based reduced models, and hierarchical models [20].

### **2.5.1 Data Fit Models**

Data-fit models include response surface methods that use interpolation or regression of simulation data to fit a model for the system output as a function of the parameters. A key benefit of data-fit approaches is that the offline process of deriving the surrogate model is non-intrusive. The high-fidelity model can be run in “black-box” mode, where the sole task is to specify input parameters and generate the corresponding system output predictions. [21]. In the literature, for aerospace applications, data-fit models include linear interpolation [4], Kriging [22],[24],[25],[26], radial basis functions [24],[25] and neural networks [23].

### **2.5.2 Projection-Based Reduced Order Models**

Projection-based reduced-order models take high-fidelity solutions and project solutions into low-dimensional subspaces. One of the potential advantages of a projection-based reduced model is that it retains the underlying structure of the model. This advantage is significant for dynamical systems because the model can be used for the prediction of the future state of a dynamical system. In the aerospace industry, projection based reduced order models are used for time-independent computational fluid dynamics solutions to calculate aerodynamic loads

[3],[18],[19],[28] and for time-dependent aero-structural coupling cases [27],[29]. They are also handy for control applications and is used in stall control [30],[31].

### **2.5.3 Hierarchical Models**

Hierarchical surrogates are derived from higher-fidelity models, simplifying physics assumptions, coarser grids, alternative basis expansions, and looser residual tolerances [21]. Hierarchical surrogate models also include multi-fidelity methods, combining low and high-fidelity solutions. In the literature, it is used for combining the experimental and computational results [32]. Hierarchical surrogate models are also used in the aeroelasticity literature to predict the flutter point of aircraft [33],[34],[35].

## **2.6 Conclusions**

This chapter briefly describes the initial design for fighter aircraft and how load analysis plays a role in the design phases. Rigid and flexible aircraft load analyses for fixed-wing aircraft are described and the need for flexible aircraft load analysis in the preliminary design stages is emphasized. Afterward, established computational approaches for aero-structural studies are reviewed and categorized as the fidelity level of the fluid and structural modeling. Because low-fidelity methods cannot capture the non-linear aerodynamic phenomena such as shocks, separations, and vortices and high-fidelity techniques require high computational resources and times, there is a need for a rapid approach that can capture the aerodynamic non-linearities. Therefore, high-fidelity-based rapid computational approaches are introduced next. These approaches are also known as surrogates in the literature and are divided into three categories. Data-fit models are response surface methods that use interpolation or regression of simulation data to fit a model for the system output as a function of the parameters. Projection-based reduced-order models take high-fidelity solutions and project solutions into low-dimensional

subspaces with low-dimensional representation. It can protect the underlying structure of the model while decreasing the computational cost. Hierarchical models are derived from high-fidelity models by using approaches like simplifying physics assumptions, coarser grids, and looser residual tolerances. Among the various computational approaches, this thesis lies in the data-fit models under the high fidelity-based rapid computational approaches for the aero-structural analyses category. High-fidelity CFD solutions are the basis for the data-fit model. With this model, all the required analyses for the initial design stages can be conducted while computational cost is significantly reduced.

And therefore, this thesis aims to propose a rapid computational methodology for integrating the aero-structural analyses into the early stages of the fighter aircraft development process.





## CHAPTER 3

### PROPOSED METHODOLOGY

#### 3.1 Introduction

This chapter introduces and explains the proposed methodology for aero-structural coupling for a generic fighter wing. First, descriptions of aerodynamic and structural modules are given. Afterward, surrogate models used with aerodynamic analyses results are explained. Finally, the aeroelastic module is described, which shows the coupling between aerodynamic and structural modules.

#### 3.2 Aero-Structural Coupling of a Generic Fighter Wing

The proposed methodology is an approach to predict flexible wing loads. This methodology is proposed in [4] to optimize flexible wing twists using rapid computational methods. The method is called as rapid because this method is much faster compared to computational fluid dynamics (CFD) and computational structural mechanics (CSM) coupling. CFD-CSM coupling takes sixty hours and the proposed rapid method only takes one second for this particular study [4]. The study uses the rapid methodology to a transport type of aircraft for a fixed Mach (M) number and changes the angle of attack (AoA) values. For finding the unknown AoA values, linear interpolation is used. This study aims to extend the proposed methodology for changing AoA and Mach numbers and apply it to a generic fighter wing. Because fighter aircraft can operate at high Mach numbers and AoA values, they experience more severe conditions than transport aircraft and it is essential to investigate these high AoA and Mach number values. The method will cover all of the regimes that a generic fighter aircraft operates for finding the flexible wing loads. The method requires aerodynamic and structural models of the generic fighter wing

to determine flexible wing loads. In addition to these models, as the approach aims to predict two unknown parameters ( $M$ ,  $AoA$ ), more complicated but still rapid models called surrogate models are used in this methodology. Finally, the aero-structural coupling can be performed by using these models.

The proposed methodology uses rigid aircraft aerodynamic solutions for its aerodynamic model. For this reason, the aerodynamic model of a generic fighter consists high-fidelity CFD database obtained for a rigid generic fighter aircraft at different Mach and  $AoA$  values. The database includes Mach numbers for subsonic, transonic, and supersonic regimes and high  $AoA$  values are also investigated. Data are generated with an Euler solver in commercial software. Instead of just modeling the wing, the fuselage is modeled in order to include the aerodynamic effects between the wing and fuselage. After obtaining the solutions for the aircraft, the wing part is mainly focused. Details about the aerodynamic model of a generic fighter are given in Chapter 4.

In the proposed methodology, the basic assumption is that there is no chordwise bending of the wing profile and the change in the local lift is purely a function of structural twist and induced incidence. Hence, the methodology uses a beam stick model (BSM) to represent the wing along the span. The BSM is created from a generic fighter wing's finite element model (FEM). When a wing undergoes a twisting motion, coordinates form a line in 3-dimensional space along the span about which the wing profiles rigidly rotate. This line is known as the elastic axis of the wing [61]. The nodes of the BSM are placed on this elastic axis. Furthermore, it is assumed the structure is linear and the deformation at any point on the wing can be defined by superpositioning the natural modes of the structure. Bar elements are generated from BSM nodes and material properties are tuned to achieve modal characteristics, namely the natural frequencies and corresponding mode shapes, similar to the baseline full FEM. Details about the structural model of a generic fighter wing are given in Chapter 5.

After the BSM nodes are determined and high-fidelity CFD solutions are obtained, they can be used by surrogate models. In this study, surrogate models are used to predict the sectional forces and moments along the generic fighter span. Figure 3.1 shows the planform section and BSM nodes for a generic fighter wing.

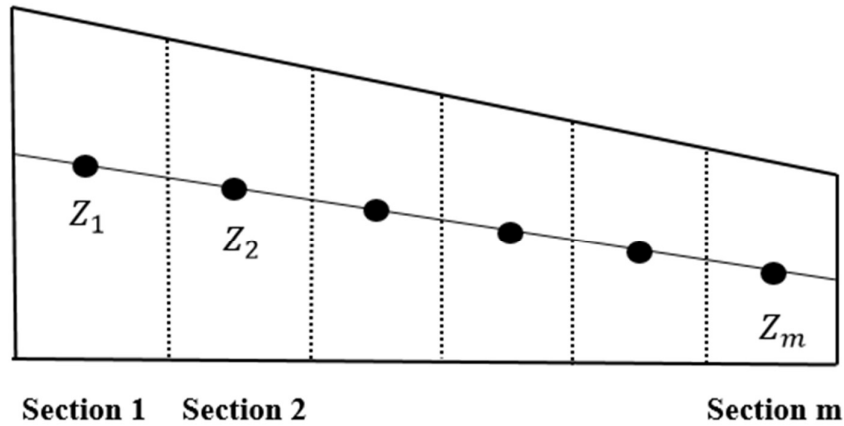


Figure 3.1 Generic fighter wing planform and BSM Nodes

From the CFD solutions, pressure distributions are obtained and forces and moments on the BSM nodes are then calculated by integrating the surface pressures on the wing from the CFD solutions with a post-processing tool. An initial aerodynamic database is created for each section and (Mach, AoA) combination for surrogate models. Table 3.1 shows the database structure for  $n$  number of Mach and  $n$  number of AoA combinations for  $m$  sections over the wing where the total number of combinations is represented with  $k$ . Additionally, in this table, the first and the second subscripts indicate the angle of attack value and the section number respectively and the superscript shows the Mach number value.

Table 3.1 Aerodynamic database structure

	<b>Section 1</b>	<b>Section 2</b>	...	<b>Section m</b>
$M_1, AoA_1$	$Z_{1,1}^{M_1}$	$Z_{1,2}^{M_1}$	...	$Z_{1,m}^{M_1}$
$M_1, AoA_2$	$Z_{2,1}^{M_1}$	$Z_{2,2}^{M_1}$	...	$Z_{2,m}^{M_1}$
⋮	⋮	⋮	...	⋮
$M_1, AoA_n$	$Z_{n,1}^{M_1}$	$Z_{n,2}^{M_1}$	...	$Z_{n,m}^{M_1}$
⋮	⋮	⋮	...	⋮
$M_n, AoA_n$	$Z_{k,1}^{M_n}$	$Z_{k,2}^{M_n}$	...	$Z_{k,m}^{M_n}$

After an initial CFD database is formed, surrogate models predict the forces and moments for unknown Mach and AoA combinations in a rapid way. These models are data-fit models that include response surface methods using interpolation or regression of simulation data to fit a model for the system output as a function of the parameters. There are many types of surrogate models used in engineering and the majority of them are covered in this study. Details about the examined surrogate models and their performance in determining aerodynamic loads are given in Chapter 6.

The final step of the methodology is to couple the aerodynamic and structural models and therefore an aero-structural coupling code is developed for this iterative process. The coupling code takes the aerodynamic loads at BSM nodes and natural frequencies and corresponding mode shapes of BSM as inputs. As a result of aero-structural coupling, the structural twist distribution of the wing is obtained. As each section's local AoA values are dependent on the induced incidence value, a numerical approach developed for non-planar wings for arbitrary loading is used to determine the induced incidence values [54]. The aerodynamic loads change for each section in every iteration and are evaluated with surrogate models. This coupling process

continues until the algorithm converges. The details about the aero-structural coupling process are given in Chapter 7.

### **3.3 Conclusions**

In this chapter, the proposed methodology for the determination of flexible wing loads for a generic fighter aircraft is briefly introduced. It can be seen from the proposed methodology that one can predict the flexible wing loads of a generic fighter aircraft over the all-flight envelope that a generic fighter can possibly operate. The main advantage of this methodology is to be able to predict flexible wing loads rapidly without compromising the accuracy that could be obtained via high-fidelity CFD solutions.



## **CHAPTER 4**

### **AERODYNAMIC MODELING AND ANALYSES OF THE GENERIC FIGHTER AIRCRAFT**

#### **4.1 Introduction**

In this chapter, the aerodynamic modeling and analyses performed on the generic fighter aircraft are explained in detail. The generic fighter is a realistic-size aeroelastic test case developed for academic studies [58]. Firstly, the generic fighter aircraft model is described, which includes the configuration and the aerodynamic mesh. Afterward, the aerodynamic analyses are conducted by using the commercial CFD software ANSYS Fluent. Aerodynamic analyses are presented by considering two different parameters: Mach and angle of attack (AoA). This study aims to cover all the regimes in which the fighter type of aircraft operates. Therefore, a wide range of Mach and AoA combinations are examined in aerodynamic analyses.

#### **4.2 Aerodynamic Model of the Generic Fighter Aircraft**

##### **4.2.1 Configuration of the Generic Fighter Aircraft**

The configuration of the fighter aircraft is called the generic fighter configuration and is created for building a realistic-size aeroelastic test case. The geometry is based on publicly available data for the F-16 and therefore the general dimensions of the configurations are similar to the F-16. However, several modifications are made to give the model a closer representation of the F-16. Improvements in the geometry include changing the twist at the wing tip and root. Also, to reduce the size of the

computational model, the tailplane is removed [58]. Figure 4.1 shows the generic fighter configuration and its dimensions.

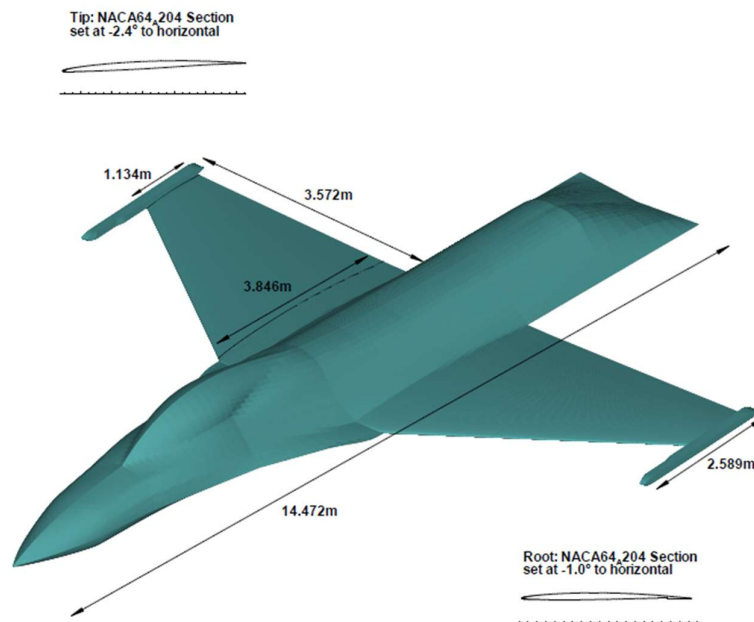


Figure 4.1 Generic fighter configuration and dimensions [58]

#### 4.2.2 Aerodynamic Mesh of the Generic Fighter Aircraft

Generic fighter configuration is meshed with an H-type block structured grid around the wing and a C-type block topology is applied around the fuselage [58]. The surface mesh has 15432 cells and 16387 nodes in total. Figure 4.2 shows the surface mesh of the generic fighter aircraft. In the volume mesh of the generic fighter, there are 600024 cells and 631973 nodes in total. Figure 4.3 shows the volume mesh of the generic fighter and Figure 4.4 shows the mesh of the fluid domain.



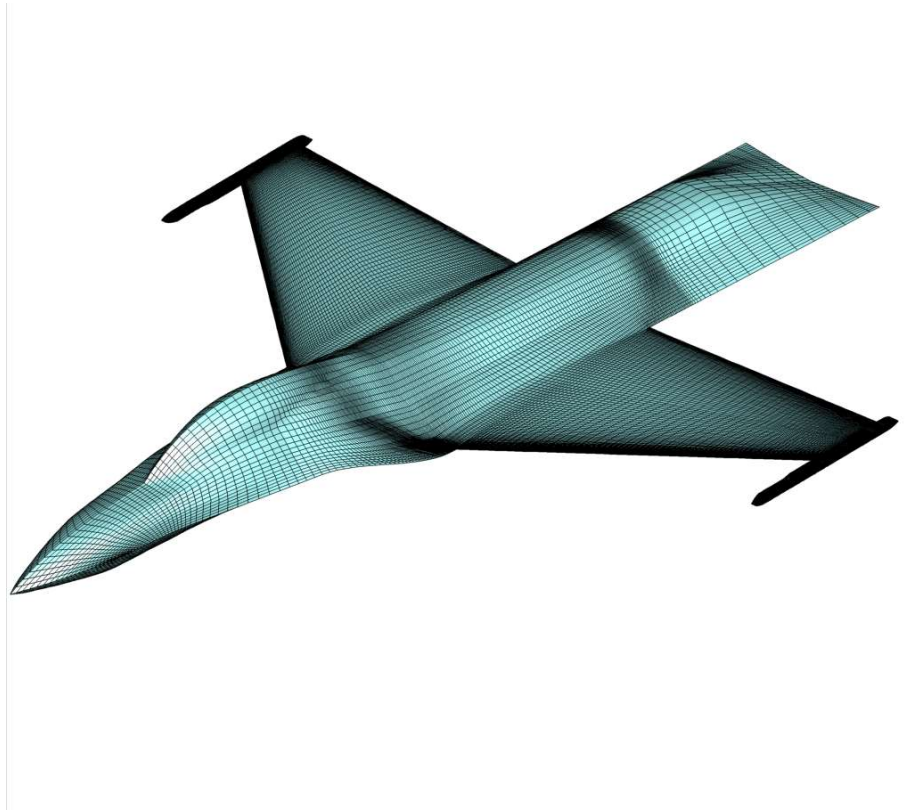


Figure 4.2 Generic fighter surface mesh [58]

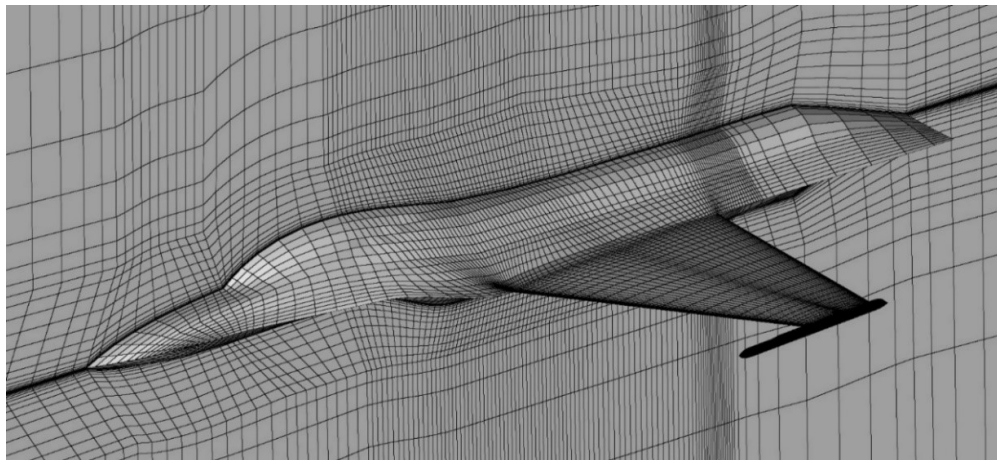


Figure 4.3 Generic fighter volume mesh

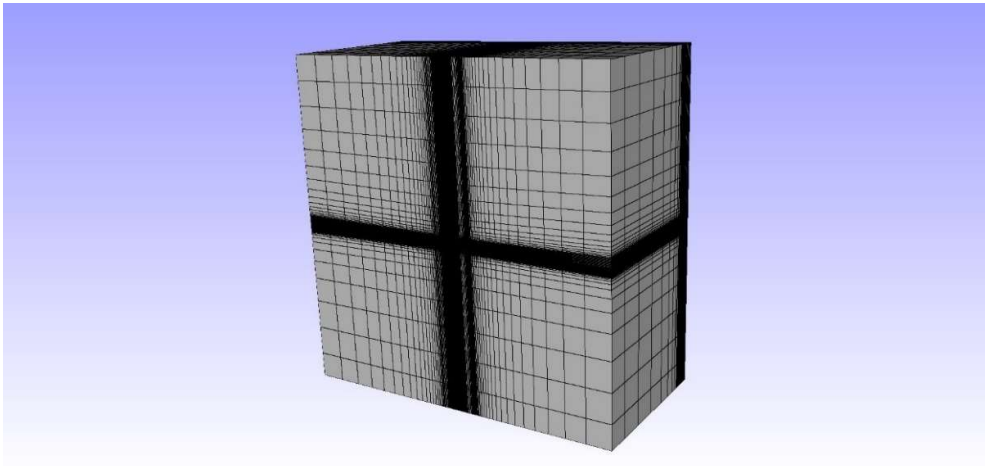


Figure 4.4 Mesh for Fluid Domain

For the generic fighter aircraft, there are multiple meshes generated. Figure 4.5 shows these meshes and compares them with the experimental results taken at Mach 0.85 with an AoA of  $2.12^\circ$ . Figure 4.5 compares different meshes generated for the generic fighter and it is evident that, among the meshes, Euler Final – Coarse Grid is in agreement with the experimental one. In this study, this mesh is utilized.

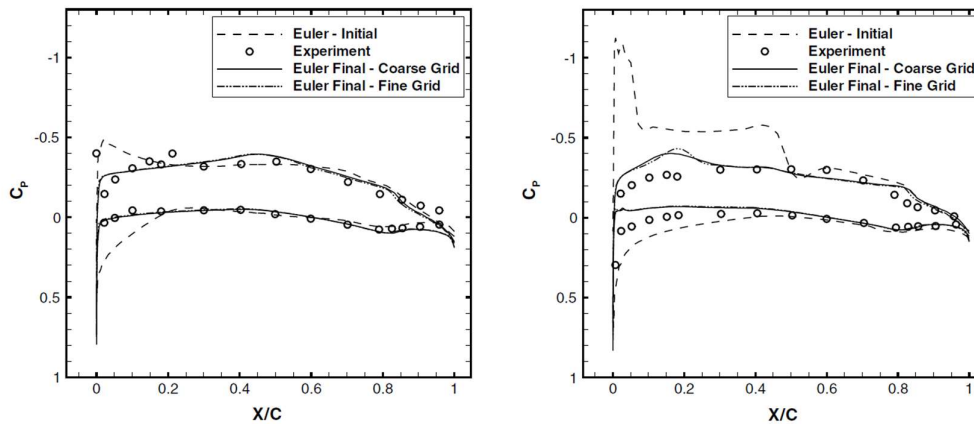


Figure 4.5 Surface pressure comparison for generic fighter  $M=0.85$ ,  $AoA=2.12^\circ$  at 59% span (left), at 85% span (right) [58]

### 4.3 Aerodynamic Model of the Generic Fighter Aircraft

#### 4.3.1 Solver Settings of Fluent

The choice of solver settings in Fluent has been based on the existing literature and guidelines for modeling large air spaces. In this thesis, one essential aspect of the setting is the governing equations used to solve the aerodynamic problem. Figure 4.6 shows the hierarchy of the governing equations. According to this figure, going up in the pyramid means increasing complexity and more accurate flow physics, which is named high-fidelity throughout the thesis, as going down in the pyramid, computational cost decreases. The figure also mentions the dates on which the governing equations are used in the industry. In the generic fighter, Euler equations are used and they are suitable for it in terms of complexity. For aeroelastic purposes of a fighter aircraft, non-linear aerodynamic phenomena are dominant. Therefore, it is essential to take these non-linearities into account during the analysis.

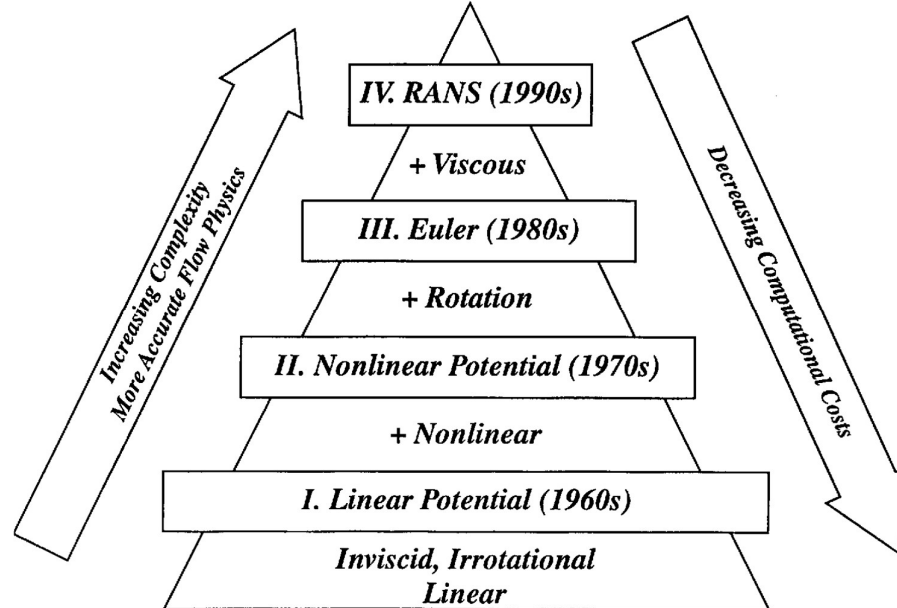


Figure 4.6 Hierarchy of governing equations [59]

After deciding the governing equations used in the problem, the following solver settings in Fluent are used in the 3D cases throughout this thesis:

- Double Precision
- Steady Condition
- Pressure Based
- Node Based Solver
- Second Order Upwind Discretization for Momentum, Turbulence and Energy Equations
- Coupled Algorithm
- Under-relaxation factors for momentum, pressure, density, body forces, energy, and temperature, are equal to 0.3, 0.3, 0.8, 0.9, 0.65, and 0.65 respectively
- Flow Courant number is 20
- Convergence criteria of  $10^{-6}$

#### **4.3.2 Analysis Results of Fluent**

In this section, aerodynamic analysis results are presented according to the Ansys Fluent settings described previously. Firstly, convergence monitoring is conducted for continuity, velocities in three directions and energy equations which are the equations used in Euler simulations. In order to be confident with the analysis, residuals are also checked. The convergence criterion is satisfied when velocity residuals are below  $10^{-3}$  [55]. Figure 4.7 shows the residuals for all of the five equations used in the Euler simulations for the increasing number of iterations. According to the convergence criteria, residuals are far below  $10^{-3}$  and for continuity equation, it becomes constant after about 500 iterations. For velocities, it becomes constant after about 750 iterations. Therefore, these results can be considered converged results.

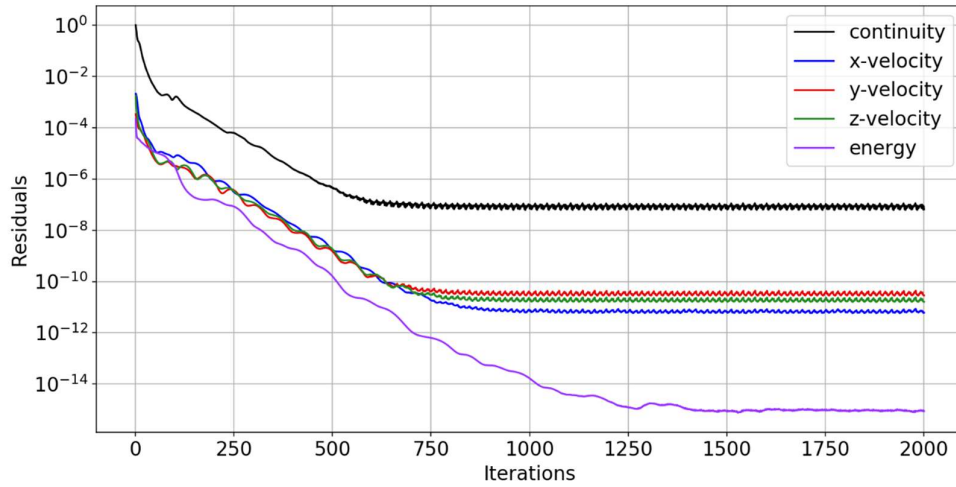


Figure 4.7 Residuals vs iteration number

After presenting the converged residuals, in order to show the analysis results are almost identical to the previously obtained results for the generic fighter, similar figures like Figure 4.5 are plotted. This time, Euler results are obtained from Fluent and experimental result data are added. Figure 4.8 and Figure 4.9 present the surface pressure distribution comparison for two different span locations. From these figures it can be observed that Fluent CFD results and experimental results are similar for 59% and 85% span. The difference in coefficient of pressure ( $C_p$ ) is less than 0.1 for both surfaces.

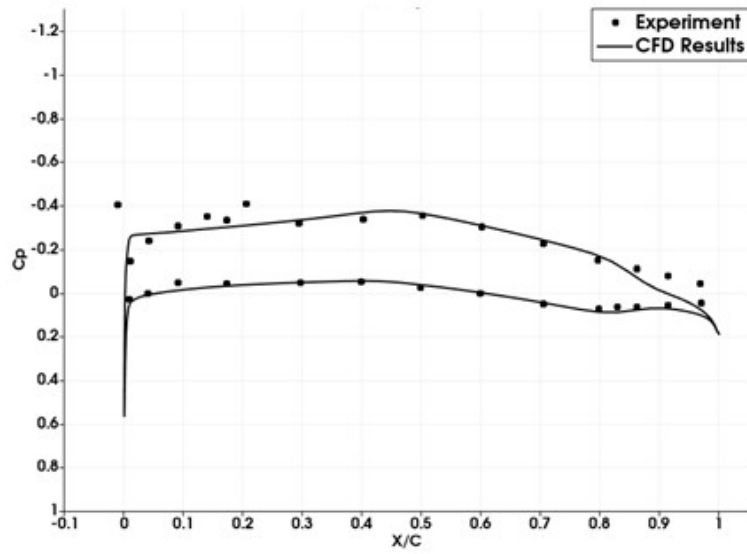


Figure 4.8 Surface pressure comparison for generic fighter  $M=0.85$ ,  $AoA=2.12^\circ$  at 59% span

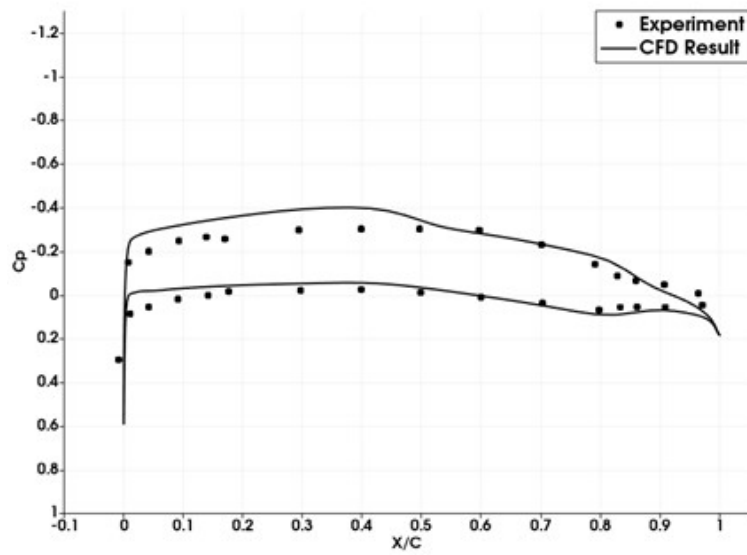


Figure 4.9 Surface pressure comparison for generic fighter  $M=0.85$ ,  $AoA=2.12^\circ$  at 85% span

This study aims to find wing loads for all of the regimes that fighter aircraft can operate. Because fighter aircraft operate at subsonic, transonic and supersonic flow regimes, analyses are conducted from 0.4 Mach to 1.8 Mach. Figure 4.11 presents the lift coefficient ( $C_L$ ) vs. AoA plot for different Mach numbers. Figure 4.11 and Figure 4.12 show the plots for the Mach value that is lower or higher than 1, respectively. In the analysis, the AoA is lower in the supersonic regime and higher in the subsonic regime and stall AoA value for subsonic regime is around  $35^\circ$  for F-16 aircraft [60]. For this reason, the AoA values are taken from 0 to 30 degrees at the subsonic regime and 0 to 16 degrees at the supersonic regime with the increment of 2 degrees.

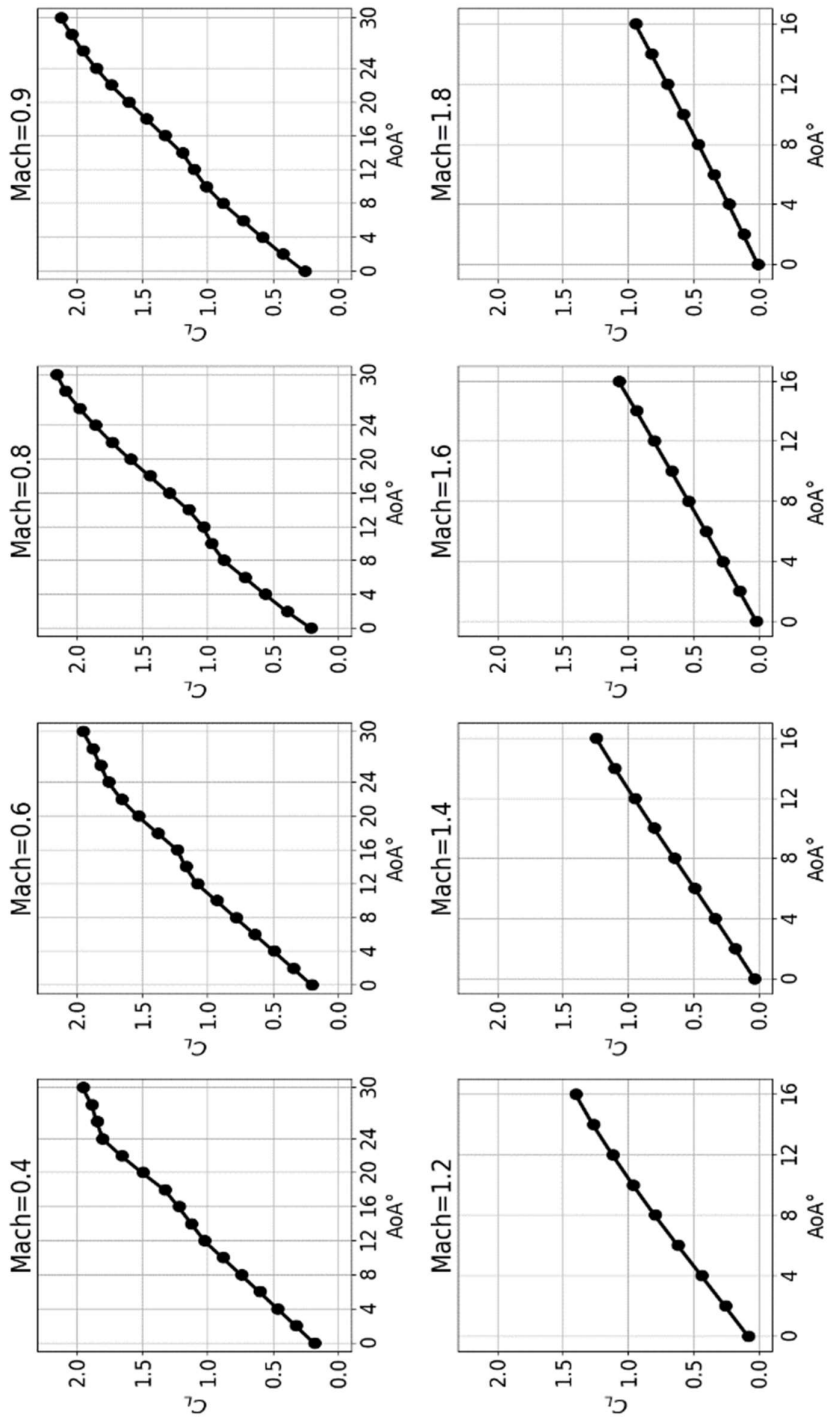


Figure 4.10  $C_L$  vs. AoA curve for different Mach numbers



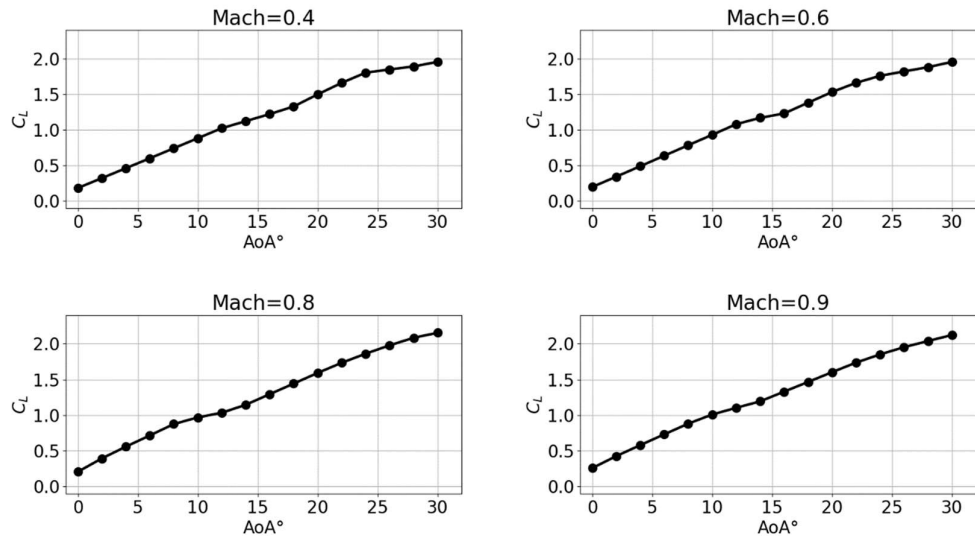


Figure 4.11  $C_L$  vs. AoA curve for Mach numbers < 1

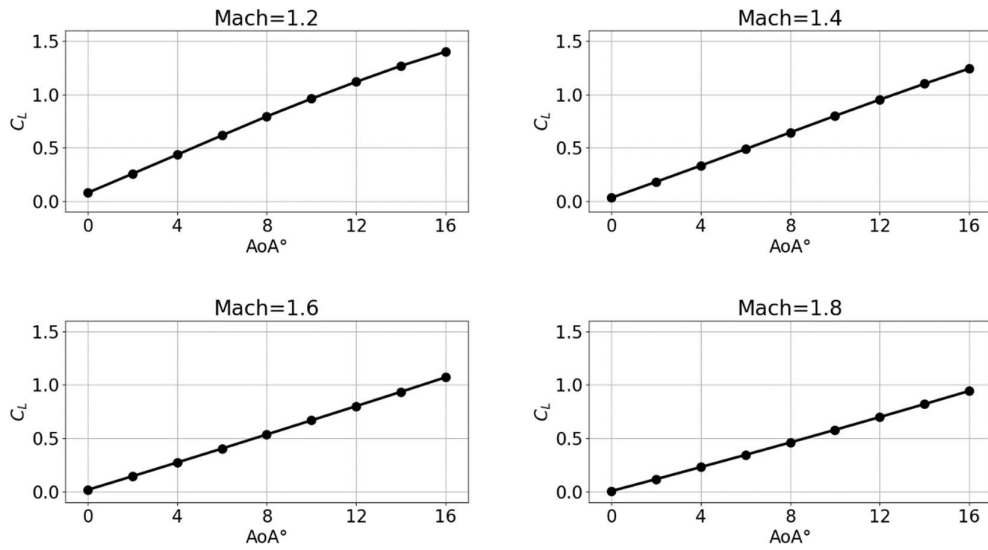


Figure 4.12  $C_L$  vs. AoA curve for Mach numbers > 1

Figure 4.11 and Figure 4.12 demonstrate that, in the supersonic regime,  $C_L$  vs. AoA curve is almost linear, on the other hand,  $C_L$  vs. AoA has a non-linear behavior for the subsonic regime. These previous plots show the total  $C_L$  values for the full configuration. Figure 4.13 demonstrates the three different sections taken at the root, middle and tip portion of the wing and Figure 4.14 presents the  $C_L$  values corresponding to each section for different Mach numbers.

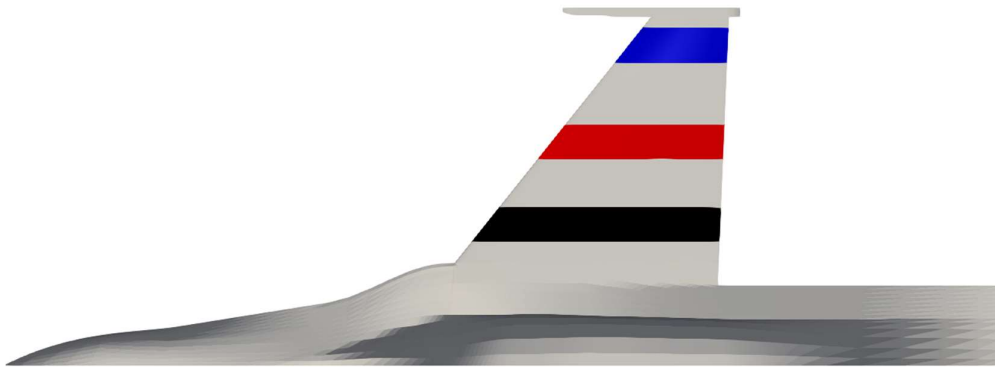


Figure 4.13 Root (black), mid (red) and tip (blue) sections on the generic fighter

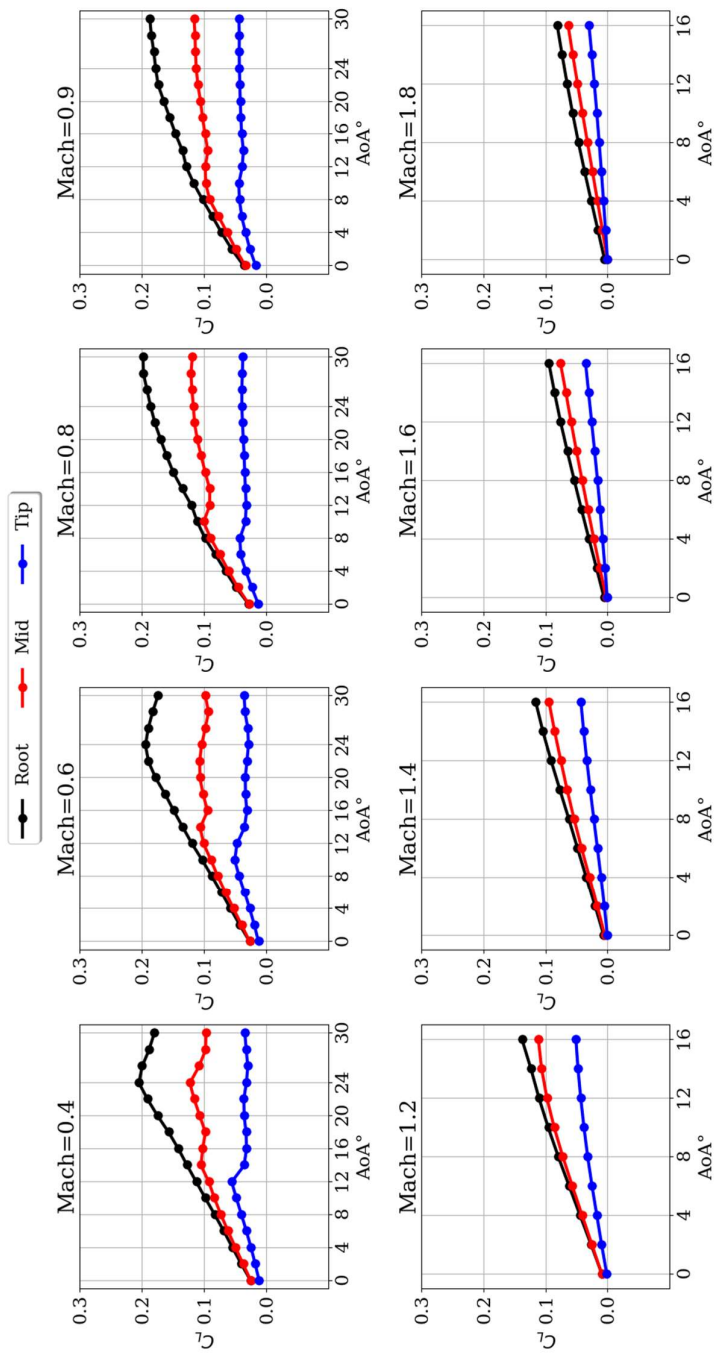


Figure 4.14  $C_L$  vs. AoA curve for different Mach numbers and three selected wing sections

Figure 4.15 to Figure 4.23 show the surface pressure distribution contours for selected Mach numbers to represent all three regimes. For this reason, 0.6, 0.9 and 1.4 Mach numbers are chosen. In these figures, left side represent lower surface and right side represents the upper surface of the generic fighter. White color corresponds to zero  $C_p$ , warm colors (red, yellow) correspond to the compression zones and cold colors (blue, purple, green) correspond to the suction regions.

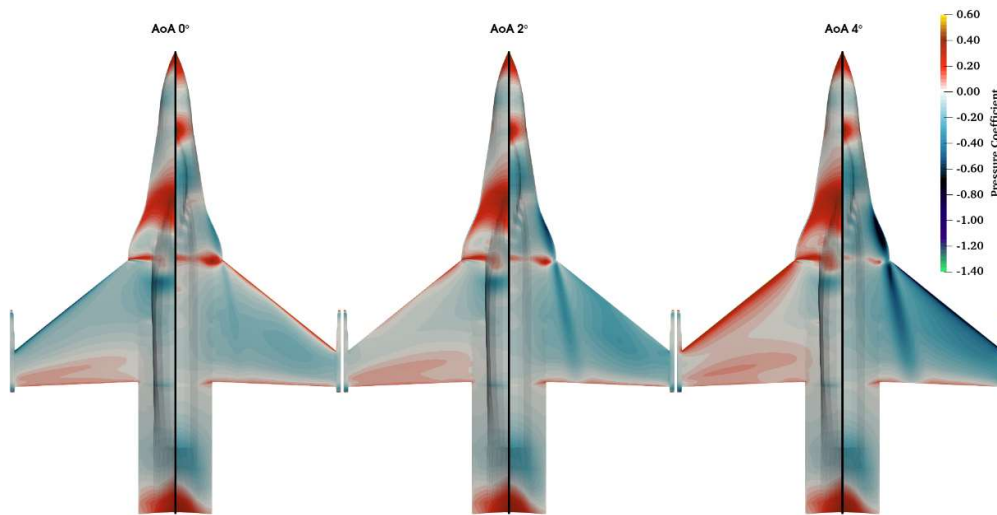


Figure 4.15 Surface  $C_p$  distributions at Mach 0.6 for  $0^\circ$ ,  $2^\circ$  and  $4^\circ$  AoA

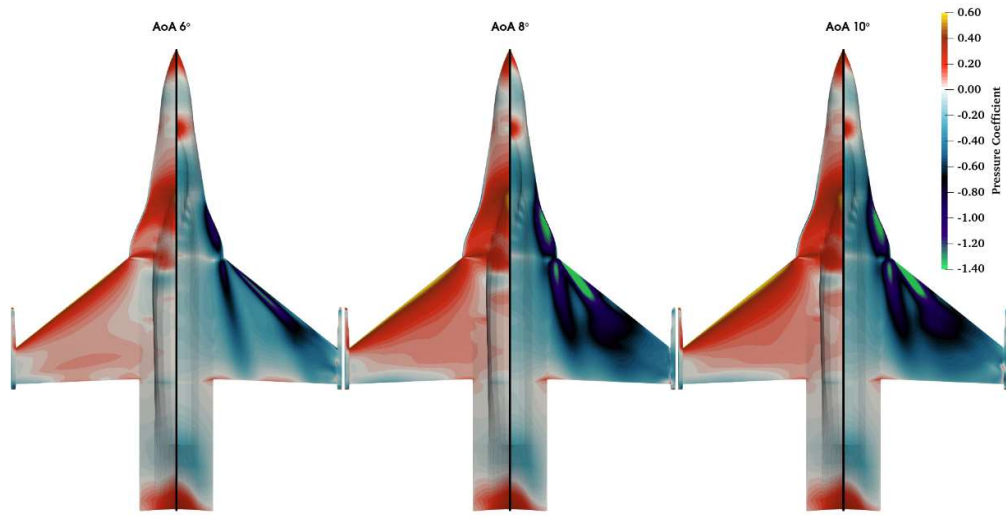


Figure 4.16 Surface  $C_p$  distributions at Mach 0.6 for 6°, 8° and 10° AoA

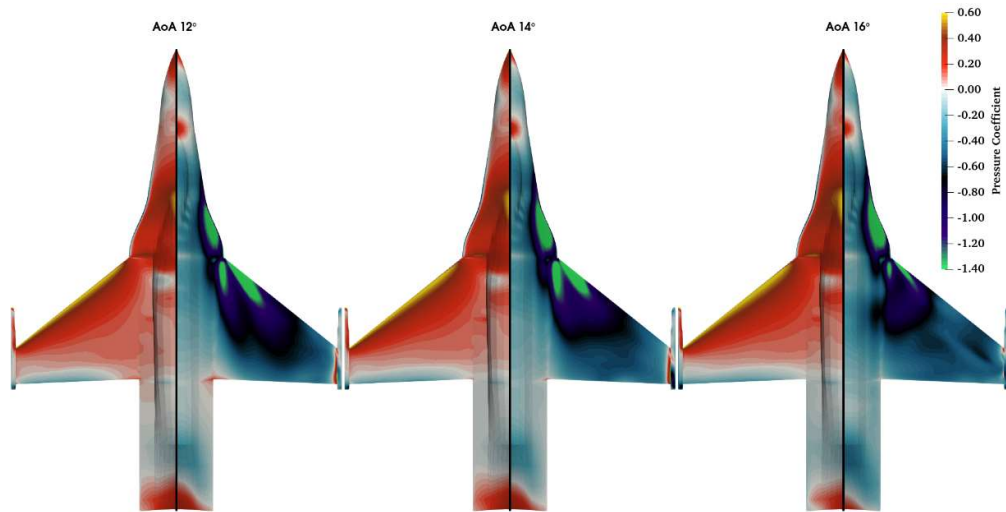


Figure 4.17 Surface  $C_p$  distributions at Mach 0.6 for 12°, 14° and 16° AoA

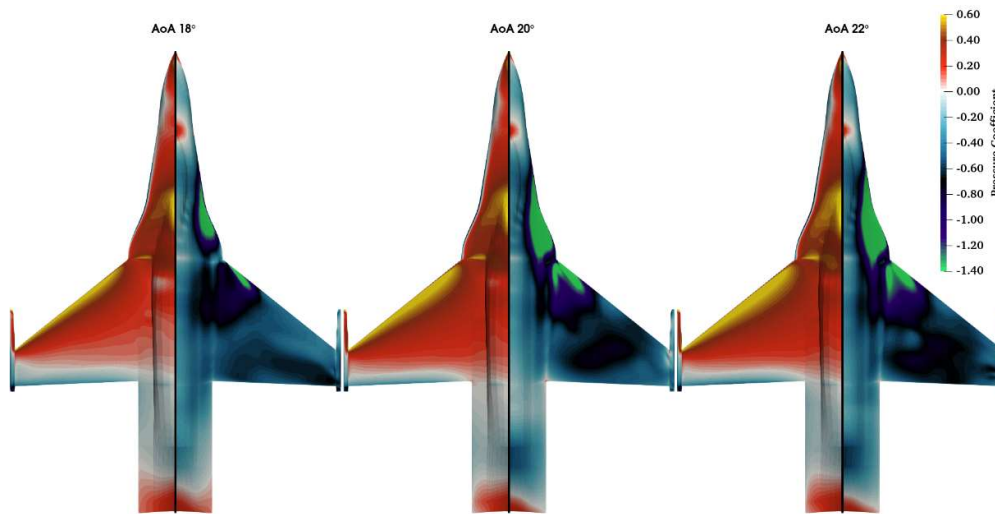


Figure 4.18 Surface  $C_p$  distributions at Mach 0.6 for 18°, 20° and 22° AoA

For Mach 0.6, the wing's leading-edge portion is under compression at 0° AoA because of a negative wing twist on both the root and tip. After 0° AoA, vortex flow becomes dominant at the subsonic region with AoA increment. Figure 4.15 and Figure 4.16 A vortex is produced from the strake region and flows towards to root portion of the wing. Also, a wing leading edge vortex is formed after 6° AoA. At higher AoA values, vortex bursts; thus, the vortex can produce more suction on the wing and lift. In addition, an interaction is observed between the strake and wing vortex after 8° AoA. It increases vortex strength, but it also causes to change vortex path of the wing and earlier vortex bursting.

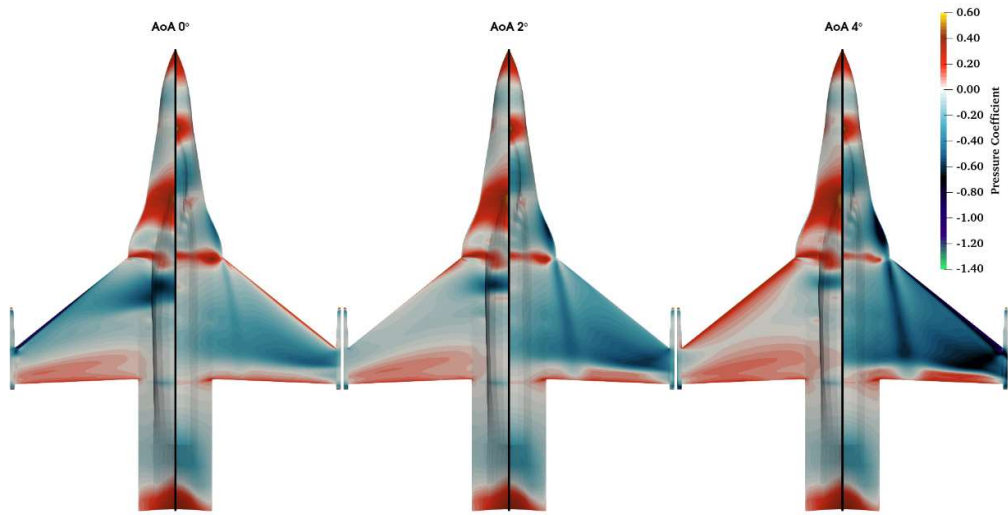


Figure 4.19 Surface  $C_p$  distributions at Mach 0.9 for 0°, 2° and 4° AoA

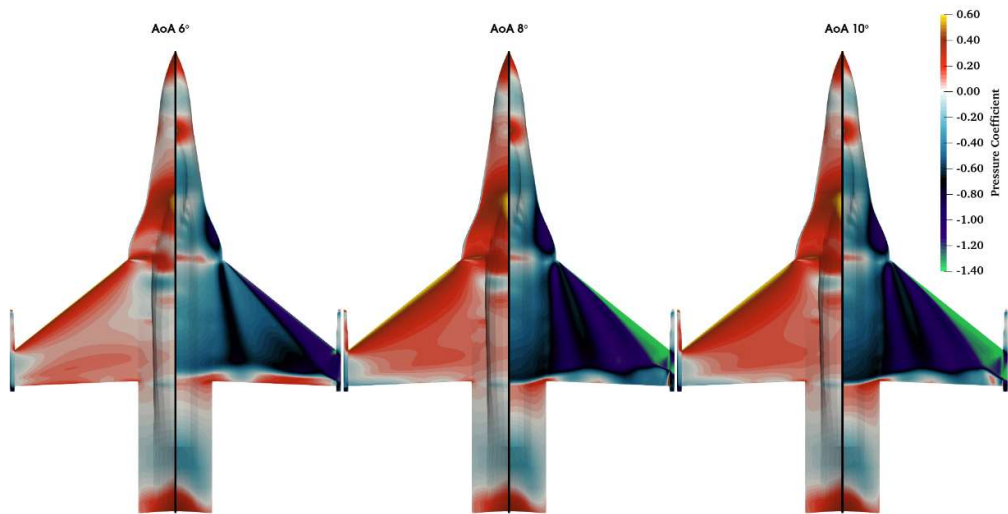


Figure 4.20 Surface  $C_p$  distributions at Mach 0.9 for 6°, 8° and 10° AoA

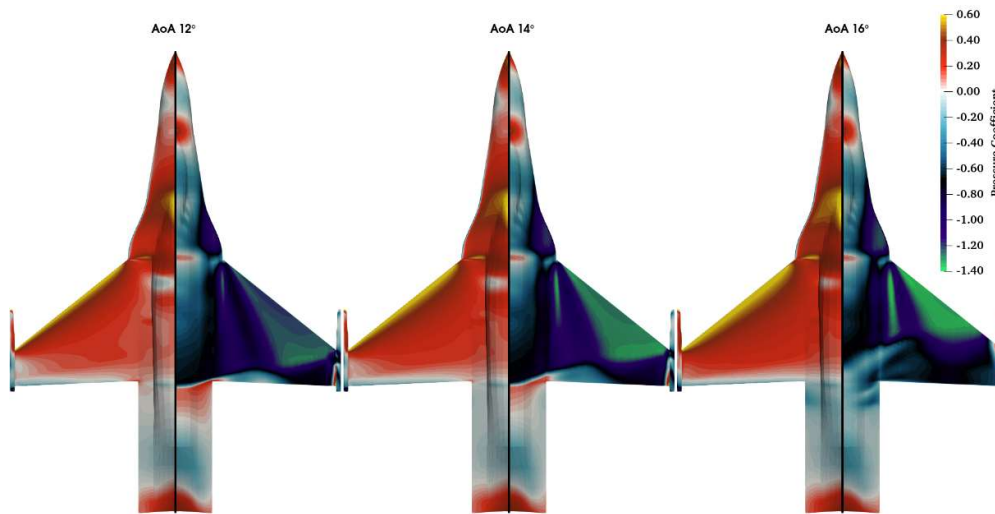


Figure 4.21 Surface  $C_p$  distributions at Mach 0.9 for 12°, 14° and 16° AoA

Pressure coefficient distribution on the surface at the transonic region is represented from Figure 4.19 to Figure 4.22. The transonic region is highly non-linear because of the shock waves. A normal shock is seen on the wing close to the wing's trailing edge at even low AoA values and the strength of shock increases with AoA increment. Also, a vortex flow occurs after 4°- 6° AoA. The supersonic flow in Mach 1.4 is given in Figure 4.22 and Figure 4.23. It has a linear behavior compared to the 0.6 and 0.9 Mach distributions. In addition, vortex flow is observed after 2° AoA, but vortex is produced with lower strength compared to subsonic and transonic due to reducing rotational flow at supersonic conditions.



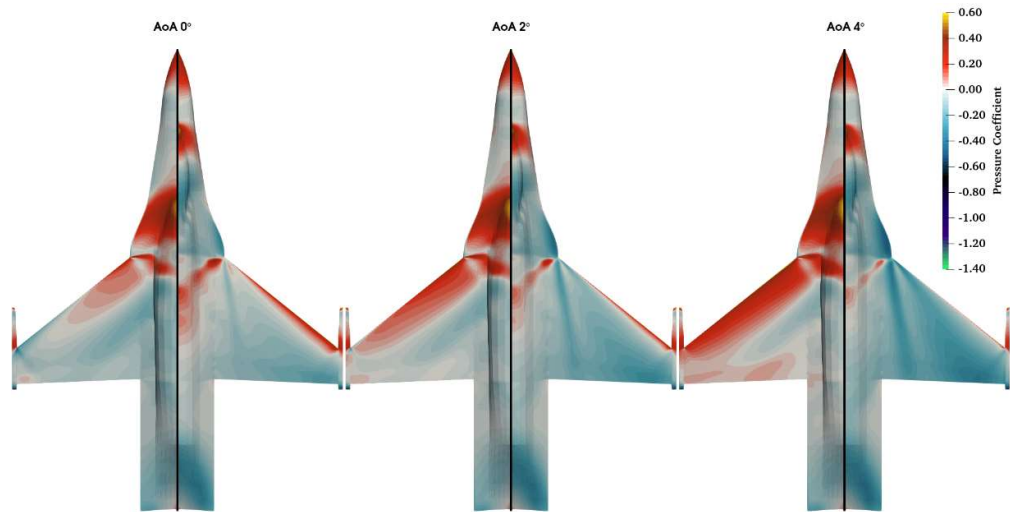


Figure 4.22 Surface  $C_p$  distributions at Mach 1.4 for  $0^\circ$ ,  $2^\circ$  and  $4^\circ$  AoA

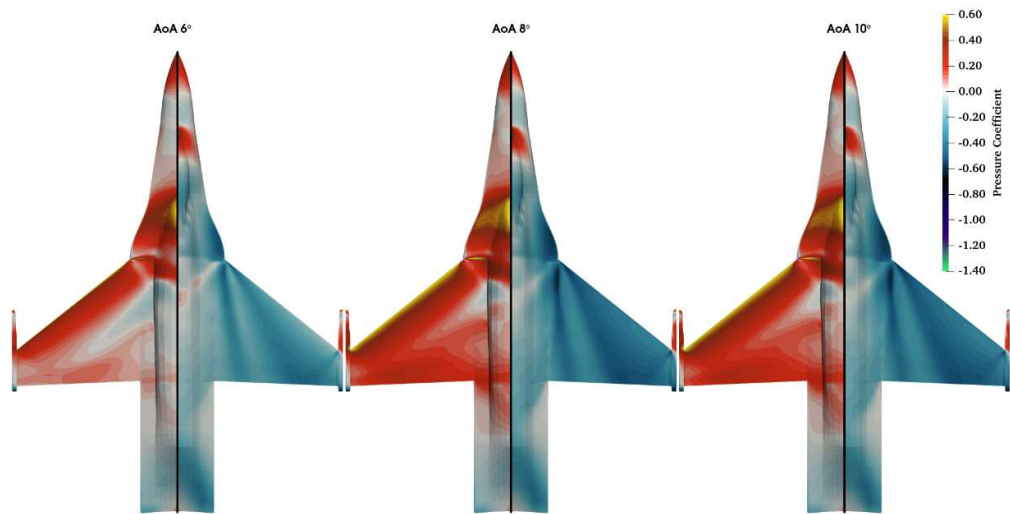


Figure 4.23 Surface  $C_p$  distributions at Mach 1.4 for  $6^\circ$ ,  $8^\circ$  and  $10^\circ$  AoA

#### 4.4 Conclusions

In this chapter, a generic fighter aircraft aerodynamic model and its analysis results are explained. The results are shown to be converged via residuals are found to be less than  $10^{-6}$  for all residuals. In addition, pressure distributions on wing sections are shown to closely agree with F-16 experimental results. In order to investigate all of the regimes that a fighter aircraft operates, aerodynamic solutions are obtained for Mach numbers from 0.4 to 1.8. In the results, the coefficient of lift is investigated and it has been seen that supersonic regimes have a linear behavior. However, subsonic and transonic regimes show a non-linear behavior for generic fighter aircraft. To investigate where the non-linearity comes from, the full aircraft's pressure distributions for all the different regimes are presented. Pressure distributions demonstrate that the non-linear aerodynamic phenomena such as shock and vortex are dominant in generic fighter aircraft and are needed to be considered in the initial design stages.

## CHAPTER 5

### STRUCTURAL MODELING OF THE GENERIC FIGHTER AIRCRAFT WING

#### 5.1 Introduction

In this chapter, the structural modeling of the generic fighter aircraft wing is elaborated. In the first section of the current chapter, the finite element model (FEM) of a generic fighter aircraft, an aeroelastic test case for academic studies is discussed in detail [58]. Later in this chapter, the basic process for creating the beam stick model (BSM) for the present case is explained. Moreover, the modal analysis of the BSM is conducted and the validation of the eigenvalue solution with the global finite element model (GFEM) is presented in this chapter.

#### 5.2 Finite Element Model of the Generic Fighter

The finite element model of the generic fighter aircraft is built in Patran structural module as proposed in [62]. The structural model comprises four components, namely; the fuselage, wing, pylon and stores. The wing and the fuselage are modeled with shell elements (CQUAD4), whereas the pylon and stores are represented as lumped masses in the current structural FEM. The wing is divided into three sections; as root, pylon and tip. Figure 5.1 shows the structural model of the generic fighter.

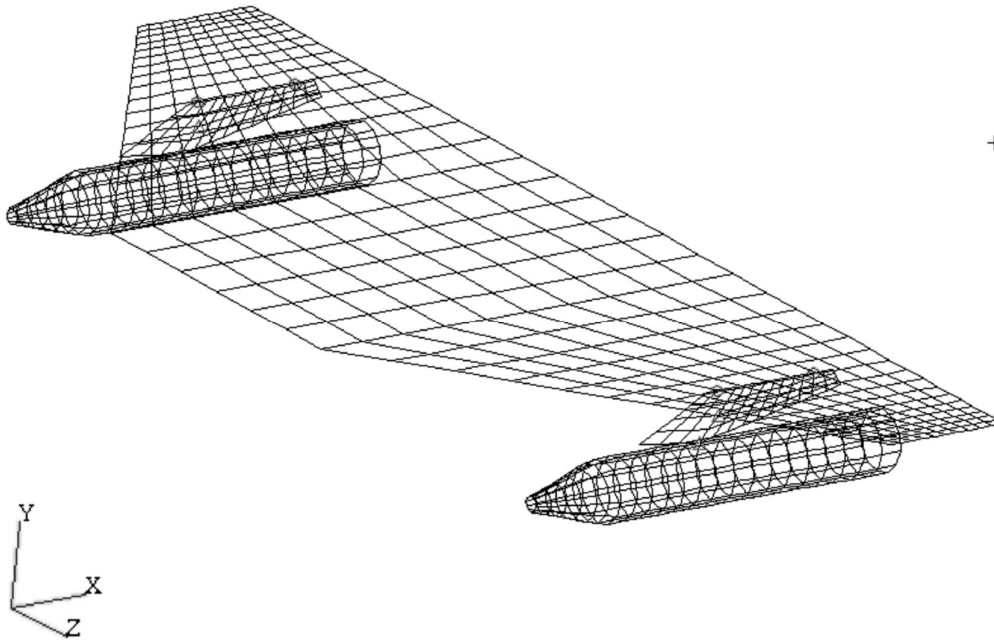


Figure 5.1 Structural finite element model for the generic fighter [58]

### 5.3 Beam Stick Model for Generic Fighter Wing

There are various structural model reduction techniques used in aerospace industries for analysis purposes and data sharing. The generation of beam stick model from GFEM is widely used for aerospace research [63].

The methodology proposed in the current study works with the beam stick structural model. The current section focuses on the generation of BSM from the subject aircraft's complete structural finite element model. The basic rules and guidelines in [63] generate a BSM from the GFEM. For the current study, only the wing section is utilized for the development of the BSM. The flow chart for the development of the BSM is shown in Figure 5.2.

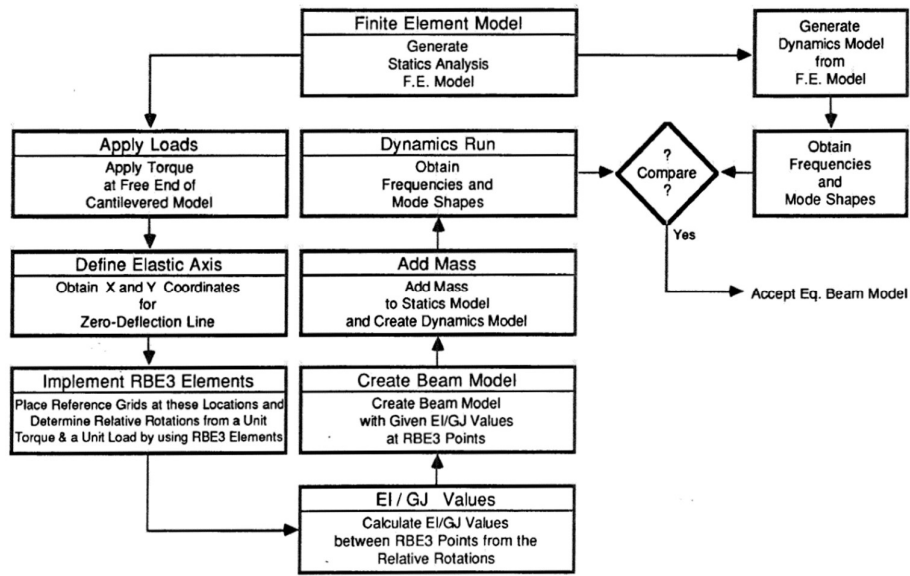


Figure 5.2 Equivalent beam reduction procedures [63]

The elastic axis of any structural component plays a critical and vital role in aeroelastic studies. The elastic axis is the points on the wing that produce almost zero or negligible twist upon applying force [63]. The initial step for generating BSM is to calculate the elastic axis of the generic fighter aircraft wing. A unit torque is applied to the wing structure and the grids with zero transverse deflections are obtained. In MSC Nastran structural module, a unit moment is applied on wing sections and the deflections are plotted. The interpolation element RBE3 is used to obtain the slope and twist at spanwise sections on the elastic axis. Figure 5.3 and Figure 5.4 show the elastic axis of the wing. The red and black QUAD elements show the deflected shape of the structure, whereas the red diamond shape grids represent the line with zero deflections. These highlighted grids form the elastic axis of the wing structure and these grids are ultimately used for the generation of BSM.

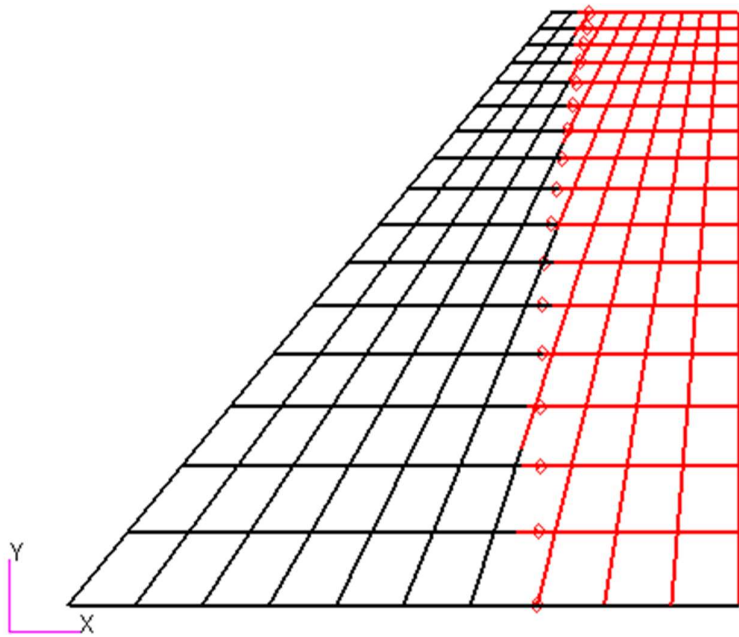


Figure 5.3 Top view for undeflected wing (red) and deflected wing (black) with BSM nodes

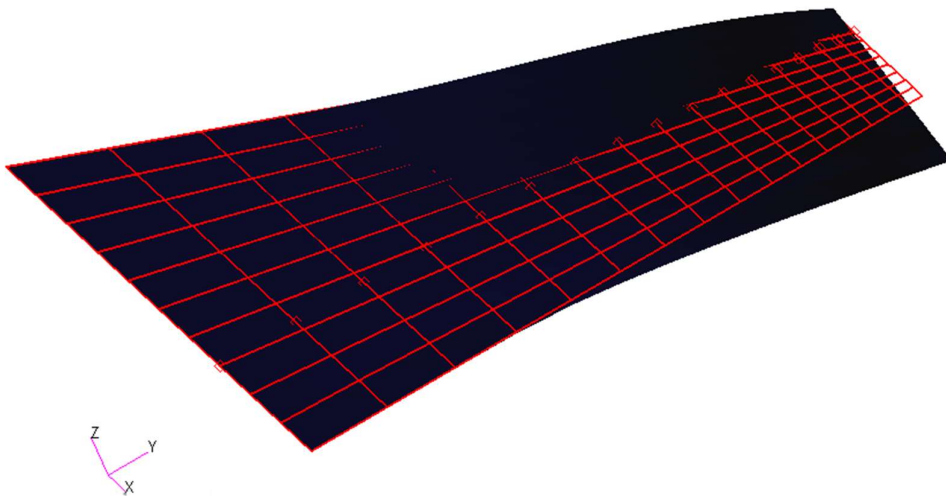


Figure 5.4 Isometric view for undeflected wing (red) and deflected wing (black) with BSM nodes

The next step is to select the number of nodes to develop a BSM that should represent the aircraft's actual wing structure. In the FEM, there are 17 nodes along the span and to represent each node of the FEM, 17 BSM nodes are placed. Because this structural model is used in the aero-structural coupling, it should be able to represent the lift distribution along the span correctly. Therefore, lift along the wing span is used as a criterion to finalize the grid points for BSM. In Figure 5.5, lift distribution along the span for three different number of structural nodes are examined. It is evident from the figure that the lift calculated with 17 grid points seems more reasonable and closer to the actual lift, i.e., with 100 nodes. From the current lift analysis, it is concluded that 17 nodes shall be used to generate the beam stick model.

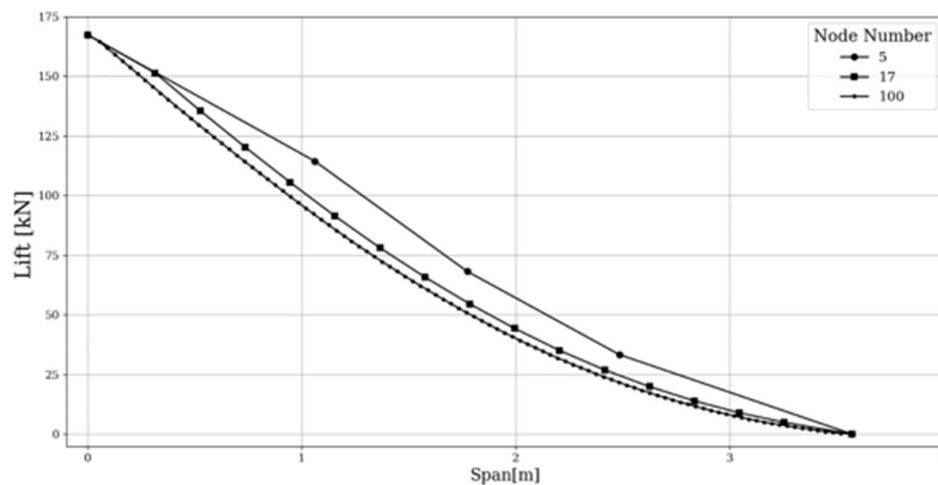


Figure 5.5 Lift distribution along the span for different numbers of beam stick nodes

Once the number of grid points is finalized for the generation of BSM, the next step is to calculate the equivalent structural beam stiffness. Namely, the flexural rigidity (EI) and torsional rigidity (GJ). Once the elastic axis is defined, with MSC Nastran analysis, the slopes and deflections of BSM nodes are obtained. For finding the EI, a transverse force  $P$  is applied at the tip and for a beam segment between points A and B formula is given as

$$EI_{AB} = \frac{1}{\Delta\beta} \int_A^B M ds \quad (5.1)$$

where  $M$  is the bending moment and  $\Delta\beta$  is the slope difference between points A and B. For a beam segment length integral is taken and the  $ds$  value is the arc length given as

$$ds = \sqrt{dx^2 + dy^2} \quad (5.2)$$

Similarly, for finding the torsional rigidity formula is given as

$$GJ_{AB} = \frac{1}{\Delta\phi} \int_A^B T ds \quad (5.3)$$

where  $T$  is the torque and  $\Delta\phi$  is the twist difference between points A and B. According to these formula, flexural and torsional rigidity values for each node along the span are obtained and shown in Figure 5.6.

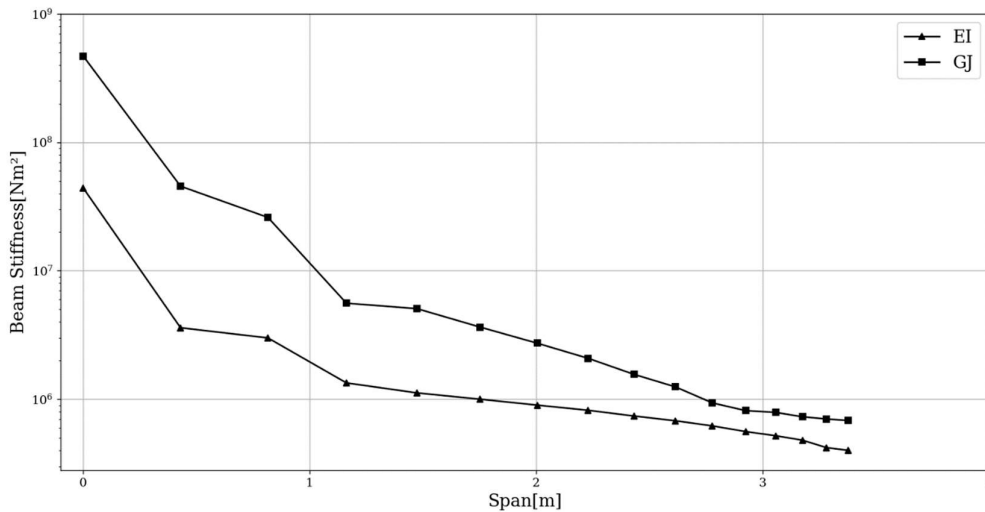


Figure 5.6 Flexural and torsional rigidity of BSM

After obtaining the bending and torsional stiffness from the structure, material properties are tuned to find similar modal characteristics with the FEM [70]. The finalized beam stick nodes on the FEM are shown in Figure 5.7.



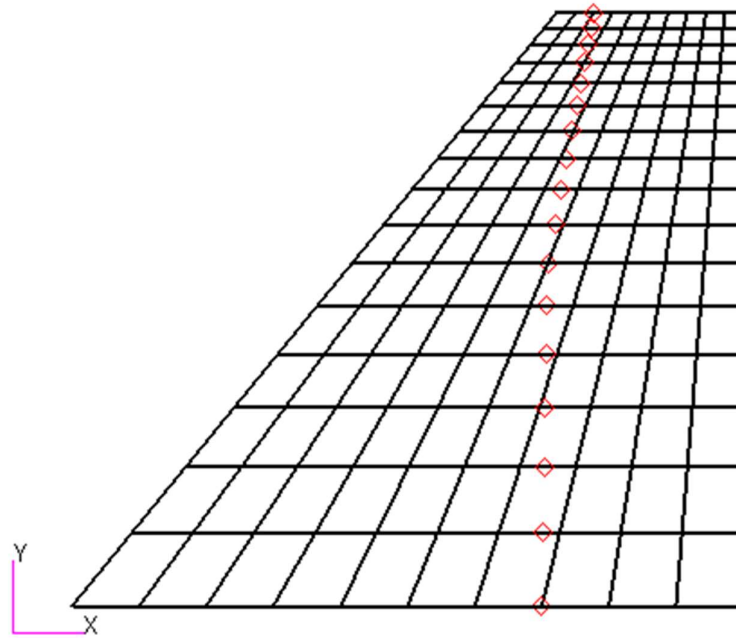


Figure 5.7 Beam stick nodes on the FEM

In order to represent the BSM similar to the 2-D FEM at the trailing and the leading edge of the wing but at the same y coordinate locations, RBE2 elements are placed. RBE2 elements are rigid body elements to add infinite stiffness to the placed points. Figure 5.8 shows the BSM nodes and RBE2 elements. With RBE2 elements placed, the BSM model is finalized and can be compared with the finite element analysis (FEA) results of 2-D FEM in terms of modal characteristics.

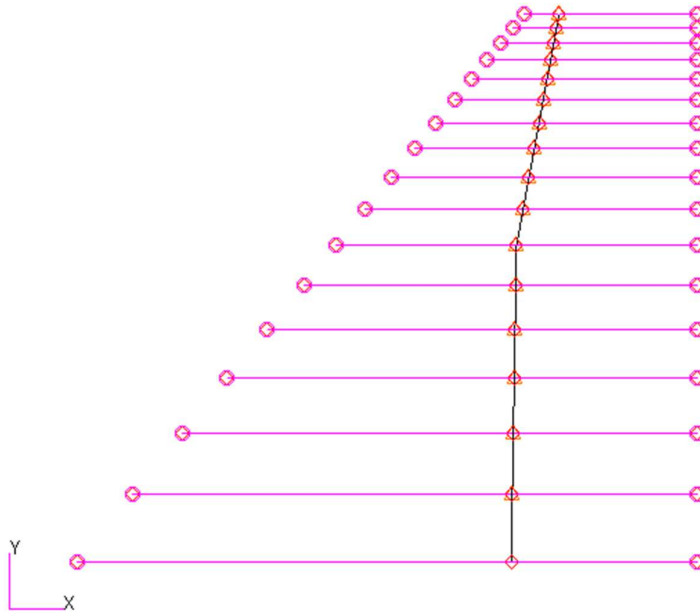


Figure 5.8 BSM nodes and RBE2 elements and leading and trailing edge of the wing

#### 5.4 Validation of the Generated Beam Stick Model

The proposed methodology in current research uses a stiffness matrix, eigenvalues and corresponding eigenvectors of the BSM. In order to efficiently use these matrices, validation of BSM is essential to be carried out. For validation purposes, a modal analysis of the BSM is conducted and the results of which are compared with that of the actual FEM. Nastran Sol 103 is used for the modal analysis. Table 5.1 shows the natural frequencies for the analysis of 2-D FEM and the BSM. Natural frequency values of BSM and FEA of the 2-D FEM show that the eigenvalue solution is in good correlation with each other. Mode shapes are shown in Figure 5.9 where red color shows the undeflected shape and the black color shows the deflected shape of the wing. Mode shapes examined for FEM and BSM are in close agreement and it can be concluded that the developed BSM can be used for the subsequent analysis.

Table 5.1 Natural frequencies of the FEA of the 2-D FEM and BSM

Modes	FEM (Hz)	BSM (Hz)
The First Bending	4.89	4.84
The First Torsion	15.82	15.41
The Second Bending	22.95	22.29

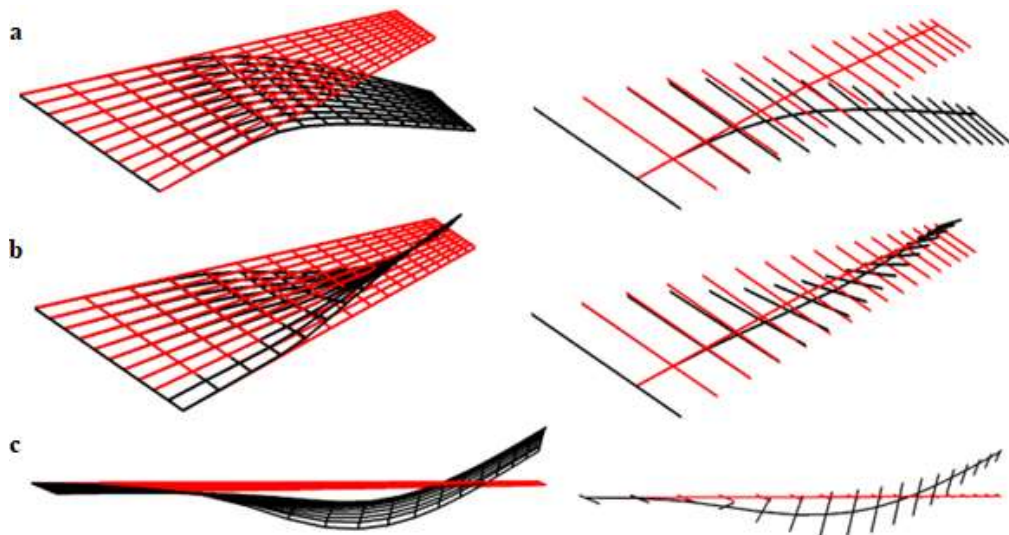


Figure 5.9 (a) The First Bending mode (b) The first torsion mode (c) The Second bending mode for FEM (left) and BSM (right)

## **5.5 Conclusions**

In this chapter, the generation of the beam stick model from the FEM of generic fighter aircraft is discussed in detail. FEM of the generic aircraft contains all the important structural components. However, only the wing structure is utilized for the current research work. The FEM of the wing structure has been reduced to the elastic axis in order to generate the BSM. Techniques for calculating the elastic axis, equivalent bending and torsional stiffness are discussed in detail. Based on the calculated stiffness and elastic axis, the beam stick model is generated and later on, the validation study of the developed beam stick model is presented. The validation study concludes that the BSM's eigenvalue solution agrees with the FEM and can be used for the proposed research methodology.

## CHAPTER 6

### AERODYNAMIC DATABASE GENERATION FOR GENERIC FIGHTER VIA SURROGATE MODELS

#### 6.1 Introduction

In engineering, a surrogate model is also referred to as a response surface or metamodel, it reflects the idea that it is a model of an underlying model. One of the most common use of surrogate models is to replace a known expensive computational model when a large number of repeated evaluations are needed, such as for optimization or uncertainty quantification. Another common application is when it is needed to obtain a continuous function from a fixed set of data, such as when the data is obtained from physical or computational experiments or from legacy code.

For surrogate models, there are two concepts, namely; the construction and evaluation of the model. In this thesis, the evaluation of the model is referred to as “prediction” and construction of the model is referred as “training”. Given  $n_x$  inputs and  $n_w$  parameters, the prediction is the evaluation of

$$y = f(x, w) \quad (6.1)$$

where  $x \in \mathbb{R}^{n_x}$  is an input vector and  $y \in \mathbb{R}$  is the output variable and  $w \in \mathbb{R}^{n_w}$  is the vector of model parameters. The objective of the training is to compute model parameters  $w$  that satisfy

$$\bar{y} \approx f(\bar{x}_i, w), 1 \leq i \leq n_t \quad (6.2)$$

where  $(\bar{x}_1, \bar{y}_1), \dots, (\bar{x}_{n_t}, \bar{y}_{n_t})$  are the  $n_t$  training points.

Surrogate modeling approaches can be divided into two main classes. It is named as interpolation if the surrogate model matches with the true function at every point given and it is named as regression when it does not match. Regression approaches used in this study includes linear regression, polynomial regression and artificial neural networks (ANN). Interpolation approaches, on the other hand, are inverse distance weights, radial basis functions, kriging and regularized minimal energy tensor-product splines [24].

This study uses surrogate models to obtain a continuous function from a fixed dataset obtained from expensive CFD simulations. With this continuous function, surrogate models create an aerodynamic database that can get the aerodynamic loads at any given input parameter space in which that surrogate model is created.

## **6.2 Aerodynamic Database Generation Methodology for Generic Fighter**

The proposed methodology is an approach to predict the load distribution along the wing span. The given method requires each section's local angle of attack (AoA) values and Mach numbers. In each iteration of the aero-structural coupling, the local AoA values change, i.e. the local AoA values cannot be determined beforehand. Therefore, there is a need for a continuous function in terms of AoA and Mach values all over the flight envelope of a generic fighter.

A conventional aircraft load envelope may require about 100000 of simulations and an unconventional plane can require up to 10 million [3]. CFD solutions with Euler equations for generic fighter aircraft take approximately 15 minutes with a 4.10 GHz processor with four cores. Figure 6.1 illustrates the computational time needed for a number of simulations with 15 minutes of simulation time. Figure 6.1 shows that for a hundred thousand simulations, it takes about a thousand days which is also approximately three years. Therefore, generating the required aerodynamic data with CFD alone is physically impossible. The computational time can be reduced with the

high-performance computing (HPC) abilities, however, with HPC the order for computational time for one simulation is in minutes and it cannot provide the required aerodynamic data in reasonable time periods.

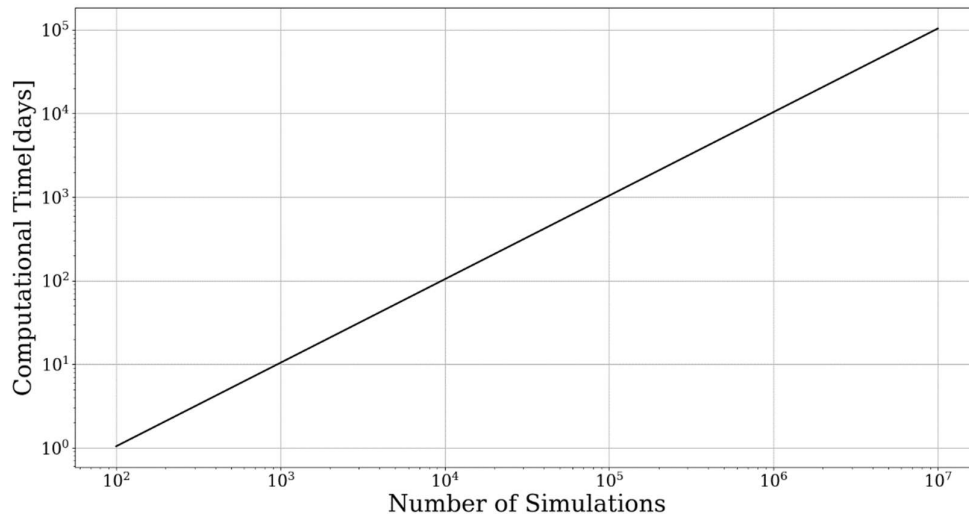


Figure 6.1 Computational time – number of simulations for CFD simulations in this study

Due to the computational limitations of the CFD, surrogate models are used to create a database. In this study, surrogate models are used as data-fit models requiring a fixed dataset to be created. Fixed datasets are created with CFD and surrogate models are trained in these points and all of the other points are called “test” points, where surrogate models are making their predictions and these points are unknown to the surrogate models. Surrogate models are making their predictions much quicker compared to the CFD analysis. Therefore, aerodynamic databases required for a load envelope can be generated within a reasonable amount of time. The aerodynamic database needs a fixed number of CFD solutions and test points are predicted with surrogate models. Mach and AoA values that CFD solutions are taken have already been mentioned in the aerodynamics chapter. Figure 6.2 illustrates the aerodynamic database generated for generic fighter. This database is a representative database aiming to cover flight regimes that F-16 like aircraft operate. It starts from 0.4 Mach

and goes up to 1.8 and the AoA values are higher at the subsonic regime than the supersonic one [60]. The aerodynamic database can be generated with the design of experiment types such as Latin hypercube sampling, optimal space-filling, box-Behnken and uniform sampling. This study generates the aerodynamic database uniformly at subsonic and supersonic regimes.

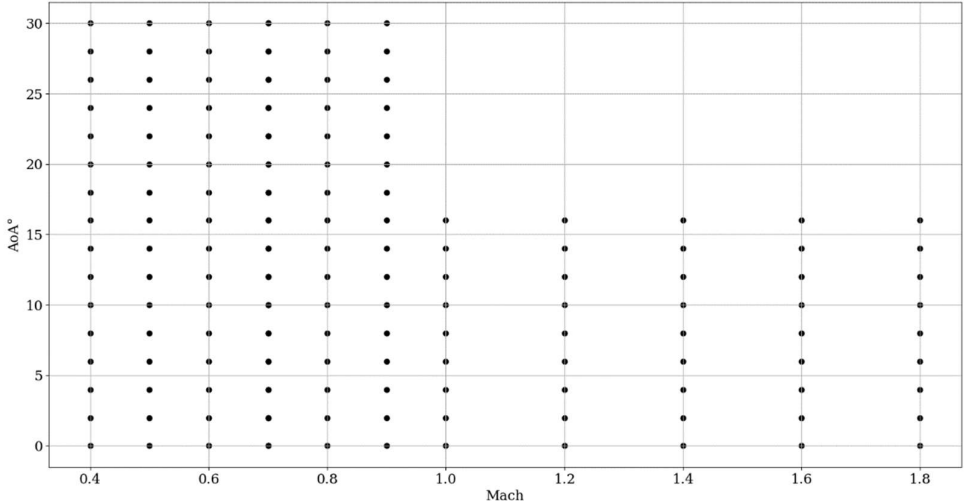


Figure 6.2 Aerodynamic database generated for generic fighter

In order for surrogate models to work, they require an initial training dataset and test dataset. For that purpose, some points should be selected as training datasets where the surrogate models are trained. Figure 6.3 shows the initial training and test points. Training points are located at the maximum and minimum AoA values for each Mach number. These points are selected to prevent surrogate models from extrapolating the data and only interpolate the data because it is known that the prediction accuracy of this type of data-based model is reduced with extrapolation [25]. Randomly selected initial training points and their accuracy results are given in Appendix A.



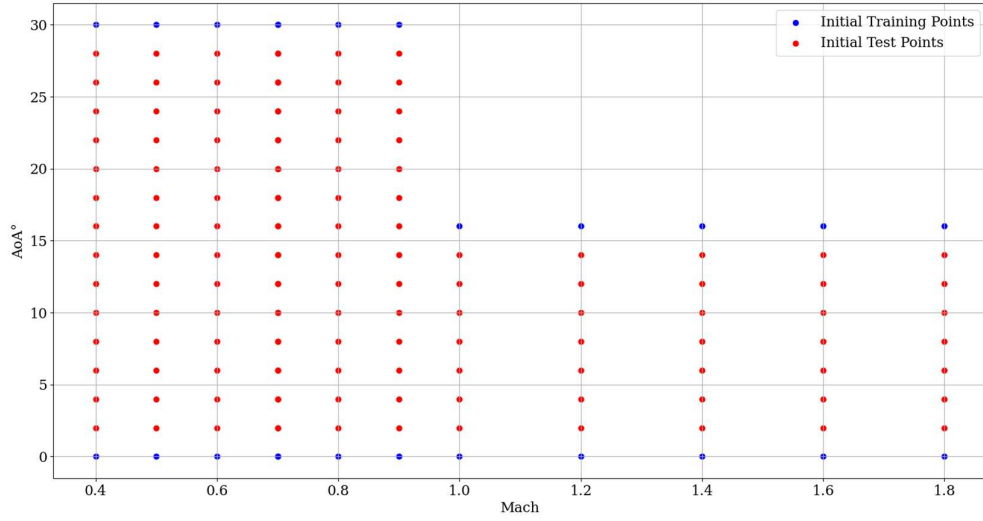


Figure 6.3 Initial training and test points for aerodynamic database

In this database, surrogate models try to predict forces and moments of beam stick model (BSM) nodes explained in structural modeling of the generic fighter aircraft wing. Figure 6.4 demonstrates the cut planes on the generic fighter wing.

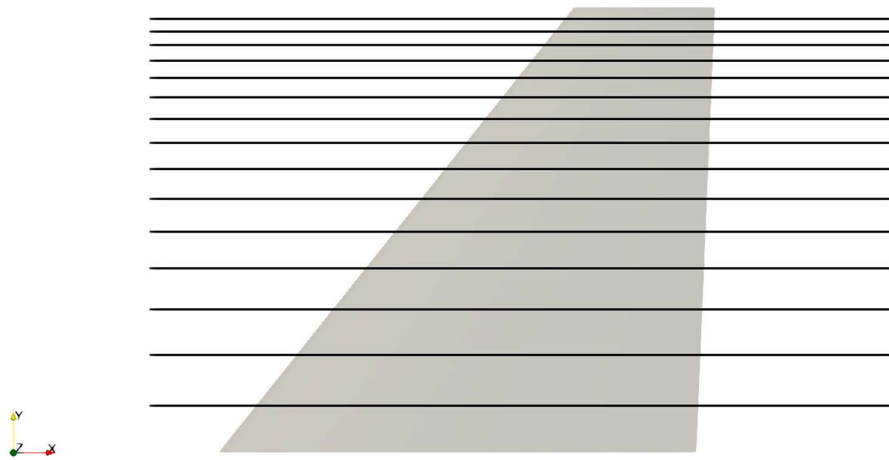


Figure 6.4 Cut planes on the generic fighter wing

For 17 sections of the generic fighter wing, forces and moments are calculated with a post processing tool Paraview [56] by integrating the pressure distributions of the CFD solutions. As Euler CFD solution takes 15 minutes with the specified computing abilities and a surrogate model prediction takes seconds when creating a database, the most critical parameter is acquiring the fewest number of CFD solutions and predicting the test points with surrogate models. According to this criterion, Figure 6.5 presents a flowchart for creating a database with surrogate models.

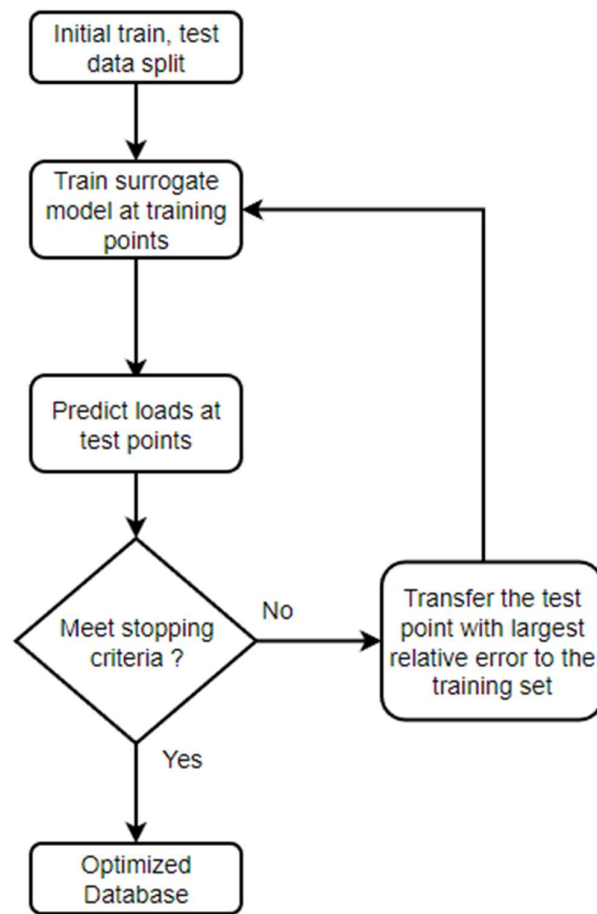


Figure 6.5 Flowchart for optimized database generation

In this flowchart, the first step starts with the initial database mentioned. Surrogate models are trained with the initial training dataset. Afterwards, surrogate models predict all of the test points. After predictions are made, the level of accuracy should be evaluated. In the literature, there are many types of accuracy measurement for surrogate models. Some of the famous ones are mean squared error (MSE), coefficient of determination ( $R^2$ ), root mean square error (RMSE) and relative maximum absolute error (RMAE). For this study, relative maximum absolute error is used. This accuracy measurement type is selected to ensure that there is a threshold value that the relative difference is always smaller than it. The equation for the relative maximum absolute error percentage is given as;

$$RMAE \% = \max_{i=1:N} \left( \left| \frac{y_i - \hat{y}_i}{y_i} \right| \right) * 100 \quad (6.3)$$

where  $N$  is the number of points,  $y_i$  is the predicted value and the  $\hat{y}_i$  is the true value of the function at that point. This formula calculates relative error percentages at each prediction point and determines the maximum value.

The algorithm developed requires a stopping criterion and the criterion is selected as a threshold value which is taken as one percent. Hence, until the surrogate model prediction error is less than one percent for all points, the algorithm continues to iterate. It transfers the test point where the maximum error occurs to the training set through the iterations. This algorithm is implemented in [68]. After the stopping criterion is reached, the optimized database is obtained.

### **6.2.1 Aerodynamic Database Generation with Surrogate Modeling Toolbox**

The surrogate modeling toolbox (SMT) is an open-source Python package that contains a collection of surrogate modeling methods, benchmark problems and sampling methods. This package provides a library of surrogate models that is simple

to use and therefore it is also suitable for this research problem. Figure 6.6 shows the architecture of the SMT.

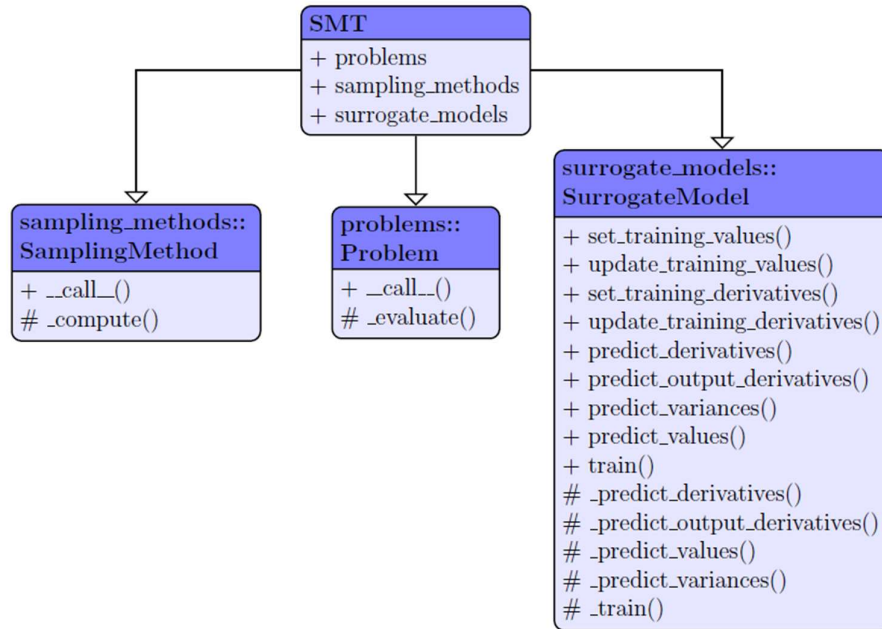


Figure 6.6 SMT Architecture [57]

In the SMT, all surrogate-modeling methods that explained previously except the ANNs are present. Therefore, ANNs will be examined by different tools. Figure 6.7 illustrates all surrogate modeling methods included in the SMT with their advantages and disadvantages.

Method	Advantages (+) and disadvantages (-)
Kriging	<ul style="list-style-type: none"> <li>+ Prediction variance, flexible</li> <li>- Costly if number of inputs or training points is large</li> <li>- Numerical issues when points are too close to each other</li> </ul>
KPLS	<ul style="list-style-type: none"> <li>+ Prediction variance, fast construction</li> <li>+ Suitable for high-dimensional problems</li> <li>- Numerical issues when points are too close to each other</li> </ul>
KPLSK	<ul style="list-style-type: none"> <li>+ Prediction variance, fast construction</li> <li>+ Suitable for high-dimensional problems</li> <li>- Numerical issues when points are too close to each other</li> </ul>
GE-KPLS	<ul style="list-style-type: none"> <li>+ Prediction variance, fast construction</li> <li>+ Suitable for high-dimensional problems</li> <li>+ Control of the correlation matrix size</li> <li>- Numerical issues when points are too close to each other</li> <li>- Choice of step parameter is not intuitive</li> </ul>
RMTS	<ul style="list-style-type: none"> <li>+ Fast prediction</li> <li>+ Training scales well up to <math>10^5</math> training points</li> <li>+ No issues with points that are too close to each other</li> <li>- Poor scaling with number of inputs above 4</li> <li>- Slow training overall</li> </ul>
RBF	<ul style="list-style-type: none"> <li>+ Simple, only a single tuning parameter</li> <li>+ Fast training for small number of training points</li> <li>- Susceptible to oscillations</li> <li>- Numerical issues when points are too close to each other</li> </ul>
IDW	<ul style="list-style-type: none"> <li>+ Simple, no training required</li> <li>- Derivatives are zero at training points</li> <li>- Poor overall accuracy</li> </ul>
LS	<ul style="list-style-type: none"> <li>+ Simple, fast construction</li> <li>- Accurate only for linear problems</li> </ul>
QP	<ul style="list-style-type: none"> <li>+ Simple, fast construction</li> <li>- Large number of points required for large number of inputs</li> </ul>

Figure 6.7 Advantages and disadvantages of surrogate modeling methods in SMT [57]

In this study, kriging (KRG), Regularized minimal energy tensor-product splines (RMTS), radial basis functions (RBF), inverse distance weighting (IDW), least squares (LS) and quadratic polynomials (QP) are investigated. Because, in this study, the number of training points and input dimensions are not high, Kriging partial least squares (KPLS) and their derivatives (KPLSK, GE-KPLS) that are suitable for high-dimensional problems are not investigated.

LS method is also known as the linear regression model and it fits a linear line, QP, on the other hand, uses a second order polynomial function. IDW calculates unknown points with a weighted average of training points and RBF uses interpolation functions as a linear combination of basis functions dependent on the distance of test points to training points. KRG is a generalization of RBF which interprets the interpolation function as a stochastic process. The function value of each training point is treated as a random variable that is correlated to the other training points. RMTS uses basis functions to calculate unknown test points and is developed for high number of training points where the computational time of KRG is relatively slow [24]. Figure 6.8 shows the elapsed time for each surrogate modeling method and the maximum relative error percentage for changing the number of the training dataset. The number of training points is increasing according to the flowchart for creating the aerodynamic database. According to the methodology for aerodynamic database creation, Table 6.1 is obtained and it presents the number of points used to create a database for each surrogate modeling method.

The surrogate modeling methods use a full database and do not take flow regimes into account. To investigate each flow regime separately, for subsonic, transonic and supersonic Mach numbers at three different databases are created with same algorithm and each surrogate model performance is then presented in Appendix B. As most of the surrogate models used in this study determine unknown points by weighted average, the performance of surrogate models is similar with three different databases. Therefore, single database that does not consider flow regimes is used throughout the study. Additionally, response surface results of all surrogate models inside SMT are given in Appendix C.

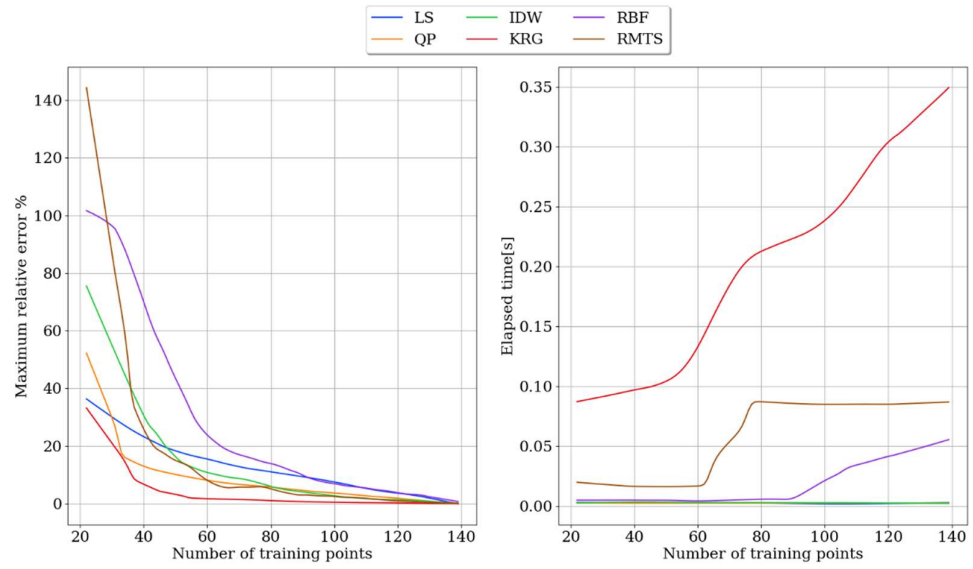


Figure 6.8 Comparisons of surrogate modeling methods in SMT

Table 6.1 Number of points used to create an aerodynamic database

Surrogate Model	Number of Training Points
	Used / All points
LS	133/141
QP	127/141
IDW	124/141
KRG	77/141
RBF	125/141
RMTS	104/141

Among the methods investigated in SMT, KRG uses the fewest points to create an optimized database according to the stopping criterion. The methodology closer to KRG is RMTS with 104 points and all other methods use above 120 points to create an optimized database. When the elapsed time comparison is made for surrogate models, KRG is the slowest one. On average, it takes 0.2 seconds. Even though KRG is the slowest, elapsed time to train and make predictions is negligible compared to the one Euler CFD solution time. Therefore, the most critical comparison criterion is usage of fewer points. Due to this reason, KRG is selected as the surrogate modeling method in the SMT for this research problem. Also, in the previous researches, KRG is introduced as the most accurate method for a small to a moderate number of training points ( $< 1000$ ) and is commonly used in engineering problems [24].

### **6.2.2 Aerodynamic Database Generation with Artificial Neural Networks**

The surrogate modeling toolbox includes many surrogate modeling methods except artificial neural networks (ANN). The most important difference between the ANNs and other surrogate models examined is that ANNs are non-linear surrogate models and therefore, they are inspected separately in this section. Many programming languages include ANNs in their libraries and this study compares famous ones within Python and MATLAB programming languages.

Python programming language has many machine learning frameworks and one of the famous ones is called PyTorch [64]. PyTorch is free and open-source software and it has built-in neural network structures, so users do not need to build them from scratch. In the ANNs, there are many parameters that are needed to be tuned to optimize the ANN performance and they are called hyperparameters. In this study, following hyperparameters, namely; number of layers, number of neurons per layer, training iterations, optimization algorithm and activation functions are investigated.



Before creating a database with ANN, the best parameters are selected with sklearn GridSearchCV [66]. It is a Python programming language module that tries all of the parameters one by one and it determines the best combination of parameters with the accuracy metric implemented. Table 6.2 presents the parameters examined in this study. Highlighted ones with the red color are the values that provide the best accuracy result and hence, the final ANN is created with those values.

Table 6.2 Hyperparameters investigated in PyTorch

<b>Hyperparameter</b>	<b>Values</b>
Number of layers	2,5, <b>10</b> ,100
Number of neurons per layer	10, <b>100</b> ,1000,10000
Number of training iterations	10,100, <b>1000</b> ,10000
Optimization Algorithms	<b>Adam</b> , Stochastic Gradient Descent (SGD)
Activation Functions	Tanh, <b>Rectified Liner Unit (ReLU)</b> , Sigmoid

Number of layers, number of neurons per layer and number of training iterations are not increased to too large values due to training time. As the best results in terms of accuracy are obtained with Adam optimization algorithm, ReLU is selected as an activation function. Same methodology for creating an aerodynamic database is followed in the ANN with PyTorch and Figure 6.9 shows the result in terms of number of points used to create the database and the elapsed time to both train and make predictions with ANN.

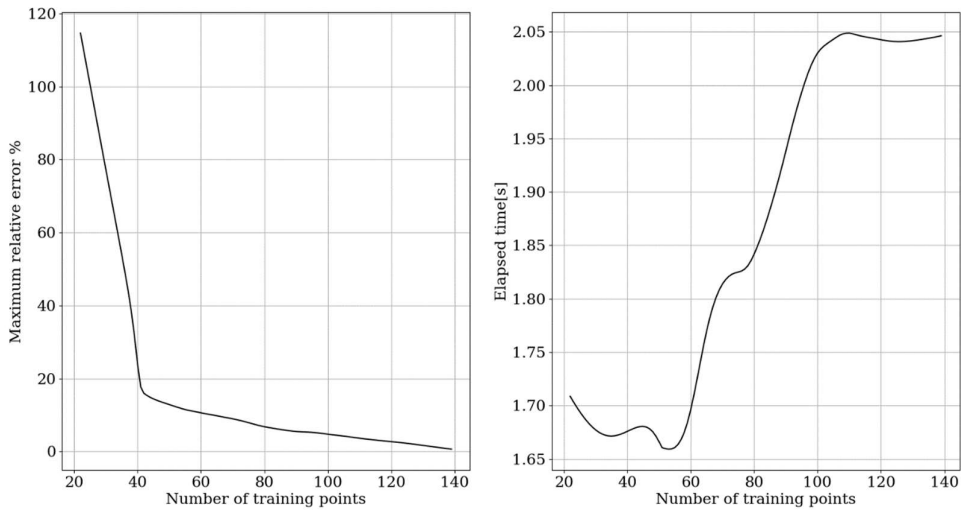


Figure 6.9 Maximum relative error (left) and elapsed time (right) - training points for ANN with Pytorch

For ANN with PyTorch, training time is now in the order of seconds and the maximum relative error distribution for the changing number of training points is higher than that of the SMT methods. In total, this method uses 127 points out of 141 points.

Another tool for the ANN is MATLAB. It has its own ANN tool called neural net fitting inside the neural network toolbox [65]. It can solve the input-output fitting problem with a two-layer feed-forward neural network which is suitable for this research problem. In MATLAB, hyperparameters are different than PyTorch. By default, it has one hidden layer and an output layer and uses a sigmoid transfer function. Table 6.3 demonstrates the hyperparameters in the neural net fitting and highlighted ones with red color are the selected parameters in terms of accuracy metric defined by MATLAB [65]. In MATLAB, the number of neurons per layer can be changed. Other parameters that can also be changed are training and validation data percentages. The training data percentage is the ANN to be trained and the validation data percentage is the data that ANN is making predictions. There are two optimization algorithms examined. The Levenberg-Marquardt algorithm is

recommended for most problems by MATLAB for some noisy and small problems, and Bayesian Regularization is recommended, but it is mentioned as taking more time to obtain a solution [65].

Table 6.3 Hyperparameters investigated in MATLAB ANN Toolbox

Hyperparameter	Values
Number of neurons per layer	10, <b>100</b> , 1000, 10000
Training data percentage	30, 50, 70, <b>90</b> , 95
Validation data percentage	70, 50, 30, <b>10</b> , 5
Optimization Algorithm	Levenberg-Marquardt, <b>Bayesian Regularization</b>

The number of neurons per layer is taken same as PyTorch and the training test split for the data is found optimal for 90-10 split. For the optimization algorithm, as MATLAB suggests, Bayesian regularization found more accurate for the small dataset. Figure 6.10 demonstrates the result in terms of number of points used to create the database and the elapsed time to both train and make predictions with ANN.

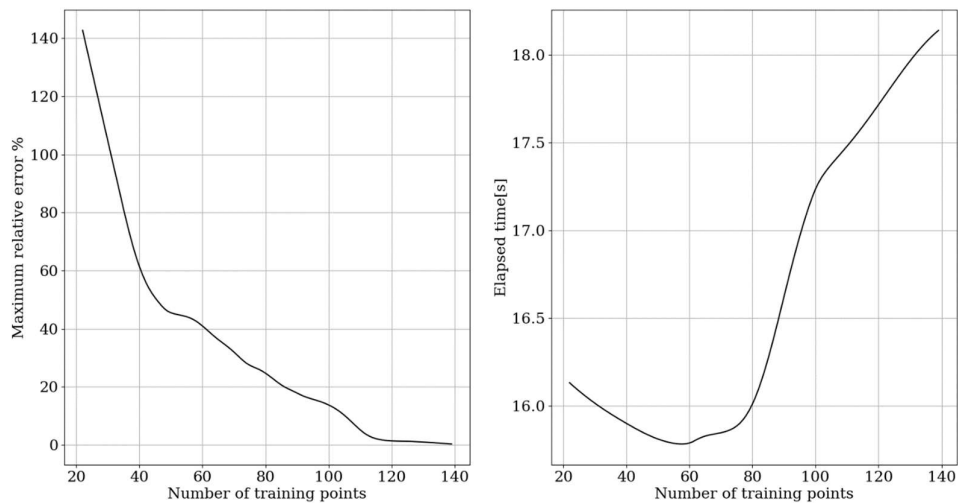


Figure 6.10 Maximum relative error (left) and elapsed time (right) - training points for ANN with MATLAB

ANN with MATLAB show slightly better accuracy than PyTorch, MATLAB uses 122 points out of 141. However, the computational cost is increased almost ten times compared to the PyTorch ANN, because it takes 17 seconds to train the ANN and makes predictions.

### 6.3 Comparisons of Surrogate Modeling Methods

In this study, the main aim is to create an aerodynamic database with surrogate modeling methods with the fewest number of points to decrease the overall computational cost of CFD. Therefore, the number of points used is the most critical parameter. Another comparison is made with average elapsed time values for each surrogate modeling method. From the SMT best-performed method, KRG is taken and ANN with PyTorch and MATLAB is compared. Table 6.4 shows the summary table for these two surrogate modeling methods.

Table 6.4 Comparison of average elapsed time and number of training points used for KRG and ANN

<b>Surrogate Model</b>	<b>Number of Training Points Used / All points</b>	<b>Average Elapsed Time [s]</b>
KRG	77/141	0.2
ANN (PyTorch)	127/141	2
ANN (MATLAB)	122/141	18

According to the convergence criterion, KRG uses only 77 points to create an aerodynamic database. However, ANN with PyTorch and MATLAB uses much more points compared to the KRG. Another significant difference is that KRG makes its predictions much faster than others. Even though ANNs are suitable for fitting non-linear data, it performs better with large datasets. This study dataset is small and therefore ANN is not good at capturing the behavior. This aspect of the ANN is also illustrated in the literature and Figure 6.11 demonstrates an example of the performance of ANNs and the data volume.

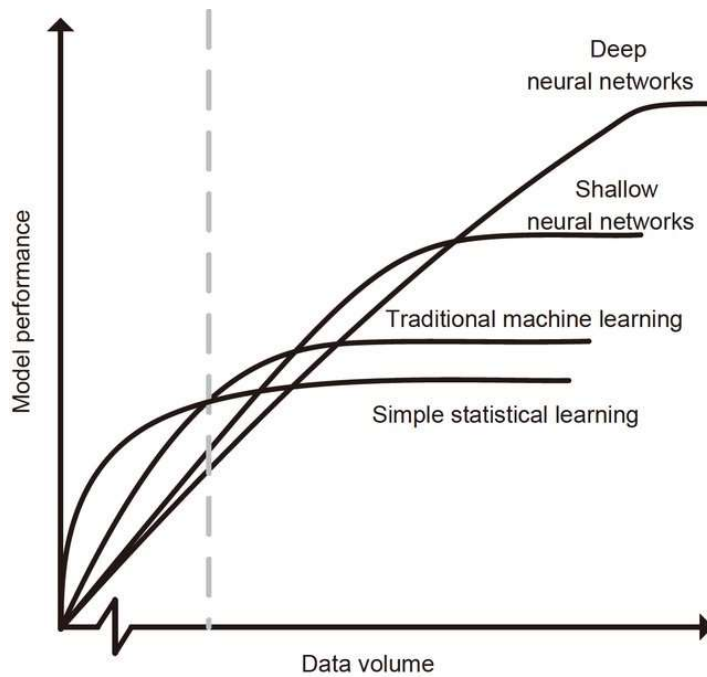


Figure 6.11 Model performance-data volume for different methods [67]

ANN used in this study is considered a shallow neural network because the hidden layer number used is small. Other surrogate modeling methods examined in this study correspond to the simple statistical learning methods. It can be seen that simple statistical learning models perform better until some threshold value with a small data volume. The data volume threshold value is not a general value but problem specific and the data volume can be considered small for the problem investigated in this study. Therefore, simple statistical learning models perform better compared to neural networks.

Another advantage of using simple statistical methods in the SMT compared to the ANNs is that ANNs have many hyperparameters to tune to obtain the optimized model for the problem. On the other hand, surrogate models in the SMT do not require tuning on many hyperparameters and can simply be used for any problem.

## 6.4 Conclusions

This chapter examines surrogate modeling methods for creating an aerodynamic database for a generic fighter aircraft. In this study, surrogate modeling methods in the SMT library and a non-linear surrogate model ANN are utilized both with PyTorch and MATLAB. Because the most time-consuming part of the aerodynamic database generation is CFD analysis, the main aim is to create a database with minimal CFD analysis and utilize surrogate models to generate all test points. With this criterion, the surrogate model is selected as KRG for this problem. KRG uses the fewest points to create an aerodynamic database in less than a second. In addition, KRG is found to be more accurate and fast compared to the ANN. This behavior is also mentioned in other research studies and the main reason is suggested as the data volume. As KRG is performed better compared to the other surrogate models for the aerodynamic database generation, it is also the suitable surrogate model to predict load distribution along the span of the generic fighter wing in aero-structural coupling.





## CHAPTER 7

### AERO-STRUCTURAL ANALYSES OF THE GENERIC FIGHTER WING

#### 7.1 Introduction

In the current chapter, the aero-structural coupling of the generic fighter wing is discussed by developing all the models, namely; the aerodynamic model of the generic fighter, the structural model of the generic fighter wing and the surrogate model for the aerodynamic database generation. In this part of the study, aerodynamic loads acquired using the kriging surrogate model are transferred onto the structural model and aero-structural coupling is performed. Nastran Flight Loads (FLDS) module is used to validate the proposed methodology. Once the validation is performed, the high-fidelity CFD-based aerodynamic loads are used to determine the flexible wing load distribution.

#### 7.2 Aero-Structural Coupling of the Generic Fighter Wing

The proposed method is an iterative process and utilizes the aerodynamic loads obtained from the surrogate model and the structural model's modal characteristics to determine the aircraft's flexible wing loads. The method can effectively determine the load distribution by getting the structural twist distribution along the wing span. Figure 7.1 illustrates the flowchart of the proposed methodology.

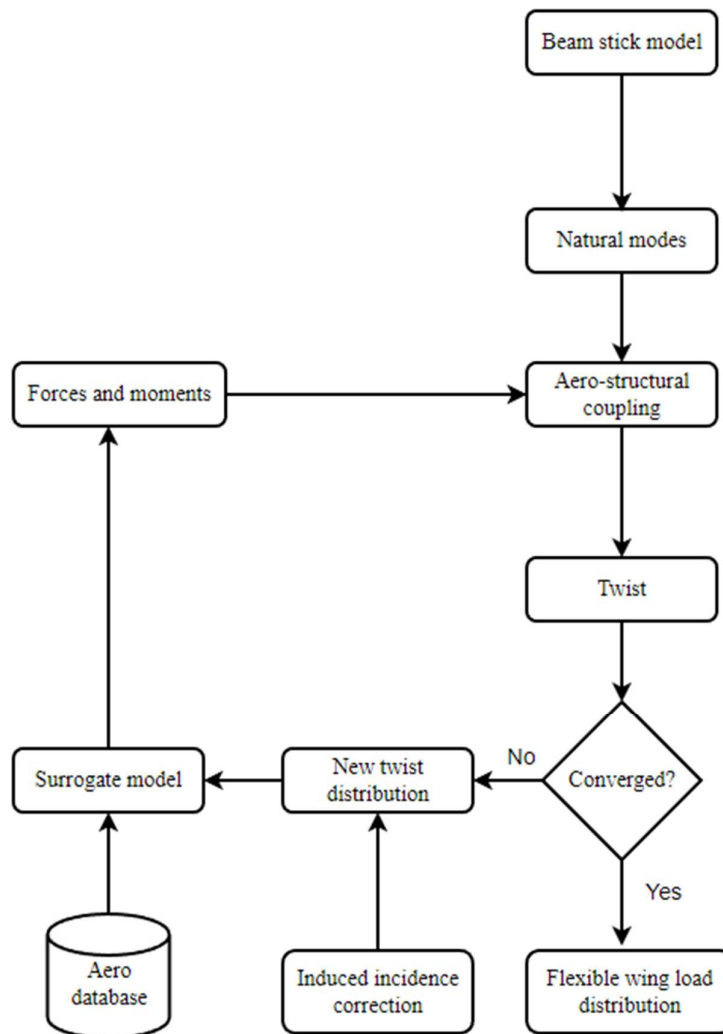


Figure 7.1 Flowchart for the proposed methodology

Aero-structural coupling is a technique that couples the aerodynamic model to the structural model for subsequent aeroelastic analyses. In the current work, the aero-structural coupling is carried out by writing a script in Python programming language. It requires two inputs: the aerodynamic loads at beam stick model (BSM) nodes and natural modes from the BSM [69]. The surrogate model is used to obtain aerodynamic loads at specified nodes rapidly. The aerodynamic database required

for building the surrogate model is obtained with aerodynamic analyses conducted on ANSYS Fluent [56]. In addition, the structural input required for the coupling script is obtained from the generated BSM. The output of this coupling process is the structural displacements and loads distribution on the flexible wing. The mathematical model described herein is used in the coupling to determine structural displacements.

Let  $[Z]$  be the six-dimensional load matrix obtained with three-dimensional force  $[F]$  and moment matrix  $[M]$

$$[Z] = ([F], [M])^T \quad (7.1)$$

Let  $[\phi]$  be the eigenvector and  $[K]$  be the stiffness matrix and  $\{u\}$  is the displacement vector.

$$[K] \{u\} = [Z] \quad (7.2)$$

By using the coordinate change,

$$\{u\} = [\phi]\{q\} \quad (7.3)$$

and by pre-multiplying with  $[\phi]^T$

$$[\phi]^T [K] [\phi] \{q\} = [\phi]^T [Z] \quad (7.4)$$

$$[\hat{K}] \{q\} = [\hat{Z}] \quad (7.5)$$

where  $[\hat{K}]$  is the generalized stiffness matrix, the displacements are obtained as follows.

$$\{q\} = [\hat{K}]^{-1} [\hat{Z}] \quad (7.6)$$

$\{q\}$  is the displacement vector containing nodal translation and rotations.

Displacements contain the twist value for each section and the twist values are the input used in the following process. New twist values are obtained from a rigid wing database and do not include the induced incidence effects. The sectional-induced incidence is a function of the coefficient of lift span-wise distribution and changes at each iteration of this loop. Therefore, induced incidence effects are added to the twist values and they are computed using a numerical approach applicable to non-planar wings with an arbitrary loading [54].

The equation for induced incidence  $\epsilon$  is given as:

$$\epsilon = \frac{V_i}{V_\infty} \quad (7.7)$$

$$V_i = \int_{-b/2}^{b/2} \frac{(d\Gamma/dy)dy}{4\pi/(y_0-y)} \quad (7.8)$$

where induced velocity  $V_i$  and free stream velocity  $V_\infty$  and circulation  $\Gamma$  is used along the span. Induced incidence values are used as

$$\alpha^{corr} = \alpha + \Delta\epsilon \quad (7.9)$$

Here,  $\alpha^{corr}$  is the absolute incidence with induced incidence correction and  $\alpha$  is the absolute incidence, whereas,  $\Delta\epsilon$  is the change in the induced incidence calculated with below equation

$$\Delta\epsilon = \epsilon^{rig} - \epsilon^{flex} \quad (7.10)$$

where  $\epsilon^{rig}$  is the induced incidence of a rigid shape and  $\epsilon^{flex}$  is the induced incidence of a flexible shape of a wing section. With the local incidence correction, new twist distribution is obtained. Twist distribution determines the new AoA values for each section and can be given to the surrogate model to compute new aerodynamic loads. These iterations continue until the wing shape does not change anymore. The convergence criterion is the change in the wing tip twist value. Let  $\theta_i$  is the tip twist value at  $i$ th iteration and  $\theta_{i+1}$  is the tip twist value at next iteration. Computations stop when the absolute difference is less than a specified tolerance value and formula for that is given as

$$|\theta_{i+1} - \theta_i| \leq Tol \quad (7.11)$$

For this study, tolerance value is taken as  $0.01^\circ$ . When the proposed methodology is converged, load distribution along the span of a flexible wing is obtained.

### 7.3 Validation of the Proposed Methodology

The proposed methodology is validated with Nastran FLDS module [51]. FLDS uses MSC Patran as the pre- and post-processor and MSC Nastran as the solver. It can calculate both the rigid and flexible structure loads. Therefore, it is an appropriate tool for validation studies. FLDS uses Doublet lattice method (DLM) for subsonic flows and ZONA51 for supersonic flows [6]. The aerodynamic theory is linearized potential flow and geometry is modeled as two-dimensional. Figure 7.2 illustrates the generated two-dimensional FLDS configuration and three-dimensional generic fighter configuration. The axes system is also shown here to present the forces and moments which will be referred in the following sections.

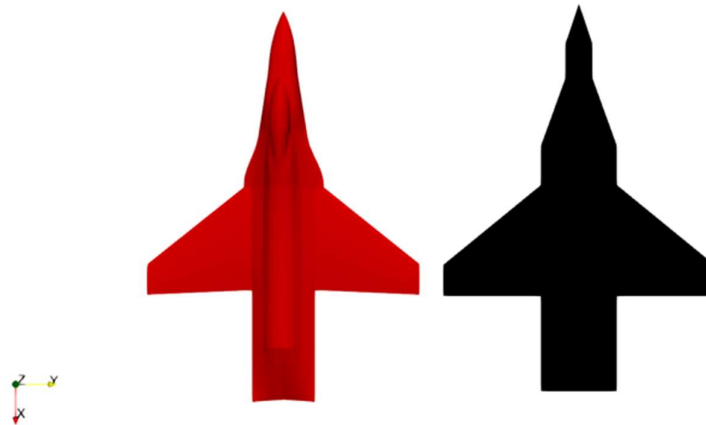


Figure 7.2 Generic fighter configuration (red) and FLDS configuration (black)

The FLDS model is two-dimensional; therefore, the three-dimensional components, such as canopy and fuselage depth, cannot be modeled in the FLDS. On the other hand, parameters important in the calculations of the wing loads, such as wing span, wing chord and the wing area are the same for both models and the top view is used for comparison purposes. It is evident from the top view that both models are almost identical. For the FLDS model, a mesh convergence study is also conducted by changing the mesh size on the wing. Mesh at the fuselage is kept constant because only the loads at the wing are considered in this study. Figure 7.3 demonstrates the different mesh densities for the model.

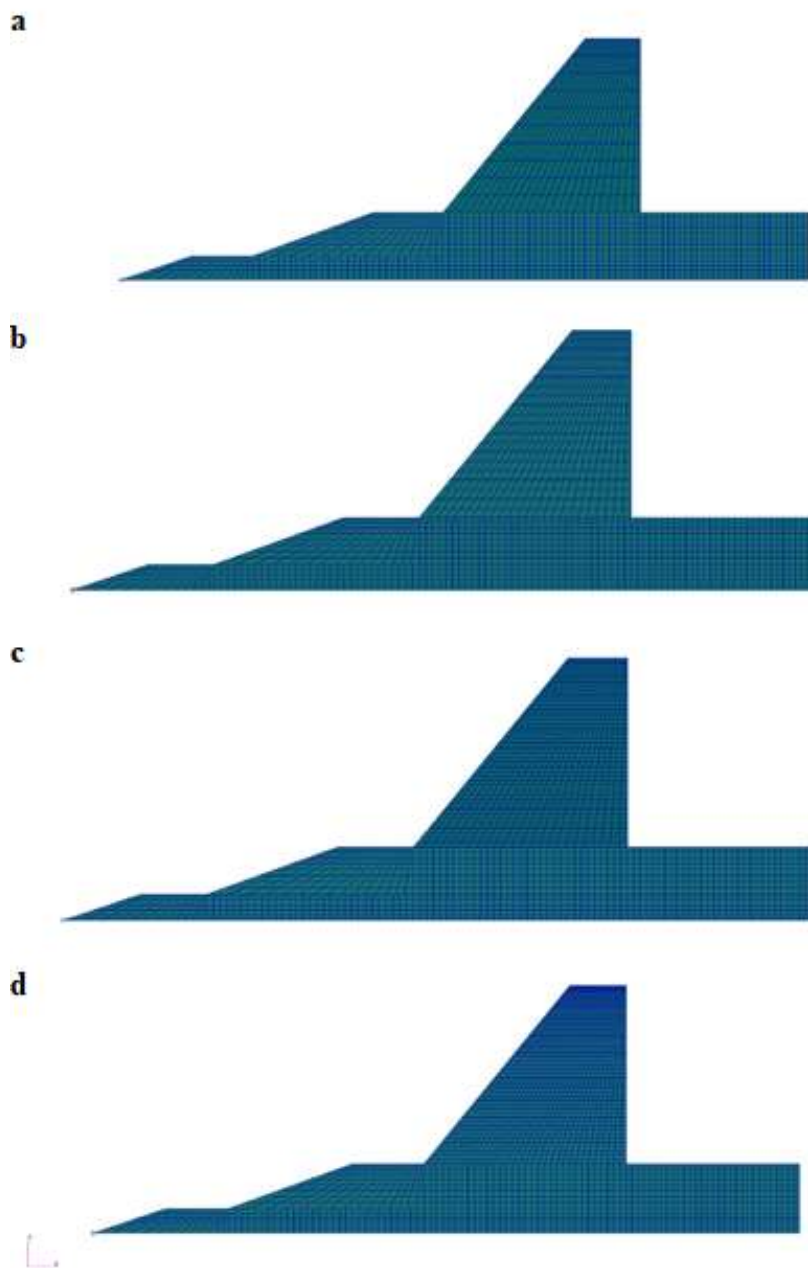


Figure 7.3 (a) 240 panels (b) 480 panels (c) 960 panels (d) 1920 for the FLDS model

Mesh numbers are doubled for each model and it has 240, 480, 960, 1920 panels respectively. Figure 7.4 presents the mesh convergence study effect on the wing  $F_z$  (i.e. force along z axis).

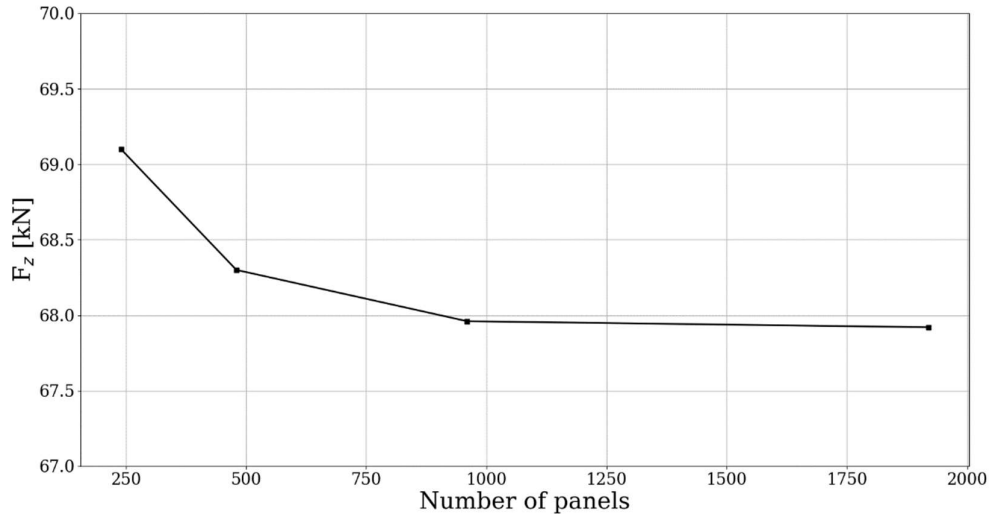


Figure 7.4  $F_z$  vs number of panels

The line plot reveals that the total wing  $F_z$  does not change between 960 and 1920 aerodynamic panels and hence the mesh is converged [6]. Considering the mesh convergence study results, the model with 1920 panels is selected as the final Nastran FLDS model. Moreover, the total wing  $F_z$  and wing  $M_y$  (i.e. moment about y axis) values are compared for Nastran FLDS and ANSYS Fluent results. For simplicity, ANSYS Fluent is referred to as Fluent and Nastran FLDS is referred to as Nastran in the following figures. Figure 7.5 illustrates the  $F_z$  and  $M_y$  values for selected Mach numbers with changing the AoA values.



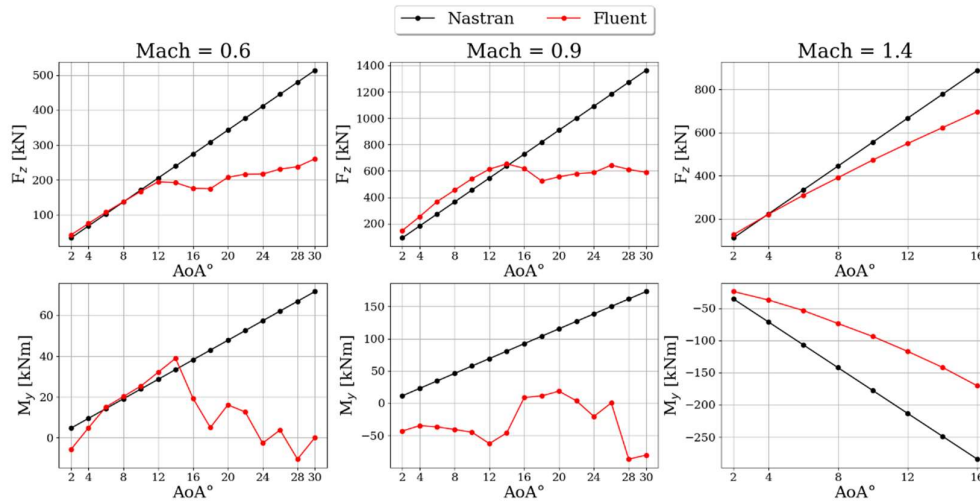


Figure 7.5 Wing  $F_z$  and  $M_y$  values for changing AoA

Nastran utilizes the linearized aerodynamic theory; therefore, it generates a linear line for both  $F_z$  and  $M_y$  values. At Mach 0.6, results up to  $12^\circ$  AoA are similar and after  $12^\circ$  AoA, Fluent Euler results are not linear anymore and the difference increases. A similar trend is also observed at 0.9 Mach for  $F_z$ , but  $M_y$  is entirely different because of non-linearities like shocks and vortices dominating at 0.9 Mach. At Mach 1.4, both trends are linear, but at higher AoA values difference is increasing due to the slope difference of these linear curves. Another comparison carried out is the center of pressure difference between Nastran and Fluent. Center of pressure ( $cp$ ) location equation can be written as,

$$x_{cp} = -\frac{M_y}{F_z} \quad (7.12)$$

$$y_{cp} = \frac{M_x}{F_z} \quad (7.13)$$

As the Nastran uses the linear flow theory, the  $M_y$ ,  $F_z$  and the center of pressure values do not change significantly with the change in angle of attack, whereas, in Fluent the values dependent upon angle of attack. Figure 7.6 and Figure 7.7 show

the center of pressure locations at the wing for different Mach numbers and constant AoA values. The BSM is also presented with red color.

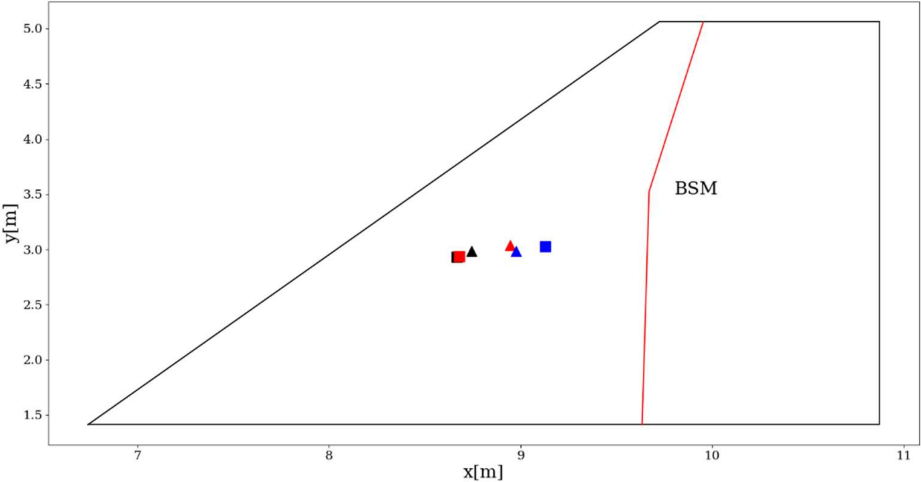


Figure 7.6 Center of pressure locations and the BSM on the wing for different Mach numbers at  $AoA = 4^\circ$

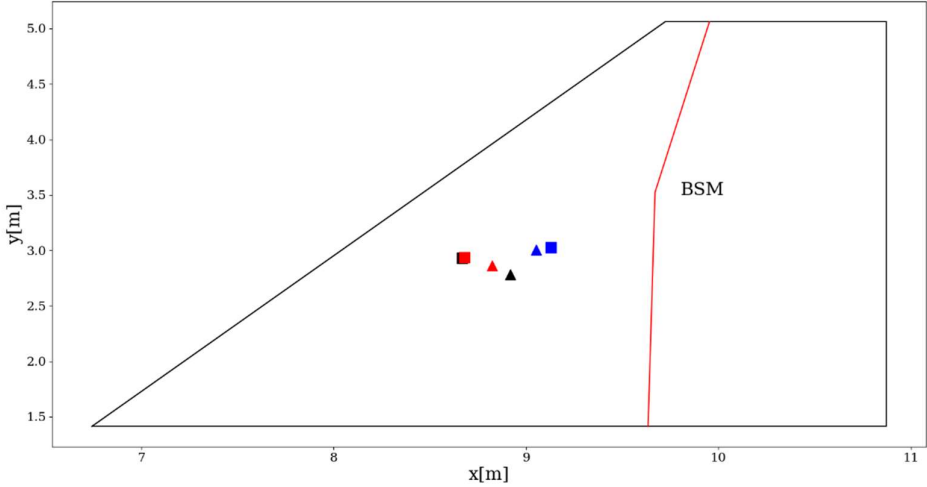


Figure 7.7 Center of pressure locations and the BSM on the wing for different Mach numbers at  $AoA = 16^\circ$

All of the center pressure locations are in front of the BSM and this creates positive twist values, which is tend to increase the angle of attack values. The center of pressure location calculated by Nastran changes drastically for a supersonic Mach number of 1.4, but there is almost no change between 0.6 and 0.9 Mach. On the other hand, the center of pressure locations calculated via Fluent is changing more compared to that of Nastran. When the center of pressure shifts backward, it gets closer to the BSM and the distance between the center of pressure and the BSM decreases. Hence, the moment arm and the local twist value also decrease.

Having presented the aerodynamic load comparison between Nastran and Fluent results, the next step is to validate the proposed methodology with Nastran data. Nastran can compute both rigid and elastic wing loads and can be used to build a surrogate model to calculate the elastic wing loads with the given methodology. The proposed methodology is named as the “Rapid Method” in the following sections. The Rapid Method can be used with and without induced incidence correction to investigate the effect of the induced incidence correction compared with Nastran results. Figure 7.8 demonstrates the  $F_z$  and  $M_y$  distributions for the wing for different Mach numbers.

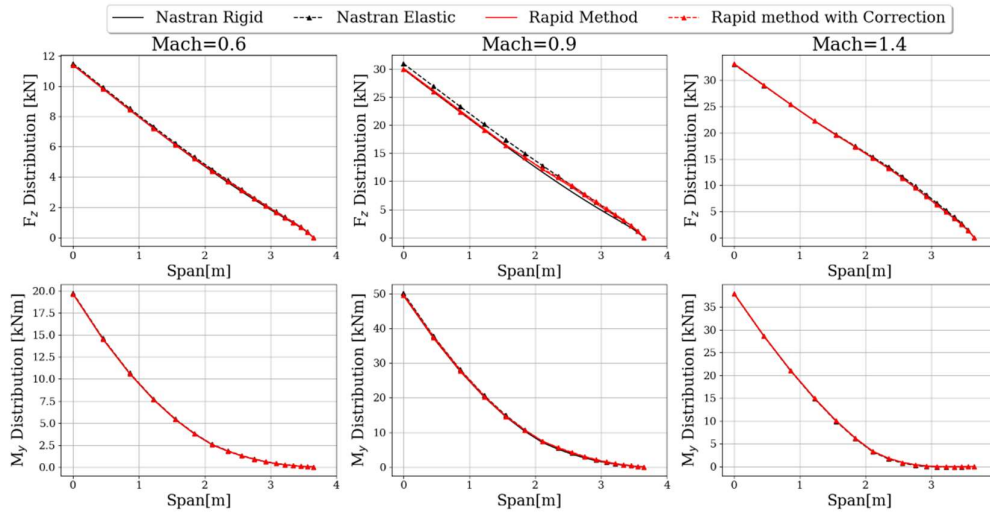


Figure 7.8  $F_z$  and  $M_y$  distributions for the wing for different Mach numbers and  $AoA = 4^\circ$

The trends are similar when the results are examined for Mach 0.6 and 1.4. All lines coincide because, at 0.6 Mach, loads are smaller than the other Mach numbers, and at 1.4 Mach, the center of pressure location is closer to the BSM. Hence moment arm is shorter. There is almost no change between rigid and elastic wing loads, which indicates that the generic fighter wing is almost rigid.

The most significant difference between rigid and elastic wing loads can be seen at the Mach 0.9 results. This Mach number is used to decide whether to use the induced incidence corrections. As the corrections are applied, Rapid Method results have shifted closer to the Nastran elastic results. Hence it is concluded that corrections are necessary for this particular research problem.

For all the Mach regimes, the results are in good agreement. Therefore, the Rapid Method is validated and can be used with an aerodynamic database obtained with higher-fidelity Fluent analyses.

## 7.4 Aero-Structural Analysis Results of the Generic Fighter Wing

The aeroelastic model is previously used with the database created with Nastran and is also validated. The next step is to obtain the same results for different Mach numbers representing subsonic, transonic and supersonic flow regimes with a database created with Fluent. Figure 7.9 and Figure 7.10 present  $F_z$  and  $M_y$  distributions for different Mach numbers and AoA values. For both of the solvers, rigid and elastic wing loads are provided. Fluent results are acquired via the Rapid Method that uses the kriging surrogate model. On the other hand, Nastran results are directly obtained from the solver output files.

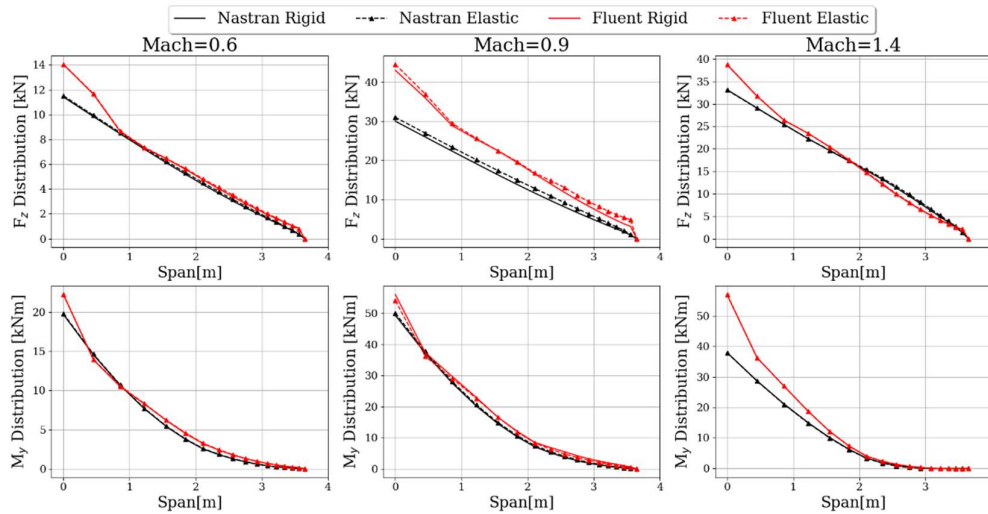


Figure 7.9  $F_z$  and  $M_y$  distributions for the wing for different Mach numbers at AoA =  $4^\circ$

The first comparison is made at  $4^\circ$  AoA for different Mach numbers. At 0.6 Mach, as it is in the linear region, Nastran and Fluent results are close to each other. In addition, at Mach 0.6, elastic wing loads are almost identical to rigid wing loads. A similar trend with Mach 0.6 is observed at 1.4 Mach. At Mach 0.9, the influence of the aerodynamic non-linearities is significant. Therefore, Fluent and Nastran  $F_z$  force

magnitudes are not close enough to each other and additionally, elastic increments are most noticeable at this Mach number.

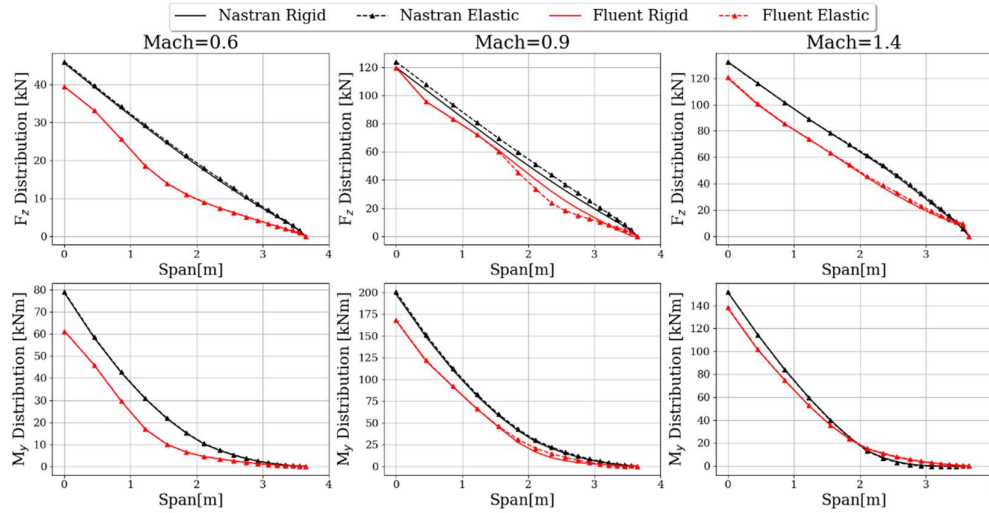


Figure 7.10  $F_z$  and  $M_y$  distributions for the wing for different Mach numbers and  $AoA = 16^\circ$

Another comparison is made at  $AoA 16^\circ$ . At this  $AoA$ , Nastran and Fluent results are not close enough because, at Mach 0.6, this  $AoA$  is no longer in the linear region. For all Mach numbers, wing  $F_z$  distributions and wing  $M_y$  distributions have a visible difference. The difference is expected because the inspected  $AoA$  value is dominated by a non-linear aerodynamic effect, which cannot be captured by Nastran but can be added with higher-fidelity simulations such as Euler simulations. The difference between elastic and rigid loads calculated through Nastran and Rapid Method is maximum at Mach 0.9. Table 7.1 elaborates on the rigid and elastic wing  $F_z$  values for both Nastran and Fluent results.

Table 7.1 Total wing  $F_z$  forces [kN] for different Mach and AoA values

Mach	AoA°	Nastran Rigid	Nastran Elastic	Fluent Rigid	Fluent Elastic
0.6	4	68.5	70.1	77.6	78.4
0.9	4	181.9	196.1	260.0	275.4
1.4	4	222.2	225.2	226.2	227.2
0.6	16	274.1	280.7	183.0	183.7
0.9	16	727.9	784.1	640.2	610.6
1.4	16	889.1	900.8	717.0	735.3

At Mach 0.6 and 1.4 for AoA 4°, the total wing  $F_z$  difference between rigid and elastic is around 1% because the force is smaller at Mach 0.6 compared to other Mach numbers and the moment arm between the center of pressure and BSM is smaller at 1.4 Mach. At 0.6 Mach for 16° AoA, the difference is more significant in Nastran results than in Fluent because the center of pressure is not changing with AoA at Nastran. However, in Fluent, the center of pressure shifts backward, shortening the moment arm. The most significant difference between rigid and elastic wing loads can be seen at Mach 0.9, which is about 10% for Nastran and 5% for Fluent. In the Fluent, elastic loads are smaller than the rigid loads, but it is the opposite for Nastran. This difference is due to the force decrease after the 16° AoA in Fluent, which cannot be seen at the Nastran because it always increases linearly. The results indicate that difference at Mach 0.9 cannot be neglected and is essential. Therefore, including flexibility effects in the analysis in the early stages of design is necessary.

The final comparison is made in terms of elapsed time for the CFD-based Rapid Method and the Nastran FLDS software to compute the elastic wing loads. Table 7.2 shows the time comparison between them.

Table 7.2 Elapsed time comparison for FLDS and Rapid Method

Model	Elapsed time [s]
Nastran FLDS	1
CFD-based Rapid Method	1

When computational costs are compared, on average, both provide results in 1 second making both methods very fast. The CFD-based Rapid Method utilizes the aerodynamic analysis results of Euler simulations and the kriging surrogate model for unknown AoA values. According to the results, it can be deduced that the CFD-based Rapid Method is an effective alternative to the Nastran FLDS because it does not increase the computational cost. Moreover, the Rapid Method has also the capability of including the non-linear aerodynamic phenomena that Nastran FLDS cannot capture.

## 7.5 Conclusions

This chapter elaborates on the proposed methodology for calculating the elastic wing loads. The methodology is also validated with a commercial tool Nastran FLDS which uses low-fidelity linearized aerodynamic theory. In the validation process, it is demonstrated that induced incidence correction in the method provides better results and agrees well with the FLDS results. After completing the validation, higher-fidelity Euler simulations are introduced to the CFD-based Rapid Method to determine flexible wing loads. The FLDS module utilizes the linear aerodynamic theory in non-linear regions. On the other hand, the CFD-based Rapid Method includes non-linear aerodynamic effects in the flexible wing load calculation.



Therefore, the difference in the computed results increases with the Fluent in these non-linear regions. In this study, subsonic, transonic and supersonic flow regimes are investigated. The difference between flexible and rigid loads for Mach 0.6 and 1.4 is within 2%, which can be considered negligible increment in the design stages. However, at 0.9 Mach, the flexible load's increment is significant. The reason is the center of pressure location and the stiffness of the wing. As the wing for the generic fighter is almost rigid and has high stiffness, the difference between rigid and elastic loads is less for shorter moment arms and loads that are not large enough to produce considerable twist at the wing. Finally, the computational cost for Nastran FLDS and the Rapid Method is compared in terms of elapsed time. On average, the elapsed time for the Rapid Method is identical to that of Nastran FLDS, which makes this method appealing to designers and engineers who want to explore the entire design space at the initial fighter development stages.



## CHAPTER 8

### CONCLUSIONS

#### 8.1 General Conclusions

In this thesis, several surrogate models are investigated for generating an aerodynamic database for a generic fighter aircraft. This database represents the fighter aircraft's flight envelope, including subsonic, transonic, and supersonic flow regimes and high angle of attack values. Because the CFD simulations are computationally expensive, surrogate models are compared in terms of their ability to generate the aerodynamic database using the fewest CFD solutions. According to this criterion, Kriging is selected as the surrogate model for this research problem.

The aerodynamic loads for the rigid wing are also generated by using the Nastran Flight Loads (FLDS) module and is used in the aeroelastic model. The flexible wing loads are calculated using a surrogate model and compared with those calculated via FLDS. It is observed that the proposed methodology provides similar results to that of the FLDS, which verifies that the presented method can be used for subsequent loads analysis.

The given method is also utilized to compute the flexible wing loads with high-fidelity CFD obtained with ANSYS Fluent. Non-linear aerodynamic phenomena that cannot be modeled or captured in FLDS are also acquired with the given methodology. With the implementation of this so-called rapid method to aero-structural coupling, the level of accuracy in CFD analyses is achieved with the significantly reduced computational cost making this methodology suitable for the initial design stages of a fighter jet.

## 8.2 Recommendations for future works

The recommendations for the future work of this study can be listed as follows:

- In this study, Mach and angle of attack are the only input parameters for surrogate models. Other parameters, such as sideslip angle and control surface deflections can also be added to the surrogate model to capture all the parameters at the design phase for the completion of the load cycle.
- This study is applied to the wing only and therefore, other lifting surfaces, such as the horizontal and vertical tail can also be investigated.
- Currently, aerodynamic solutions are taking Euler solutions into account. High-fidelity solutions like Reynolds-averaged Navier-Stokes (RANS) simulations can also be performed, especially for stall and separated flow conditions at high AoA and transonic conditions.
- Two-way fluid structure interaction can be performed to compare its results with the proposed methodology.

## REFERENCES

- [1] Daniel, P. (2018). Raymer--‘Aircraft Design: A Conceptual Approach’. AIAA Education Series.
- [2] Lomax, T. L. (1996). Structural loads analysis for commercial transport aircraft: theory and practice. American Institute of Aeronautics and Astronautics.
- [3] Ripepi, M., Verveld, M. J., Karcher, N. W., Franz, T., Abu-Zurayk, M., Görtz, S., & Kier, T. M. (2018). Reduced-order models for aerodynamic applications, loads and MDO. CEAS Aeronautical Journal, 9(1), 171-193.
- [4] Agostinelli, C., & Allen, C. (2012, June). Flexible Wing Twist Optimisation using Rapid Computational Methods. In 30<sup>th</sup> AIAA Applied Aerodynamics Conference (p. 2661).
- [5] Wright, J. R., & Cooper, J. E. (2008). Introduction to aircraft aeroelasticity and loads (Vol. 20). John Wiley & Sons.
- [6] MSC Software Corporation, *MSC Nastran 2018 Aeroelastic Analysis User’s Guide*. 2018.
- [7] Guruswamy, G. P. (2002). A review of numerical fluids/structures interface methods for computations using high-fidelity equations. Computers & structures, 80(1), 31-41.
- [8] Eldred, M., & Dunlavy, D. (2006, September). Formulations for surrogate-based optimization with data fit, multifidelity, and reduced-order models. In 11th AIAA/ISSMO multidisciplinary analysis and optimization conference (p. 7117).

- [9] Albano, E., & Rodden, W. P. (1969). A doublet-lattice method for calculating lift distributions on oscillating surfaces in subsonic flows. *AIAA journal*, 7(2), 279-285.
- [10] Giesing, J. P., Kalman, T. P., & Rodden, W. P. (1972). *Subsonic Unsteady Aerodynamics for General Configurations. Part 2. Volume 1. Application of the Doublet-Lattice Method and the Method of Images to Lifting-Surface/Body Interference.* DOUGLAS AIRCRAFT CO LONG BEACH CA.
- [11] Giesing, J. P., Kalman, T. P., & Rodden, W. P. (1972). *Subsonic Unsteady Aerodynamics for General Configurations. Part 2. Volume 1. Application of the Doublet-Lattice Method and the Method of Images to Lifting-Surface/Body Interference.* DOUGLAS AIRCRAFT CO LONG BEACH CA.
- [12] Giesing, J. P., Kalman, T. P., & Rodden, W. P. (1972). *Subsonic Unsteady Aerodynamics for General Configurations. Part 2. Volume 2. Computer Program N5KA.* DOUGLAS AIRCRAFT CO LONG BEACH CA.
- [13] Giesing, J. P., Kalman, T. P., & Rodden, W. P. (1972). Subsonic steady and oscillatory aerodynamics for multiple interfering wings and bodies. *Journal of Aircraft*, 9(10), 693-702.
- [14] Liu, D. D., James, D. K., Chen, P. C., and Pototzky, A. S. (1991). Further Studies of Harmonic Gradient Method for Supersonic Aeroelastic Applications. *J. Aircraft*, Vol. 28, pp. 598-605.
- [15] Van Muijden, J., Prananta, B. B., & Veul, R. P. G. (2008). Efficient aeroelastic simulation in a parametric procedure for fatigue analysis. In *26th International Congress of the Aeronautical Sciences* (pp. 1-10).
- [16] Raveh, D. E., & Karpel, M. (1999). Structural optimization of flight vehicles with computational-fluid-dynamics-based maneuver loads. *Journal of aircraft*, 36(6), 1007-1015.

- [17] Sobester, A., Forrester, A., & Keane, A. (2008). *Engineering design via surrogate modelling: a practical guide*. John Wiley & Sons.
- [18] Fossati, M. (2015). Evaluation of aerodynamic loads via reduced-order methodology. *AIAA Journal*, 53(8), 2389-2405.
- [19] Eldred, M., & Dunlavy, D. (2006, September). Formulations for surrogate-based optimization with data fit, multifidelity, and reduced-order models. In *11<sup>th</sup> AIAA/ISSMO multidisciplinary analysis and optimization conference* (p. 7117).
- [20] Benner, P., Gugercin, S., & Willcox, K. (2015). A survey of projection-based model reduction methods for parametric dynamical systems. *SIAM review*, 57(4), 483-531.
- [21] Yondo, R., Andrés, E., & Valero, E. (2018). A review on design of experiments and surrogate models in aircraft real-time and many-query aerodynamic analyses. *Progress in aerospace sciences*, 96, 23-61.
- [22] San, O., Maulik, R., & Ahmed, M. (2019). An artificial neural network framework for reduced order modeling of transient flows. *Communications in Nonlinear Science and Numerical Simulation*, 77, 271-287.
- [23] Liem, R. P., Mader, C. A., & Martins, J. R. (2015). Surrogate models and mixtures of experts in aerodynamic performance prediction for aircraft mission analysis. *Aerospace Science and Technology*, 43, 126-151.
- [24] Hwang, J. T., & Martins, J. R. (2018). A fast-prediction surrogate model for large datasets. *Aerospace Science and Technology*, 75, 74-87.
- [25] Brunton, S. L., & Kutz, J. N. (2022). *Data-driven science and engineering: Machine learning, dynamical systems, and control*. Cambridge University Press.
- [26] Lindhorst, K., Haupt, M. C., & Horst, P. (2014). Efficient surrogate modelling of nonlinear aerodynamics in aerostructural coupling schemes. *AIAA Journal*, 52(9), 1952-1966.

- [27] Alsayyari, F., Perkó, Z., Lathouwers, D., & Kloosterman, J. L. (2019). A nonintrusive reduced order modelling approach using proper orthogonal decomposition and locally adaptive sparse grids. *Journal of Computational Physics*, 399, 108912.
- [28] Xiao, D., Yang, P., Fang, F., Xiang, J., Pain, C. C., & Navon, I. M. (2016). Non-intrusive reduced order modelling of fluid–structure interactions. *Computer Methods in Applied Mechanics and Engineering*, 303, 35-54.
- [29] Mohan, A. T., & Gaitonde, D. V. (2017). Analysis of airfoil stall control using dynamic mode decomposition. *Journal of Aircraft*, 54(4), 1508-1520.
- [30] Mariappan, S., Gardner, A. D., Richter, K., & Raffel, M. (2014). Analysis of dynamic stall using dynamic mode decomposition technique. *AIAA journal*, 52(11), 2427-2439.
- [31] Kuya, Y., Takeda, K., Zhang, X., & Forrester, A. I. (2011). Multifidelity surrogate modeling of experimental and computational aerodynamic data sets. *AIAA journal*, 49(2), 289-298.
- [32] Kou, J., & Zhang, W. (2021). Data-driven modeling for unsteady aerodynamics and aeroelasticity. *Progress in Aerospace Sciences*, 125, 100725.
- [33] Thelen, A. S., Leifsson, L. T., & Beran, P. S. (2020). Multifidelity flutter prediction using regression cokriging with adaptive sampling. *Journal of Fluids and Structures*, 97, 103081.
- [34] Taira, K., Brunton, S. L., Dawson, S. T., Rowley, C. W., Colonius, T., McKeon, B. J., ... & Ukeiley, L. S. (2017). Modal analysis of fluid flows: An overview. *AIAA Journal*, 55(12), 4013-4041.
- [35] Amsallem, D., Cortial, J., & Farhat, C. (2010). Towards real-time computational-fluid-dynamics-based aeroelastic computations using a database of reduced-order information. *AIAA journal*, 48(9), 2029-2037.



- [36] Lieu, T., & Farhat, C. (2007). Adaptation of aeroelastic reduced-order models and application to an F-16 configuration. *AIAA journal*, 45(6), 1244-1257.
- [37] Lillian, C., McDaniel, D., & Morton, S. (2011). An efficient method of computing maneuvering aircraft surface loads using CFD, proper orthogonal decomposition, and system identification. In 49<sup>th</sup> AIAA Aerospace Sciences Meeting including the New Horizons Forum and Aerospace Exposition (p. 1177).
- [38] Klimmek, T., Ohme, P., Ciampa, P. D., & Handojo, V. (2016). Aircraft loads-an important task from pre-design to loads flight testing.
- [39] Dupuis, R., Jouhaud, J. C., & Sagaut, P. (2019). Improved Surrogate Modeling using Machine Learning for Industrial Civil Aircraft Aerodynamics. arXiv preprint arXiv:1912.04706.
- [40] Nazzeri, R., Haupt, M., Lange, F., & Sebastien, C. (2015). Selection of critical load cases using an artificial neural network approach for reserve factor estimation. Deutsche Gesellschaft für Luft-und Raumfahrt-Lilienthal-Oberth eV.
- [41] Cumnuantip, S., Kier, T., Risse, K., & Chiozzotto, G. P. (2016). Methods for the quantification of aircraft loads in DLR-Project iLOADS. Deutsche Gesellschaft für Luft-und Raumfahrt-Lilienthal-Oberth eV.
- [42] Dharmasaroja, A., Armstrong, C. G., Murphy, A., Robinson, T. T., McGuinness, S. H. M., Iorga, N. L., & Barron, J. R. (2017). Load case characterization for the aircraft structural design process. *AIAA Journal*, 55(8), 2783-2792.
- [43] Dupuis, R., Jouhaud, J. C., & Sagaut, P. (2018). Aerodynamic data predictions for transonic flows via a machine-learning-based surrogate model. In 2018 AIAA/ASCE/AHS/ASC Structures, Structural Dynamics, and Materials Conference (p. 1905).

- [44] Han, Z. H., & Görtz, S. (2012). Hierarchical kriging model for variable-fidelity surrogate modeling. *AIAA journal*, 50(9), 1885-1896.
- [45] Ruiz Juretschke, I., García Bosque, A., Hilario Montes, J., & Calvo Blanco, M. (2019). Developments in optimized load calculation and extreme load detection: summary of EADS-CASA's main static loads activities in CleanSky Smart Fixed Wing Aircraft, work package on Advanced Loads Control Techniques. *CEAS Aeronautical Journal*, 10(4), 1089-1100.
- [46] Tartaruga, I., Cooper, J. E., Lowenberg, M. H., Sartor, P., Coggon, S., & Lemmens, Y. (2016). Prediction and uncertainty propagation of correlated time-varying quantities using surrogate models. *CEAS Aeronautical Journal*, 7(1), 29-42.
- [47] Cesnik, C. E., Palacios, R., & Reichenbach, E. Y. (2014). Reexamined structural design procedures for very flexible aircraft. *Journal of Aircraft*, 51(5), 1580-1591.
- [48] Hesse, H., & Palacios, R. (2014). Reduced-order aeroelastic models for dynamics of maneuvering flexible aircraft. *AIAA journal*, 52(8), 1717-1732.
- [49] Dussart, G., Portapas, V., Pontillo, A., & Lone, M. (2018). Flight dynamic modelling and simulation of large flexible aircraft. *Flight Physics-Models, Techniques and Technologies*.
- [50] McDaniel, D. R., Cummings, R. M., Bergeron, K., Morton, S. A., & Dean, J. P. (2009). Comparisons of computational fluid dynamics solutions of static and manoeuvring fighter aircraft with flight test data. *Proceedings of the Institution of Mechanical Engineers, Part G: Journal of Aerospace Engineering*, 223(4), 323-340.
- [51] Chajec, W. (1999, June). Aeroelastic analyses in "PZL-Mielec" using MSC/NASTRAN. In *MSC Worldwide Aerospace Conference*.
- [52] Whiting, B., & Neill, D. J. (1997, November). Interfacing external, high order aerodynamics into MSC/NASTRAN for aeroelastic analyses. In *MSC Aerospace User's Conference*.

- [53] Kaneko, H., & Furukawa, T. (2004). Operational Loads Regression Equation Development for Advanced Fighter Aircraft. In Paper ICAS 24th International Congress of the Aeronautical Sciences. Japan (pp. 1-9).
- [54] Blackwell Jr, J. A. (1976). Numerical method to calculate the induced drag or optimum loading for arbitrary non-planar aircraft. NASA. Langley Res. Center Vortex-Lattice Utilization.
- [55] Fluent, A. N. S. Y. S. (2016). Fluent 15 users guide. Lebanon, USA.
- [56] Ayachit, U. (2015). The paraview guide: a parallel visualization application. Kitware, Inc..
- [57] Bouhlel, M. A., Hwang, J. T., Bartoli, N., Lafage, R., Morlier, J., & Martins, J. R. (2019). A Python surrogate modeling framework with derivatives. *Advances in Engineering Software*, 135, 102662.
- [58] Marques, S., Badcock, K. J., Khodaparast, H. H., & Mottershead, J. E. (2010). Transonic aeroelastic stability predictions under the influence of structural variability. *Journal of Aircraft*, 47(4), 1229-1239.
- [59] Jameson, A., & Fatica, M. (2006). Using computational fluid dynamics for aerodynamics.
- [60] Knapp, M., Berger, T., Tischler, M., Cotting, M., & Marcus, A. (2018). Development of a full flight envelope F-16 VISTA simulation model from closed-loop flight data. *AIAA Paper*, 525, 2018.
- [61] Tatham, R. (1951). Fz centre, flexural centre and flexural axis: an attempt to clear up current confusion and provide definitions differentiating between the three terms. *Aircraft Engineering and Aerospace Technology*.
- [62] Cattarius, J. (1999). Numerical wing/store interaction analysis of a parametric F16 wing (Doctoral dissertation, Virginia Tech).
- [63] Singh, A. K., & Nichols, C. W. (1988). Derivation of an equivalent beam model from a structural finite element model. In *Proceedings of the MSC 1988 World Users Conference*.
- [64] Pytorch, A. D. I. (2018). Pytorch.

- [65] MATLAB. (2018). 9.7.0.1190202 (R2019b). Natick, Massachusetts: The MathWorks Inc.
- [66] Pedregosa, F., Varoquaux, G., Gramfort, A., Michel, V., Thirion, B., Grisel, O., ... & Duchesnay, E. (2011). Scikit-learn: Machine learning in Python. the Journal of machine Learning research, 12, 2825-2830.
- [67] Guo, Q., Jin, S., Li, M., Yang, Q., Xu, K., Ju, Y., ... & Liu, Y. (2020). Application of deep learning in ecological resource research: Theories, methods, and challenges. Science China Earth Sciences, 63(10), 1457-1474.
- [68] Timme, S., Rampurawala, A., & Badcock, K. J. (2010). Applying interpolation techniques to search for transonic aeroelastic instability: ANN vs kriging. In The RAES Aerodynamics Conference, Bristol, United Kindom.
- [69] Ö. Zafer and M. Şahin (2022, September). Bir esnek savaş uçağı kanat yüklerinin vekil modeller kullanılarak belirlenmesi. 9. Ulusal Havacılık ve Uzay Konferansı, İzmir
- [70] CIRILLO, R. (2011). Detailed and condensed finite element models for dynamic analysis of a business jet aircraft.

## APPENDICES

### A. Initial Training and Test Points for Aerodynamic Database Generation

In the surrogate modeling part, initial training points are selected at the minimum and maximum AoA values to prevent extrapolation. In this part, two randomly selected initial training points and test points named as case A and case B are demonstrated, allowing surrogate models to extrapolate as well. In Figure A. 1 and Figure A. 2, the number of points used according to the algorithm described in section 6.2 is also listed in Table A.1 and Table A.2.

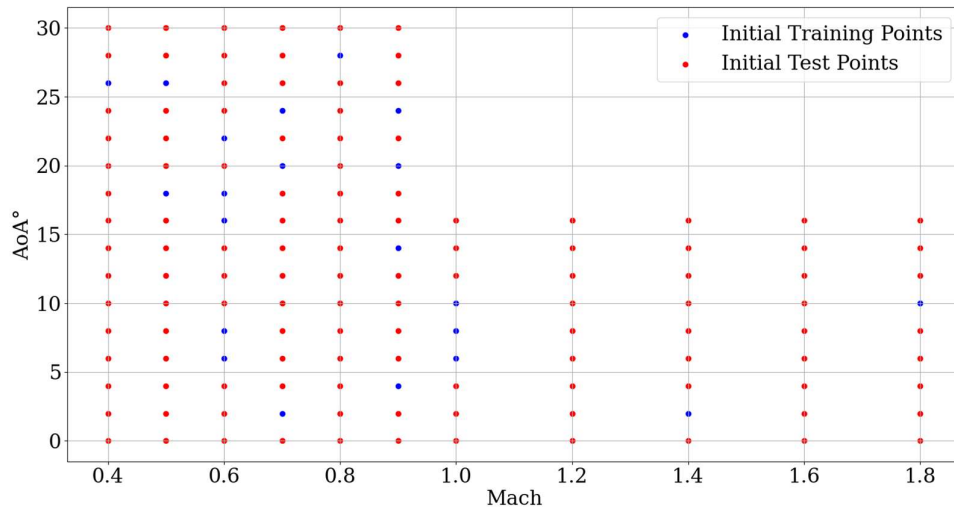


Figure A. 1 Randomly selected initial training and test points for aerodynamic database (Case A)

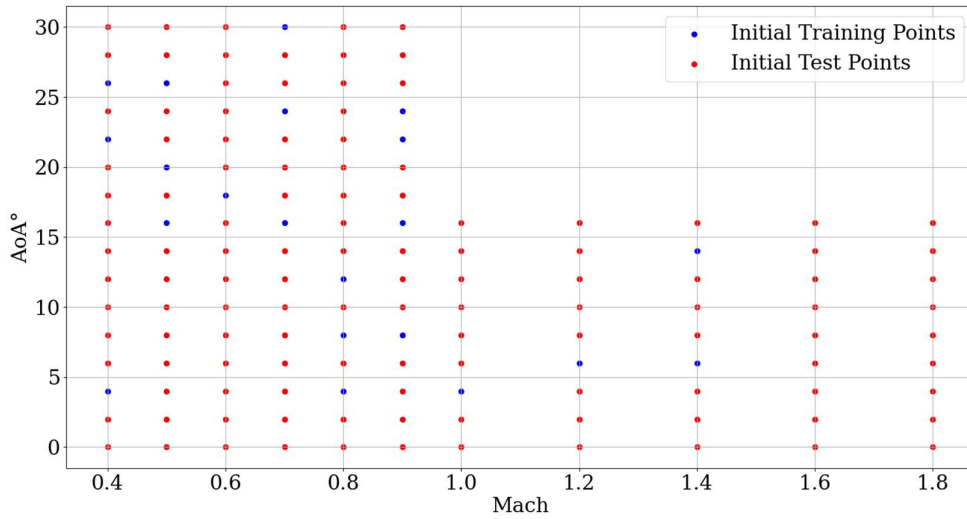


Figure A. 2 Randomly selected initial training and test points for aerodynamic database (Case B)

Table A.1 Number of points used to create an aerodynamic database with initial training points (Case A)

Surrogate Model	Number of Training Points
	Used / All points
LS	135/141
QP	133/141
IDW	127/141
KRG	84/141
RBF	129/141
RMTS	111/141

Table A.2 Number of points used to create an aerodynamic database with initial training points (Case B)

<b>Surrogate Model</b>	<b>Number of Training Points Used / All points</b>
LS	135/141
QP	132/141
IDW	126/141
KRG	83/141
RBF	133/141
RMTS	117/141

### **B. Aerodynamic Database Generation with Three Different Databases**

In this part, the surrogate models are trained in three different databases, which are divided according to the flow regime, namely subsonic, transonic and supersonic regimes. Subsonic regime is taken as below 0.8 Mach, between 0.8 and 1.2 is selected as transonic and above 1.2 Mach is referred as the supersonic region. Figure B.1 illustrates these regions. Surrogate models are trained for each regime with the same database generation algorithm and the number of points used for each surrogate model is given at Table B.1.

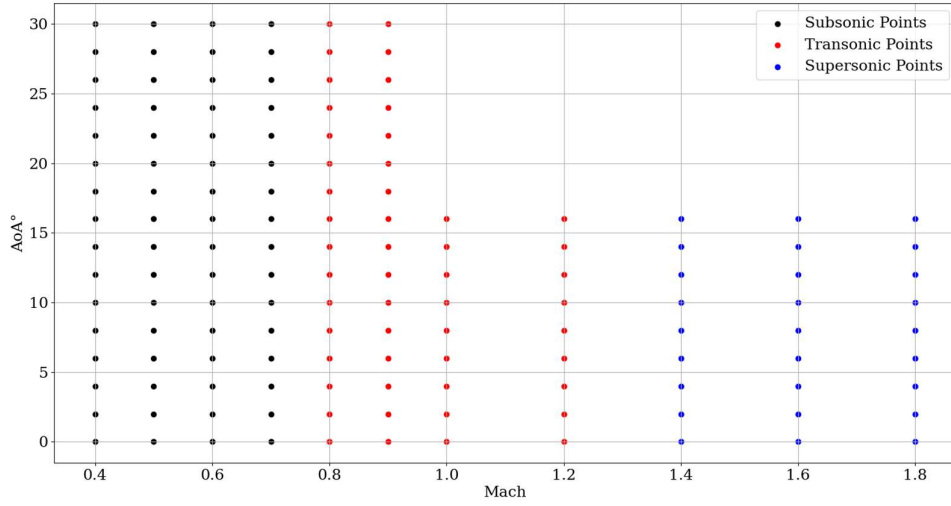


Figure B.1 Aerodynamic database divided according to flow regimes

Table B.1 Number of points used to create an aerodynamic database with three different databases

Surrogate Model	Number of Training Points
	Used / All points
LS	133/141
QP	127/141
IDW	125/141
KRG	79/141
RBF	127/141
RMTS	109/141



### C. Response Surfaces for Surrogate Models

In this part, response surfaces for each surrogate model and the used sample points are given in Figure C.1 to Figure C.6. Sample points are the values obtained directly from the CFD analysis. The response surfaces show the predictions made by the surrogate model. In order to use the same amount of training points, each surrogate model is trained with 80/141 points.

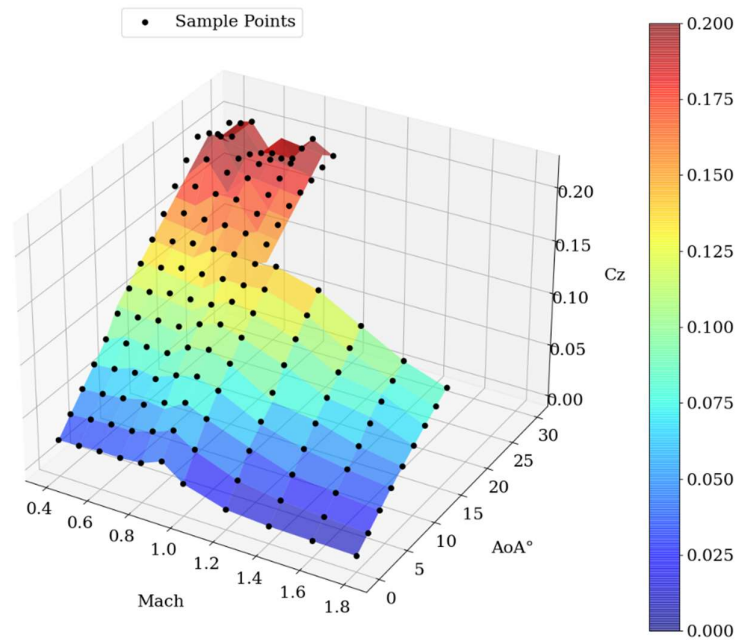


Figure C.1 Response surface of LS

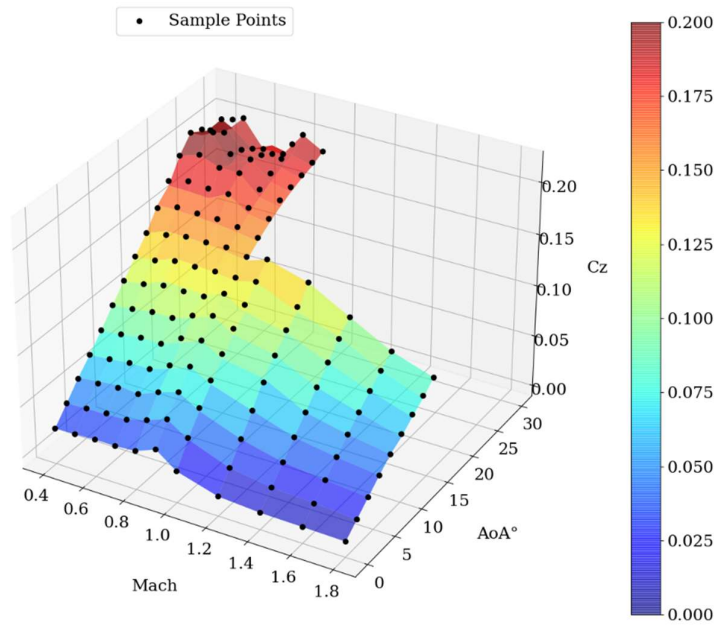


Figure C.2 Response surface of QP

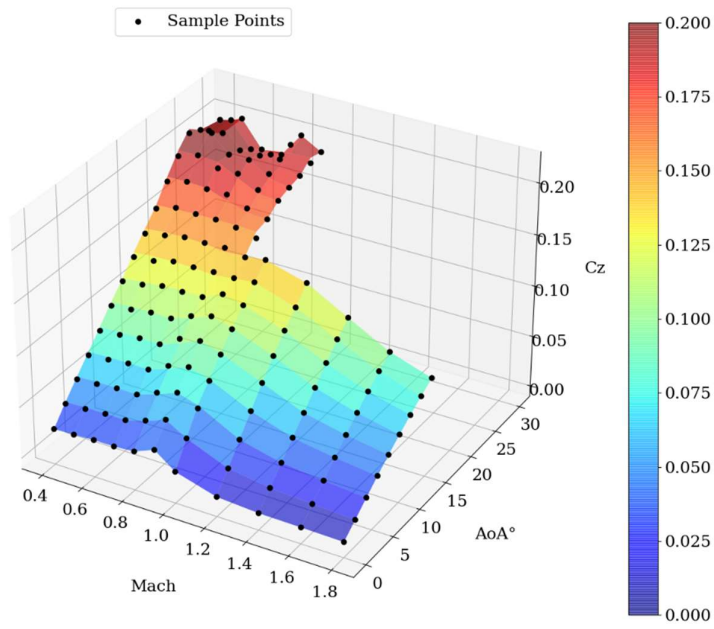


Figure C.3 Response surface of IDW

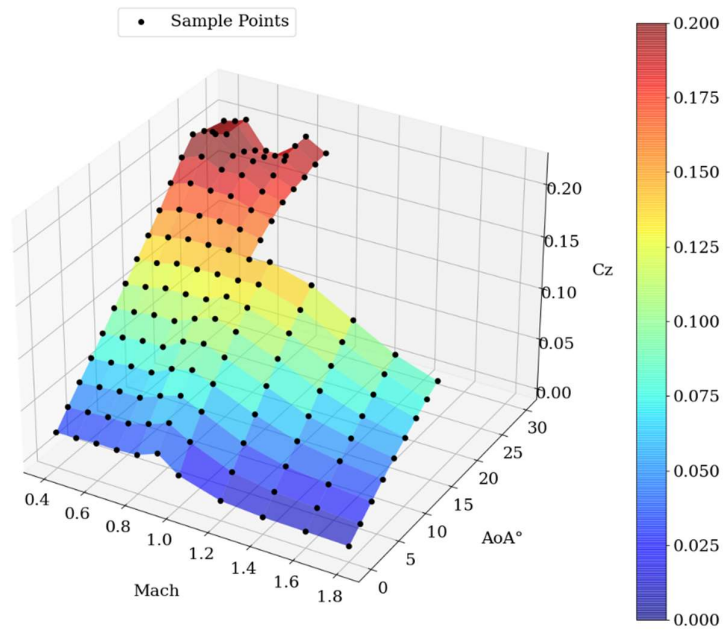


Figure C.4 Response surface of KRG

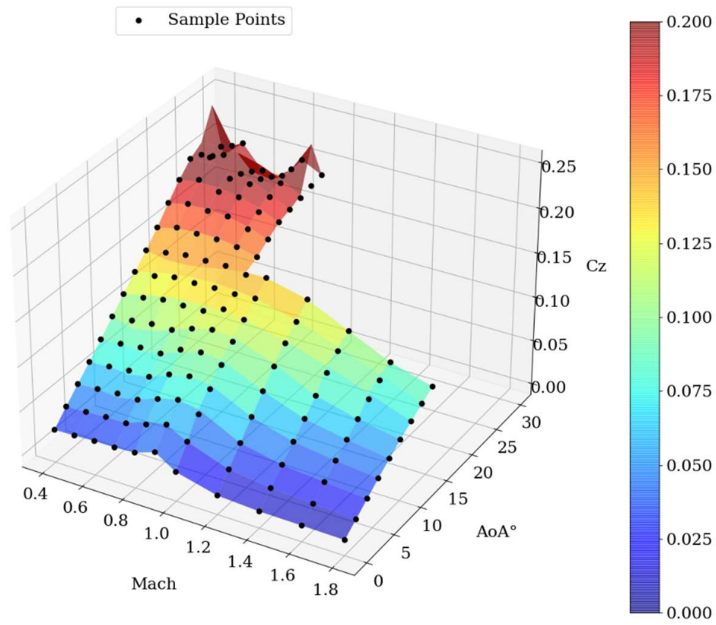


Figure C.5 Response surface of RBF

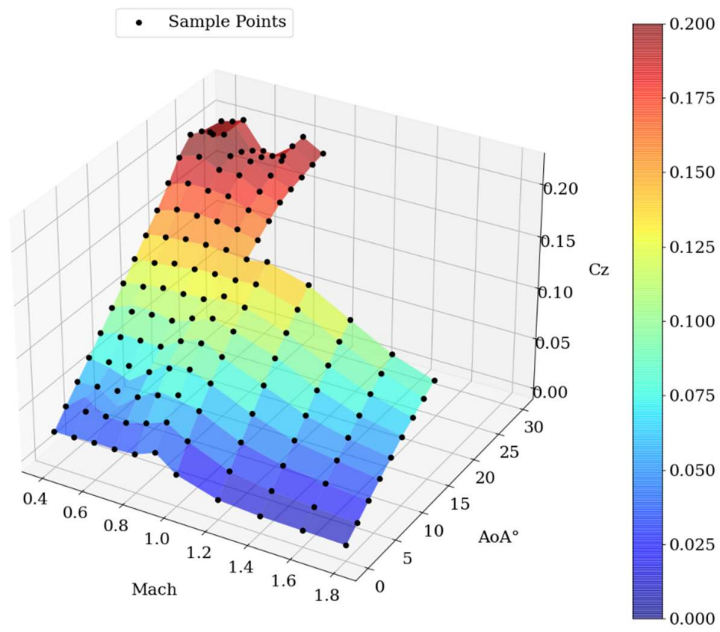


Figure C.6 Response surface of RMTS